A basal forebrain to midbrain circuit drives exploratory locomotion

Doctoral thesis

to obtain a doctorate (PhD)

from the Faculty of Medicine

of the University of Bonn

Petra Mocellin

from Marostica, Italy

2023

Written with authorization of

the Faculty of Medicine of the University of Bonn

First reviewer: Prof. Dr. Stefan Remy

Second reviewer: Prof. Dr. Dirk Isbrandt

Day of oral examination: 17.10.2023

From the German Center for Neurodegenerative Diseases (DZNE)

Director: Prof. Dr. Pierluigi Nicotera

To Lidia and Günther,

Table of Contents

List of abbreviations

4-AP: 4-amynopyridin
AAV: adeno-associated virus
ACh: acetylcholine
Amy: amygdala
AP: action potential
bAP: backpropagating action potential
BNST: bed nucleus of the stria terminalis
CB: calbindin
Cc: corpus callosum
ChAT: cholinergic
ChR: channelrhodopsin
CLi: caudal linear nucleus
CR: calretinin
cTRIO: cell-type-specific tracing the relationship between input and output
Ctrl: control
DA: dopamine
D-AP5: D-2-amino-5-phosphonopentanoate
DAT: dopamine transporter
DLC: DeepLabCut
EC: entorhinal cortex
EnvA: envelope protein of the subgroup A avian sarcoma and leukosis virus
EPSP: excitatory post synaptic potential
Gad: glutamate decarboxilase
GECI: genetically encoded calcium indicator
CaM:calmodulin
GFP: green fluorescent protein
HCN: hyperpolarization-activated cyclic nucleotide-gated cation channel
HPC: hippocampus
IF: interfasciculate nucleus
Ih: hyperpolarization-activated current
IP: interpeduncolar nucleus
PN: paranigral nucleus
IR: input resistance
LDT: laterodorsal tegmentum
LFP: local field potential
LH: lateral hypothalamus
LHb: lateral habenula
LS: lateral septum
MSDB: medial septum and diagonal band of Broca
$MSDB_{glu}$: VGluT2+ medial septal neurons
NAc: nucleus accumbens
NBQX: 2,3-dioxo-6-nitro-7-sulfamoyl-benzo[f]quinoxaline
NI: nucleus incertus
Nts: neurotensin
OF: Optical Flow

PAG: periaqueductal grey
PBP: parabrachial pigmented nucleus
PFC: prefrontal cortex
PH: posterior hypothalamic nucleus
POA: preoptic area
PPT: peduncolopontine tegmentum
PV: parvalbumin
PVH: paraventricular hypothalamic nucleus
RABV: rabies virus
RG: rabies glycoprotein
RLi: rostral linear nucleus
RPE: reward prediction error
SN: substantia nigra
SST: somatostatin
SuM: supramammillary nucleus
TF: septofimbrial and triangular septal nuclei
TH: tyrosine hydroxylase
THIP: 4,5,6,7-tetrahydroisoxazolo[5,4-c]pyridin-3-ol
TS: triangular septal nuclei
TTX: tetrodotoxin
VGluT2: vesicular glutamate transporter type 2
vHPC: ventral hippocampus
VMAT: vesicular monoamine transporter 2
VTA: ventral tegmental area
VTA_{glu}: VGluT2+ ventral tegmental area neurons

1. Introduction

Movement is a key feature of almost every living being. However, not all living organisms are capable of moving voluntarily through space. The voluntary aspect of movement seen in higher-order animal species has spurred scientific investigation into how the brain refines and regulates motor control and execution. Animals move for various reasons, such as foraging, fleeing, mating, or exploring the environment (Mogenson et al., 1980b), (Mogenson et al., 1980b). All of these reasons require a finely tuned and specific orchestration of an animal's internal drive and representation of external cues, that will give rise to a broad range of behavioral outcomes. This work aims at elucidating how the medial septum and diagonal band of Broca, a major component of the basal forebrain, influence the locomotor activity of mice via its projections to the ventral tegmental area, a brain region linked to motivation for reward consumption, learning, and memory.

1.1 Locomotion and exploration

Locomotion is a fundamental behavior shared among all mammalian species. It is defined as a movement of the animal's body in space, resulting in a change of its position in the environment. Depending on the internal state and the external demands, different motivations to move exist (Mogenson et al., 1980b). The environment presents resources that the animal aims to reach such as food, water, conspecifics, or shelter; but also dangers that it needs to avoid as predators or aggressions from other conspecifics. The motivation to move and be exposed to the environmental conditions is heavily influenced by the animal's internal state (Berlyne, 1966; Belzung, 1999). Homeostatic needs, such as thirst or hunger, represent strong internal drives. The resulting behavior motivated by needs like food or water is defined as goal-oriented and terminates when the animal satiates its needs (including also social needs as reviewed by (Matthews and Tye, 2019)). Goal-oriented behaviors can be related to both positive and negative valences. While food and water are considered rewarding, escaping actions are aversive experiences substantiated by a similar goal-oriented trait (Kesner et al., 2022).

Seminal studies conducted in the '50s across different species showed that all animals have in common an intrinsic drive to move in the environment, even in the absence of an immediate reward. For example, rats will choose to spend more time in a complex labyrinth rather than in a simple corridor (Tolman, 1948) and monkeys will engage in

operant tasks in order to access new environmental information (Butler, 1953). This drive towards gaining information about the surroundings in the absence of an immediate goal or reward is referred to as exploratory or information-seeking behavior (Kesner et al., 2022).

1.1.1 Behavioral correlates of exploration

Exploratory or information-seeking behavior is defined as a series of responses including walking, sniffing, rearing, leaning, jumping and digging (Belzung, 1999) and is most prominently observed within a novel environment or in the presence of a novel cue. However, novelty is often accompanied by both positive (neophilia) and negative (neophobia) valence. Novelty elicits curiosity and exploration to access more information (neophilia), but the absence of previous knowledge is also linked to stress and anxiety (neophobia) (Berlyne, 1955, 1966). Thus, exploratory and information-seeking behaviors are complex, multiplexed, and, given the diversity of their triggers, likely exhibit a high intra-animal variability. They depend on the animal's internal state (more anxious animals will have a lower exploratory drive), on the environmental condition (higher degrees of novelty can cause more neophobia, while lower degrees may favour neophilia), and on the previous experience (animals used to novel environments will have more exploratory drive than animals that are not used to it). Moreover, depending on the environment and the animal previous experience, exploration is a mixture of some, sometimes all, of the above-mentioned behavioral responses, in a non-specific order and with hardly predictable transitions between them.

1.1.2 Neural circuits underlying exploratory behavior

Given the multiplexed nature of exploratory behaviors, it is not surprising that numerous brain areas and neural circuits contribute to it. In order to explore, an animal must perform several cognitive and motor tasks. First of all, it needs to compare its current status with its past experience: only when there is a discrepancy from what the animal knows to what it is exposed to, exploratory behavior initiates. A key brain region involved in memory acquisition, consolidation and retrieval is the hippocampal formation (Carr et al., 2011; Buzsáki and Moser, 2013; Joo and Frank, 2018). Indeed, lesions and pharmacological silencing of the hippocampus resulted in impaired spatial navigation and reduced performances in cognitive and memory tasks (Aggleton et al., 1986; Jarrard, 1993; Hollup

et al., 2001). Once such a discrepancy is detected, the animal needs a motivation in order to engage in exploratory actions. Midbrain circuits involved in dopaminergic signalling are classically considered central for motivated behaviors (Mogenson and Huang, 1973; Schultz, 1999). This has been particularly reported for the ventral tegmental area (VTA) and its reciprocal projections to the nucleus accumbens (NAc) (Mogenson et al., 1980b; Yang et al., 2018; Mohebi et al., 2019). When VTA projections to NAc were pharmacologically silenced, rodents reduced the exploration of a novel environment, while no impairment was detected in familiar spaces (Hooks and Kalivas, 1995).To execute these kinds of actions, animals must be able to move. Thus, cortical and subcortical motor circuits also play a role in this behavior (motor cortex, dorsal striatum, mesencephalic locomotor region, and the spinal circuits just to mention the most relevant ones (Parker and Sinnamon, 1983; Capelli et al., 2017; Caggiano et al., 2018; Ferreira-Pinto et al., 2018)). However, movement and motivation may not be sufficient to define exploration. In rodents, sniffing, rearing, and leaning are motor outputs underlying curiosity and interest towards the environment (Berlyne, 1966; Belzung, 1999; Kurnikova et al., 2017). Detecting salient stimuli is therefore a necessary component of the network and is mediated, among other regions, by the medial septum and diagonal band of Broca (MSDB) (Zhang et al., 2018a, 2018b; Kesner et al., 2021). This brain region is of particular interest in the context of locomotor and exploratory behavior given its crucial position in the basal forebrain which is at the interface of the navigational, limbic, and motor systems.

1.2 The medial septum and diagonal band of Broca

The septum is a brain area located in the middle of the basal forebrain and delimited on the superior part by the lateral ventricles and the corpus callosum. It extends for around 1 mm in the anterior-posterior axis, it is surrounded by the striatum in the more anterior parts (NAc, caudoputamen, substantia innominata and ventral pallidum) and by the hypothalamic preoptic area (POA) as well as the bed nucleus of the stria terminalis in the more posterior parts (Figure 1). It has initially been studied as a whole, but it is now established that it comprises at least three anatomically distinct parts located in the medial, lateral, and posterior regions. These three structures are named: the medial septum and diagonal band of Broca (MSDB), the lateral septum (LS), and the septofimbrial and triangular septal nuclei (TF). Those regions are evolutionary well-

conserved parts of the limbic systems, highly interconnected with the hippocampal formation and the hypothalamus in all vertebrate groups (Lanuza and Martínez-García, 2009). Embryonically, MSDB and LS cells originate from the subpallium and the neighbouring progenitor regions of the telencephalon (medial ganglionic eminence, preoptic area, and medial pallial-subpallial boundary) (Wei et al., 2012), while TF cells belong to an independent stream of migrating neurons born in the more caudal thalamic eminence (Watanabe et al., 2018).

1.2.1 Cell type diversity

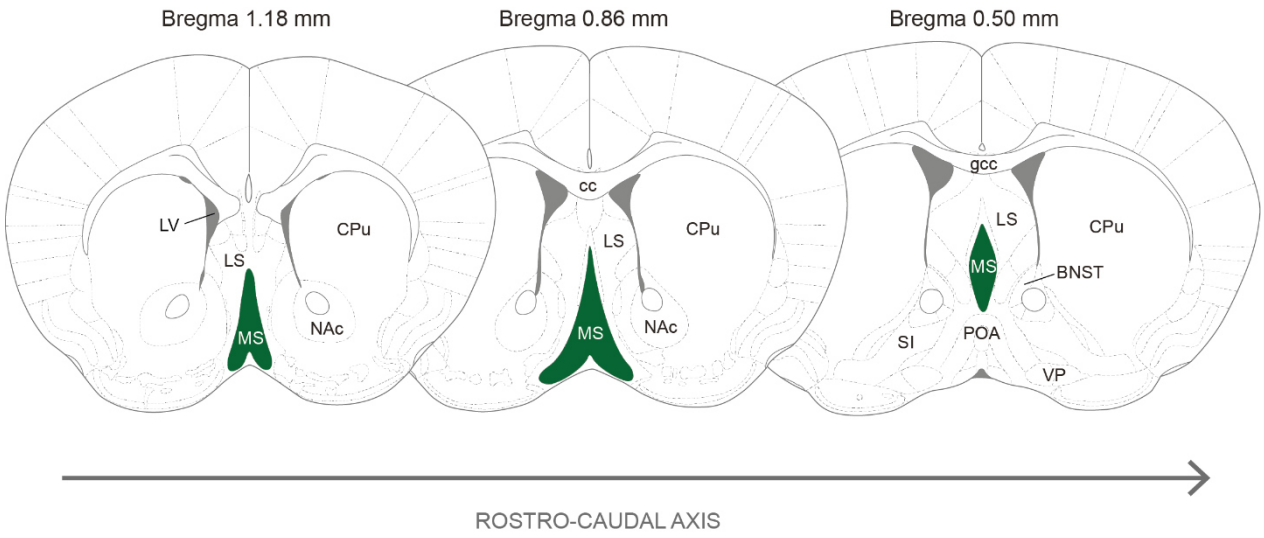

Figure 1 – MSDB anatomy. Position of the MSDB (abbreviated MS) along the rostro caudal axis. BNST: bed nucleus of the stria terminalis; CPu: caudoputamen; cc: corpus callosum; LS: lateral septum; LV: lateral ventricle; NAc: nucleus accumbens; POA: preoptic area; SI: substantia innominata; VP: ventral pallidum

The different embryonic origins give rise to different cell types in the septal region. The TF neurons are positive for the vesicular glutamate transporter type 2 (VGluT2) and considered to be mostly excitatory cells releasing glutamate as a neurotransmitter (Watanabe et al., 2018). The MSDB and LS neurons arise from the same regions, thus spatial and temporal developmental control allows for neuronal diversity. Most septal neurons are generated after the embryonic day 10.5 from residential precursors in the septal neuroepithelium. A remarkable exception are the parvalbumin positive (PV^+)

interneurons of the MSDB that are embryonically distinct from the PV^+ interneurons in the LS and originate outside the septum at earlier embryonic stages (Magno et al., 2022). It is still not fully resolved how septal neurons differentiate, as it could be that the neuronal precursors segregate into the septum, or that bipotential precursors exist whose differentiation is dependent on intrinsic factors. Indeed, several transcription factors influence the development of septal neurons. The most relevant ones comprise Zic4, Nkx2.1, and the recently identified Bsx. The expression of the Zic family transcription factors is crucial to distinguish septal progenitors zone from adjacent regions (Inoue et al., 2007). Overall, MSDB neurons develop first from there and LS neurons raise later and occupy progressively more lateral position in what was referred as a “onion-skin like” organization (Wei et al., 2012). Most of those LS and MSDB neurons are positive for Zic4, and comprise the largest proportion of progenitors that will develop into different kind of interneurons in both LS and MSDB. However, MSDB has been largely studied for its cholinergic (choline acetyltransferase (ChAT) positive neurons) cell population. Indeed, a specific reporter, namely Nkx2.1, is highly specific for these ChAT neurons releasing acetylcholine (ACh) (Magno et al., 2017). While the presence of interneurons and ACh neurons in the MSDB has been largely established since the 1980’s (Griffith and Matthews, 1986), the first evidence of excitatory glutamatergic cells in this area of the basal forebrain dates to 2003 (Sotty et al., 2003). Only recently, a transcription factor has been identified as specific for those neurons at the embryonic level: Bsx. Those cells of the MSDB were also positive for VGluT2 markers but interestingly do not correspond to the full population of identified glutamatergic neurons in the MSDB (Magno et al., 2022). Overall, it is known that the LS population is substantially inhibitory and comprised of spiny neurons releasing GABA. On the other side, it is widely accepted that at least three different population of neurons exists in the MSDB: ChAT, GABAergic, and glutamatergic. While four subpopulations of GABAergic interneurons can be identified with classical markers (PV, SST, Gad65 and Gad67), some overlap between ACh and interneurons markers at the transcriptomic level, and between glutamatergic and interneurons marker at late embryonic stages has also been reported. Thus, it is still debated how many subclusters of MSDB neurons exist (see (Turrero García et al., 2021; Magno et al., 2022)).

1.2.2 Input-output connectivity

Positioned in the middle of the basal forebrain, the MSDB constitutes a strongly interconnected region of the brain. It has bidirectional input-output relationships with the nearby LS, the hippocampal formation (including both the hippocampus proper (HPC) and the entorhinal cortex (EC)), the hypothalamic region (in particular the POA, the lateral hypothalamus (LH), and the supramammillary nucleus (SuM)) It is also connected with key brain areas involved in the generation, and suppression of hippocampal rhythmogenesis in the brainstem (the raphe nuclei and the nucleus incertus (NI)). It receives inputs from the cerebellum and the thalamus, while it sends output projections to the cingulate and insular cortices, the olfactory bulb, the medial and lateral habenula, and the VTA (Figure 2) (Meibach and Siegel, 1977; Fuhrmann et al., 2015; Agostinelli et al., 2019).

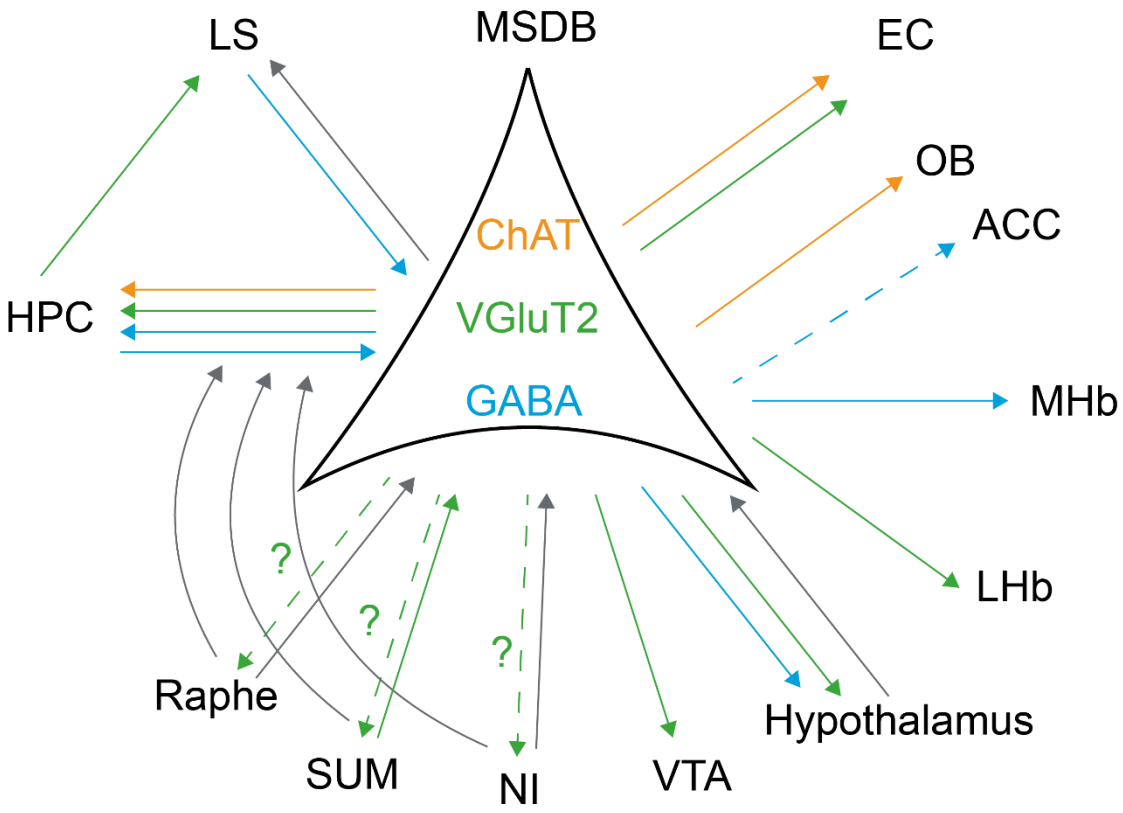

Figure 2 – Cell-type specific MSDB neurons efferent projections. Overview of ChAT (orange), VGluT2 (green) and GABA (blue) MSDB neurons efferents to cortical and subcortical structures. Dotted lines indicate tracing observations not yet confirmed by functional and/or behavioral data. Gray arrows indicate projections whose cell-type has not been identified. Adapted from Mocellin & Mikulovic, 2021.

1.2.3 Behavioral correlates of MSDB activity

Although anatomical studies have shed some light on the way the information is routed in the brain, the understanding of how those networks shape behavior have to come from a functional analysis of those input-output connections. In neuroscience, two main approaches have been used to understand the role of a brain area in influencing behavior: 1) monitoring of the cell activity during a task via electrophysiological or calcium imaging approaches; or 2) manipulation of the brain area via either activation or inhibition of the neurons. In the past, the latter was achieved by electrical stimulation, lesions, or pharmacology. However, those techniques did not allow for a precise spatial and temporal control over the circuit. The development of novel tools such as optogenetics and chemogenetics, together with the genetic access to specific cell types via transgenic animals, is currently allowing for a more precise control over specific types of neurons during behaviorally relevant activities. First, electrical stimulation of the MSDB enabled the identification of this brain region as a hub for motivated actions and self-reinforcement (Olds and Milner, 1954; Gordon and Johnson, 1981; Cazala et al., 1988), while a decrease in exploratory locomotor behavior (Lee et al., 1988), rate of habituation in novel environments (Decker et al., 1992), and deficits in spatial tasks (Fraser et al., 1991) was described upon MSDB lesion. Similarly, inhibition of MSDB neuronal activity using GABA A agonist like muscimol or Na^+ channels blocker like lidocaine resulted in impaired memory and navigation (Chrobak et al., 1989; Nagahara and McGaugh, 1992; Walsh et al., 1998). This effect was not surprising in light of the strong projections of the MSDB to the HPC formation, constituting the most extensively studied septal circuit: the so-called septohippocampal network. The septohippocampal network is necessary for the rhythmogenesis in the HPC ranging between 3 and 12 Hz and classically referred as theta oscillations. Two types of theta rhythm have been described (Kramis et al., 1975). Type 1 theta (8-12 Hz) is recorded in association with voluntary locomotion, it is strongly correlated with the animal speed, and it is believed to be a way for the brain to constantly update the voluntary motor system with the changes in the environmental conditions (Vanderwolf, 1969). Conversely, type 2 theta (3-8Hz) typically occurs during arousal episodes in immobile animals and it is thought to play a major role in sensorimotor integration (Bland et al., 1984; Bland and Oddie, 2001). Disruption of theta oscillations causes severe impairment of both animal and human behavior, including spatial and

memory deficits. Thus, the impairments in movement, exploration, and navigation observed following MSDB inactivation are consistent with the impairments observed with theta oscillation disruption in the HPC, and emphasises the importance of the MSDB to HPC projections in HPC rhythmogenesis. More recently, specific manipulation of the different cell types in the MSDB have shed new light on the role of MSDB neuronal populations in animal behavior.

1.2.4 Cholinergic neurons and their network

For a long time, MSDB received attention as one of the basal forebrain regions with the highest concentration of cholinergic neurons and the major source of cholinergic inputs to the HPC. ACh is a neuromodulator whose function is to potentiate ongoing adaptive and complex behaviors, while supressing responses to stimuli that do not require an immediate action (Picciotto et al., 2012). In simple terms, it has been linked to the level of arousal and attention of an organism, thus high levels of ACh are linked to high alertness and increased attention levels, while low level of ACh were detected during resting and sleep (Hasselmo and McGaughy, 2004). The ChAT-Cre mouse line has been extensively used to study the cholinergic systems in the mouse brain. In particular, chemogenetic silencing of ChAT neurons in the MSDB reduced anxiety-like behaviors (Jiang et al., 2018), while activation of those neurons and their projections in the ventral HPC (vHPC) and prefrontal cortex (PFC) were related to alert responses (Adhikari et al., 2010; Mikulovic et al., 2018). Interestingly, those responses were also linked to slower oscillations in the HPC, resembling type 2 theta rhythm and supporting the role of the ACh MSDB neurons in modulating attention and arousal.

1.2.5 GABAergic neurons and their network

The population of MSDB GABAergic neurons is quite heterogeneous, densely project to the HPC, and comprises neurons that express PV, somatostatin (SST), calretinin (CR) and calbindin (CB) at different level and with different combinations. Those neurons can be targeted using different transgenic mouse lines. Gad65-Cre and Gad67-Cre are broadly labelling all GABAergic neurons as glutamate decarboxylase (Gad) is an enzyme present in two isoforms (Gad 65 and Gad67) and necessary to synthetize the neurotransmitter GABA. PV-Cre and SST-Cre mouse lines are specific for interneurons that express PV or SST. In particular, MSDB PV expression overlaps with the

hyperpolarization-activated cyclic nucleotide-gated (HCN) channel, making those neurons capable of pacemaker activity (Hangya et al., 2009). Indeed, optogenetic activation of this cell population is sufficient to elicit theta oscillations in the HPC (Varga et al., 2008). Conversely, MSDB SST^+ neurons appear to be responsible for spatial working memory: when optogenetically inhibited, they disrupt the alternation index in a Y maze test (Espinosa et al., 2019). While PV and SST manipulation appear to have an impact on HPC firing or HPC-related behaviors as memory and spatial tasks, little is known about the role of MSDB interneurons outside the septohippocampal circuit. So far, only the habenula has been functionally characterized as a target of the MSDB GABA neurons projections and seem to be involved in the modulation of anxiogenic and depressive states (Choi et al., 2016; Vickstrom et al., 2021). This is not surprising, as most of the interneurons throughout the brain exert their activity in local microcircuits, and only recently, the idea of long-range interneurons activity has started to become investigated (Melzer et al., 2012).

Overall, MSDB ACh and GABA neurons exert most of their influence locally in the MSDB or via their projections to the HPC. The septohippocampal network, as a whole, plays a role in theta generation (via PV neurons) and modulation (via ACh release), thus it is involved in an animal's ability to navigate an environment and memorize what it is experiencing

1.2.6 Glutamatergic neurons and their network

The $VGluT2^+$ population of the MSDB ($MSDB_{glu}$) is the most recently described population (Sotty et al., 2003)and constitutes around 25% of the neurons in this area (Colom et al., 2005). Early studies of slice physiology and anatomy revealed that those neurons are not homogeneous, having at least two different types of morphology and forming four different clusters based on their electrophysiological properties. Optogenetic activation of the $MSDB_{glu}$ neurons was sufficient to elicit HPC oscillations (Fuhrmann et al., 2015; Robinson et al., 2016), likely due to the local connectivity with the MSDB interneurons, and in particular the PV subpopulation. However, another more surprising effect was described upon stimulation of the $MSDB_{glu}$ neurons: the reliable initiation of locomotor activity (Fuhrmann et al., 2015). Recently, it has been shown that the motor output is not dependent on MSDB interconnectivity, as the application of blockers cocktail is not preventing the locomotor effect, but seems to rely on the persistent firing of the $MSDB_{glu}$

neurons (Korvasová et al., 2021). Looking at the projections of this cell population via tracing studies (Fuhrmann et al., 2015; Zhang et al., 2018a; Agostinelli et al., 2019) it appears that, unlike ChAT and GABA MSDB neurons, the $MSDB_{glu}$ neurons target a broader range of brain areas: HPC, EC, lateral habenula (LHb), POA, LH, paraventricular (PVH) and posterior (PH) hypothalamic nuclei, SUM, VTA, NI, and raphe nucleus. Even more interestingly, activation of $MSDB_{glu}$ axons in those areas exert different behavioral effects. In the LH, optogenetic activation of $MSDB_{glu}$ inputs induce wakefulness and increase theta power, while their silencing prolonged the NREM sleep phases (Manseau et al., 2005). In the LHb, place aversion can be optogenetically induced (Zhang et al., 2018a), while in the POA it was possible to control the speed of locomotion (Zhang et al., 2018a) in a similar way to what was reported in an earlier study using somatic activation of $MSDB_{glu}$ neurons (Fuhrmann et al., 2015). Inputs to the HPC modulate theta oscillations (Fuhrmann et al., 2015) while projections to the EC convey speed-dependent (Justus et al., 2017) and salient auditory (Zhang et al., 2018b) stimuli. Finally, $MSDB_{glu}$ inputs are also targeting the VTA, one of the key regions in the brain for motivated and reinforcing behaviors (Faget et al., 2016; Kesner et al., 2021).

Taken together, the $MSDB_{glu}$ neuron population is positioned at the interface of navigational, limbic, and motor brain circuits. Through its MSDB interconnectivity and projections to the HPC, it modulates theta oscillations and conveys speed-dependent information to the EC, thus allowing an animal to receive an on-line update of its movement in space. Its inputs to the LHb and the EC convey salient stimuli, allowing the organism to promptly respond to unexpected changes in the environment. In addition, $MSDB_{glu}$ neuronal stimulation through their pathway to the POA elicited a locomotor response (Zhang et al., 2018a). The MSDB has also been shown to be related to reinforcement and self-stimulation (Olds and Milner, 1954; Kesner et al., 2021) but the downstream targets mediating this behavior are still unknown. Tracing experiments indicated the ventral tegmental area (VTA) as a putative candidate for this role. VTA neurons are multiplexing information: they tune an animal's behavior via NAc projections (Mingote et al., 2019) and receive inputs from several brain regions (Morales and Margolis, 2017). Moreover, the VTA projects to motor cortex and striatum (Hosp et al., 2011; Howe and Dombeck, 2016), and VTA neurons can fire in an onset-, acceleration- and speed-dependent manner (Engelhard et al., 2019; Kremer et al., 2020). Thus,

$MSDB_{glu}$ neurons interaction with VTA could represent a key pathway bridging the septo-hippocampal spatial network, the limbic motivational systems and rewarding dopaminergic circuits.

1.3 The ventral tegmental area

The VTA has been extensively studied for its role in motivated behaviors. In particular, it is known to be involved in the regulation of mood, reward, learning, detection of salient stimuli, and the pathologies associated with all of the above (Nestler and Carlezon, 2006; Fields et al., 2007; Grace et al., 2007; Bromberg-Martin et al., 2010; Creed et al., 2014; Gillies et al., 2014; Ikemoto and Bonci, 2014; Meye and Adan, 2014; Overton et al., 2014; Walsh and Han, 2014). It is located around the midline of the midbrain floor and it was initially considered an extension of the substantia nigra (SN) (Castaldi, 1923). In 1925, Tsai argued that those midline neurons, smaller in size and delimited by the medial lemniscus, were anatomically and functionally different from the SN (Tsai, 1925). This observation was then confirmed by later studies in the ‘50s that used for the first time the name of ventral tegmental area of Tsai (Nauta, 1958). With the advent of the formaldehyde histofluorescence method in 1964 by Falck and Hillarp, it the distribution of catecholamines-containing neurons in the brain was described. 12 groups of neurons were identified and they were designated A1 to A12 (Carlsson et al., 1964; Fuxe, 1965). In particular, the A9 and A10 dopaminergic groups corresponded roughly to the SN and VTA, respectively. For years, attempts were made to anatomically define the borders of those two regions and classify their different subnuclei. Using Nissl staining, a first distinction was made between the highly packed neurons in the SN and the scattered neurons in the VTA. If a clear distinction was observed dorsally and ventrally at the boundary with the red nucleus and the interpeduncular nucleus (IP); anterior, lateral and posterior VTA borders are not easily visible. Indeed, the VTA neurons merge with the SUM, SN and reticular formation neurons making it difficult to define clear edges (Oades and Halliday, 1987).Only the density and morphology of DA neurons can help distinguishing the different brain structures (Phillipson, 1979). The VTA itself also presents different subnuclei: the more lateral VTA neurons cluster, close to the SN, is called paranigral nucleus (PN) and share morphological features with the nearby SN pars compacta neurons (Poirier et al., 1983). Medially, the interfascicular nucleus (IF) is

characterized by round, small, and densely packed cells dorsal to the IP. Above the PN, sits the parabrachial pigmented nucleus (PBP). The main difference between the two nuclei is the orientation of their cells: PN neurons have a horizontal orientation, while PBP neurons are haphazardly arranged dorsal to them. Finally, the rostral linear (RLi) and the caudal linear (CLi) nuclei are positioned above the IF, following the anterior-posterior axis. RLi is visible in the more anterior coronal slices, while CLi appears in the more rostral ones. It is still debated if those two nuclei are part of the VTA or belong to the neighbouring raphe nuclei in the reticular formation (as proposed by (Swanson, 1982; Kalivas, 1993; Ikemoto, 2007)). However, given the presence of DA neurons in those two areas and their proximity to the VTA proper, CLi and RLi are here considered part of the VTA formation together with the IF, PBP, and PN nuclei (Figure 3; see (Oades and Halliday, 1987; Sanchez-Catalan et al., 2014; Morales and Margolis, 2017)).

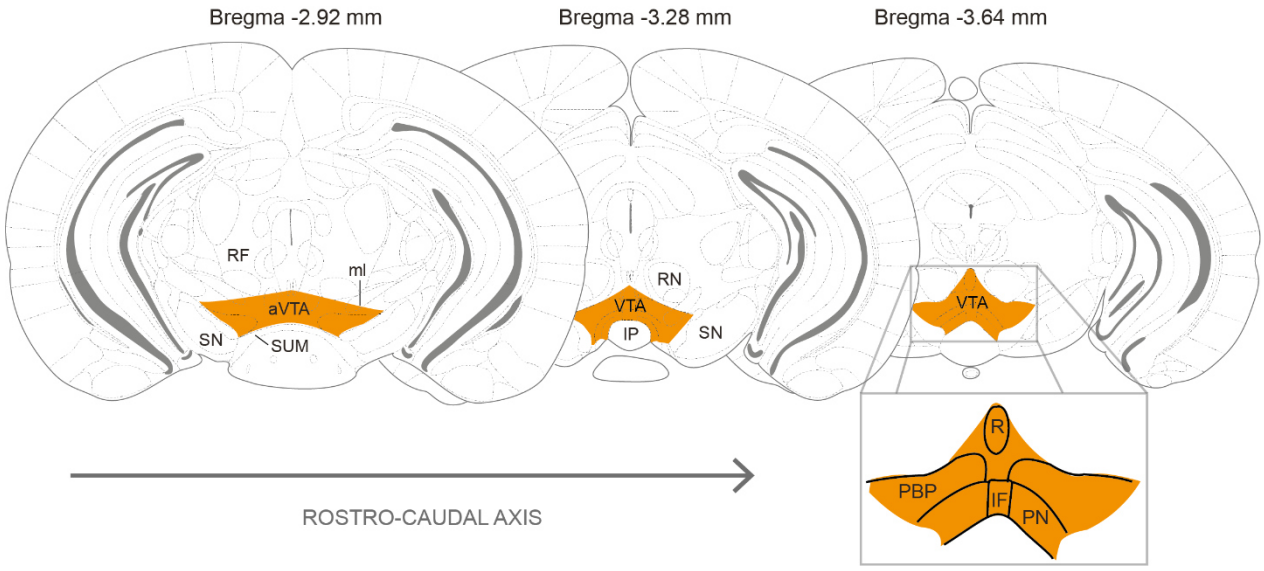

Figure 3 – VTA anatomy. Position of the VTA along the rostro caudal axis. aVTA: anterior VTA; IF: interfascicular nucleus; IP: interpeduncular nucleus; ml: medial lemniscus; PBP: parabrachial pigmented nucleus; PN: paranigral nucleus; R (abbreviation for RLi): rostral linear nucleus; RF: reticular formation; RN: red nucleus; SN: substantia nigra; SUM: supramammillary nucleus.

1.3.1 Heterogeneity of the VTA neuronal population

VTA is mostly known for the DA population that accounts for almost 70% of its neurons (Nair-Roberts et al., 2008). Early studies reported one third of VTA neurons to be non-dopaminergic (Swanson, 1982). Indeed, more recent quantifications of VTA cell types found that around 35% of VTA neurons are positive for GAD mRNA, and 3 to 5 % are positive for VGluT2 mRNA (Nair-Roberts et al., 2008; Yamaguchi et al., 2015). However, despite the broad use of in situ hybridization and immunostaining techniques to identify cell types in different brain areas, in the VTA several drawbacks have been reported (Margolis et al., 2006). If on one side there is a general agreement that those three cell types (DA, GABA and glutamate positive neurons) are part of the VTA, it is still not fully understood how do they differ from each other and how to uniquely identify them. Moreover, VTA neurons can co-release GABA and glutamate, DA and glutamate and DA and GABA, making the identification of specific neural markers even more complex (Hnasko et al., 2010; Root et al., 2014; Ntamati and Lüscher, 2016; Miranda-Barrientos et al., 2021). Several attempts have been made in order to differentiate the neuronal subpopulation of the VTA: anatomy, morphology, mRNA expression, protein expression, electrophysiological properties, afferent and efferent projections target, and the use of transgenic reporter lines.

1.3.2 Anatomy

Anatomically, a first distinction exists between anterior (aVTA) and posterior (pVTA), as well as between medial (mVTA) and lateral (lVTA) regions (Sanchez-Catalan et al., 2014). The delivery of GABA agonists and antagonists in the aVTA and pVTA resulted in a discrepancy of behavioral responses (Arnt and Scheel-Krüger, 1979a). The main reason was found in the relatively higher abundance of GABA neurons in the aVTA and their progressive reduction along the rostro-caudal axis (Olson, 2005). Conversely, there is a slight predominance of DA neurons in the pVTA, even though DA neurons can be found all along the medio-lateral and rostro-caudal axes. Regarding glutamatergic neurons, they are mostly located in the IF and CLi nuclei close to the midline (Yamaguchi et al., 2015). Thus, a medio-lateral gradient of glutamatergic VTA neurons can be observed, similar to the expression pattern of the DA-glutamate co-releasing neurons.

1.3.3 Transcriptomics and proteomics

To identify different cell types, it is common in neuroscience to use techniques that label specific markers expressed in the neurons as in situ hybridization does with mRNA and antibody immunostaining does with proteins. There are pro and cons of both techniques: while mRNA is a transient transcript of DNA and does not necessarily translate into a protein, the protein itself can be difficult to label using antibodies and the success of the technique is linked to the availability and localization of the protein in the cell. Thus, a combination of both in situ and immunostaining have been used to classify VTA neurons. A classical marker for DA neurons is tyrosine hydroxylase (TH), the rate-limiting enzyme of catecholamine biosynthesis. For years, immunostaining for TH was the golden standard to identify VTA DA neurons. However, it was found that not all the TH^+ neurons in VTA were encoding for other two necessary proteins involved in the cellular re-uptake of DA (the dopamine transporter – DAT) and in its accumulation into vesicles (the vesicular monoamine transporter 2 – VMAT2)(Margolis et al., 2006). Moreover, some neurons expressing TH mRNA were lacking detectable levels of TH protein (Margolis et al., 2010). Thus, while still broadly used to identify DA neurons, it must be considered that the VTA neuronal population is heterogeneous and that TH protein expression may not necessarily indicate an active release of DA from the labelled neuron. On the other side, the use of GAD to label VTA GABA neurons seem to give a more homogeneous labelling, while it is still necessary to consider that sharing the expression of GAD does not necessarily make interneurons a homogeneous population (Margolis et al., 2012). Indeed, only some GABA neurons responded to certain drugs (DRD2 receptor or u-opioid receptor agonists) and most, but not all, expressed the hyperpolarization activated current (Ih) (Olson and Nestler, 2007; Wang and Morales, 2008). However, when considering the glutamatergic population, VGluT2 expression is considered a hallmark of VTA glutamatergic neurons as there is compelling evidence that those neurons indeed utilize glutamate as a neurotransmitter (Kawano et al., 2006; Yamaguchi et al., 2015).

1.3.4 Electrophysiology

Electrophysiologically, DA and GABA VTA neurons have been initially identified both *in vivo* and *in vitro* based on their action potential (AP) duration, their firing frequency, their input resistance (IR), and the presence or absence of Ih. Ih is defined as the current generated through the hyperpolarization-activated cyclic nucleotide-gated cation channels

(HCN) and for several years was thought to be a distinctive feature of VTA DA neurons together with their long AP duration (Lammel et al., 2008). However, more recent data have shown that not all DA neurons have Ih and that also GABA and glutamatergic neurons sometime possess the HCN channels. Classically, GABA neurons are characterized by a high firing frequency and short AP duration (Chieng et al., 2011). This partially holds true also in VTA, but subsets of GABA neurons do not share those electrophysiological properties (Chieng et al., 2011; Margolis et al., 2012). Finally, glutamatergic neurons are the most recently described in this area, but have not been extensively studied partly due to their small percentage. However, they have been reported to have a fast spontaneous firing rate ex vivo and a small or no Ih (Hnasko et al., 2012). Only few studies have focused on the co-releasing populations, given that targeting those neurons requires a more complex genetic approach including the crossing of Cre and Flp reporter lines. Recently, the generation of a VGluT2 Cre/VGat Flp mouse line allowed the intersectional study of GABA only, glutamate only, and GABA-glutamate co-releasing neurons (Miranda-Barrientos et al., 2021). The authors identified 4 clusters of neurons and showed that it was not possible to predict their nature purely based on the recorded electrophysiological properties. However, they showed that most of the glutamate only and GABA-glutamate co-releasing neurons were characterized by a high input resistance, indicating the need for stronger excitatory drive to fire action potentials. Overall, the VTA presents a complex and heterogeneous population of neurons hard to unequivocally classify using only one of the current available techniques. However, given that protein expression and, therefore, electrophysiological properties are influenced not only by the cell intrinsic properties but also by the surrounding network activity, it is relevant to further investigate the input and output relationship of the different VTA cell types.

1.3.5 Input/output connectivity

Three streams of dopaminergic neurons arise from the ventral midbrain: the nigrostriatal, the mesolimbic, and the mesocortical pathways. The first originating from SN to dorsal striatum, the others originating in the VTA and targeting the NAc, amygdala (Amy), and LHb on one side, and the PFC on the other. Despite having two major output targets, VTA neurons are projecting to a wide variety of brain regions including somatosensory, motor, limbic, prefrontal and association cortices; the hippocampal formation and limbic

structures, striatum, and pallidum; hypothalamic nuclei; and some thalamic and brainstem structures; as demonstrated by VTA single-cell axon tracing analysis (Aransay et al., 2015). Moreover, VTA neurons are highly interconnected. First, DA neurons act through volume diffusion via D2 receptors that have been found in both GABA and VGluT2 VTA neurons (Delle Donne et al., 1997; Hnasko et al., 2012). Thus, DA release influences the firing activity of the nearby non-DA neurons. GABAergic neurons form local synapses onto both DA and VGluT2 neurons (Omelchenko and Sesack, 2007; Yu et al., 2019) allowing the interneurons to restrain the neuronal activity of the surrounding cells. Finally, 50% of VTA fibres forming local synaptic contacts are VGluT2^{+} and establish asymmetric synapses into both DA and non-DA neurons (Dobi et al., 2010). Taken together, the VTA presents a highly interconnected network with reciprocal connections between all cell types. However, how this network influences behavior is still under investigation. In particular, electrophysiological and pharmacological studies showed that DA VTA neurons receive excitatory inputs from the PFC (Carr and Sesack, 2000), bed nucleus of the stria terminalis (BNST, (Georges and Aston-Jones, 2001)), LHb (Omelchenko et al., 2009), periaqueductal grey (PAG,(Omelchenko and Sesack, 2010)), raphe nucleus (Qi et al., 2014), pedunculopontine tegmentum (PPT, (Charara et al., 1996)), and laterodorsal tegmentum (LDT, (Omelchenko and Sesack, 2005)) and inhibitory inputs from PAG (Omelchenko and Sesack, 2010), raphe nucleus (Qi et al., 2014), LH (Nieh et al., 2016) and VP (Hjelmstad et al., 2013). GABAergic VTA neurons receive both glutamatergic and GABAergic inputs from PAG (Omelchenko and Sesack, 2010), raphe nucleus (Beier et al., 2015), LH (Nieh et al., 2016) and BNST (Kudo et al., 2012), while they get exclusively glutamatergic inputs from LHb (Omelchenko et al., 2009) and PFC (Carr and Sesack, 2000), and exclusively inhibitory inputs from NAc (Bocklisch et al., 2013). Up to now, only few studies focused on inputs to VGluT2^{+} VTA neurons (VTA_{glu}) (Faget et al., 2016; Beier et al., 2019) and only one could functionally prove that LH glutamatergic neurons target monosynaptically VTA_{glu} neurons (Barbano et al., 2020). Thus, further studies are needed to elucidate which brain regions functionally synapse into the VTA_{glu} population.

1.3.6 Behavioral correlates of VTA activity

DA neurons are mostly studied for their contribution in reward prediction error (RPE), processing of salient information, and motivated behaviors; but the role of GABA and VGluT2 VTA neurons has only recently received attention. Local optogenetic activation of

GABA VTA neurons disrupts reward consumption (van Zessen et al., 2012) and drives conditioned place aversion (Tan et al., 2012), most likely by inhibiting VTA DA neurons activity. For VTA_{glu} neurons the functional scenario is more complex. Their optogenetic activation elicited both positive and negative actions in mice. Indeed, it was shown that these neurons are tuned to both rewarding and aversive stimuli (McGovern et al., 2020) and when optogenetically stimulated can induce both conditioned place preference, appetitive instrumental conditioning, and reinforcement (Wang et al., 2015; Yoo et al., 2016; Zell et al., 2020) as well as avoidance and escaping behavior (Yoo et al., 2016; Barbano et al., 2020). Currently, it is hypothesised that VTA_{glu} neurons form a heterogeneous cluster that may be differentially activated based on the frequency of the optogenetic stimulation (Zell et al., 2020). Furthermore, those neurons can co-release both glutamate and other neurotransmitters. For example, it was demonstrated that VTA_{glu} projections to LHb and VP are eliciting both excitatory and inhibitory post synaptic currents (Yoo et al., 2016), thus proving their ability to both activate or silence their target region. Interestingly, recent anatomical studies using a combination of retrograde tracing and genetic mouse lines showed that DA, GABA and $VGluT2^{+}$ VTA neurons not only project to similar region, but they also receive qualitatively similar, though quantitatively different, inputs (Faget et al., 2016; Beier et al., 2019).

1.3.7 Multiplexing locomotor activity

VTA neurons are known for their multiplexed activity underlying motivated behaviors. This means that different information, like the position of the animal or the reward location, are not computed in different VTA regions or by different neurons, but rather encoded by different firing modes within the same neuronal population. Classical *in vivo* studies showed that VTA DA neurons signal RPE, namely the difference between experienced and expected reward (Schultz, 1997, 2016; Cohen et al., 2012). However, recent studies using GRIN lens and silicon probes during freely moving behavioral tests, showed that VTA neurons do much more than exclusively signalling reward (Engelhard et al., 2019; Kremer et al., 2020). Indeed, VTA neurons' activity was also tuned to the animal's position and kinematics (Engelhard et al., 2019; Kremer et al., 2020), and sent an acceleration-dependent output to the dorsal striatum (Howe and Dombeck, 2016). Moreover, these neurons increased their activity when novelty and salient stimuli were detected (Horvitz, 2000; Morrens et al., 2020) and during locomotion in novel environments (Fink and Smith,

1979; Hooks and Kalivas, 1995; Cador et al., 2002). Thus, alongside their role in reward and RPE, VTA neurons are responsible for a wider variety of behaviors, most of which include a locomotor response. Indeed, early studies searching for locomotor regions in the cat and rat brains have identified movement initiation upon VTA stimulation. Electrical stimulation of VTA in awake cats elicited locomotion (Parker and Sinnamon, 1983) and its lesion impairs the locomotor effect induced by the medial forebrain bundle stimulation (Sinnamon et al., 1984). Pharmacological treatments were also effective: picrotoxin (a GABA receptors antagonist) increased locomotion (Mogenson et al., 1980a), while baclofen (a GABA B receptor agonist) reduced it (Olpe et al., 1977). The same occurred with GABA A receptor agonists, as muscimol and 4,5,6,7-tetrahydroisoxazolo[5,4-c]pyridin-3-ol (THIP): both modulated animal's movement. Injections of these substances into the caudal VTA lead to hypermotility, while in more rostral parts caused a reduction in activity (Arnt and Scheel-Krüger, 1979a), reflecting the higher abundance of GABA neurons in the caudal, compared to rostral, VTA (Nair-Roberts et al., 2008). These data point to a role of inhibitory inputs to VTA neurons: when the inhibition was reduced, the locomotor effect arose. Moreover, the neuropeptide neurotensin (Nts) seems to play an important role in the modulation of VTA locomotor effects: injections of Nts in VTA increased both locomotion and rearing (Kalivas et al., 1983). A confined subpopulation of LPO neurons expresses Nts and projects specifically to VTA in rats making them a suitable input candidate to mediate this behavior. However, not many studies have attempted to identify their functional role *in vivo*. Recent studies on LH Nts^+ projections to VTA have shown their role in promoting reward (Kempadoo et al., 2013; Petzold et al., 2023) but interestingly the lesions of both LHA and POA did not reduce the Nts terminals in VTA (Geisler and Zahm, 2006) suggesting the existence of other sources of Nts inputs. Another line of evidence focused on the GABAergic projections to VTA as a possible source of inputs driving locomotion. Activation of all GABA neurons, as well as a subpopulation of GABA neurons co-expressing galanin ($GABA^+/Gal^+$) in the LH promoted operant food-seeking behavior. When optogenetically stimulated they both induced locomotion, but $GABA^+/Gal^-$ neurons mediated compulsive and repetitive movements associated with anxiogenic valence; while $GABA^+/Gal^+$ neurons seem to mediate a more natural behavior with frequent transitions across diverse state with a possible anxiolytic valence (Qualls-Creekmore et al., 2017). The authors reported that LH Gal^+ neurons

stimulation possibly reflected an increase in arousal and exploratory patterns. However, this outcome was not mediated by a direct LH to VTA projection, since only the GABAergic neurons not expressing galanin send direct inputs to VTA and mediate negative valence and anxiogenic effects (Qualls-Creekmore et al., 2017). More recently, an excitatory LH input to VTA was described (Barbano et al., 2020). Interestingly, its activation can also induce locomotion but in the form of escaping behavior and innate defensive responses. Apparently, hypothalamic inputs to VTA could produce locomotor responses, but they seemed to be associated with specific aversive internal states such as anxiety or fear.

1.3.8 VTA and exploration

In the previous chapters, I presented evidence of VTA-related circuits that are involved in locomotion, negative valence, and feeding behaviors. It has been hypothesized (Sinnamon, 1993) that three types of locomotor behaviors exists driven by three different systems: 1) the primary appetitive system that brings an organism in contact with incentive and consummatory stimuli; 2) the primary defensive system, that increases the distance between an organism and threatening or painful stimuli; 3) the exploratory system, that directs the organism's attention to distal stimuli which define the environmental features. It is likely that POA projections to VTA underlie the locomotion mediated by the primary appetitive system, while LH projections are involved in the primary defensive system (Barbano et al., 2020). Given the central position of the VTA in weighting different reward-, valence-, and internally generated stimuli, it is conceivable that a third input to VTA exists and is capable of driving exploratory behaviors. In this scenario, VTA acts as a hub where internal homeostatic and motivational stimuli converge with external environmental cues. Even in Schultz's classical experiment it was shown that VTA DA neurons are no longer active when the environment is static (Mirenowicz and Schultz, 1994). Thus, the VTA circuit is not only well positioned to identify salient stimuli like reward, but can also detect novelty based on environmental information. Indeed, it was shown that the mesoaccumbal-pallidal pathway is mediating novelty-induced motor response in naïve animals, but not in habituated ones (Hooks and Kalivas, 1995). Moreover VTA projections to HPC and cortical circuits contributes to the formation of long-term memories (Lisman and Grace, 2005) and VTA inactivation results in a transient loss of hippocampal theta (Orzeł-Gryglewska et al., 2006). These data highlight the existence of a network that links memory and navigation (via the HPC formation and theta oscillations), with the

investigation of a novel environment (as shown by Hooks and Kalivas), and an adaptive behavioral and motor response (through the mesoaccumbal pathway). For decades, the VTA circuit was believed to be linked solely to the detection and acquisition of reward. However, the recent discovery of VTA_{glu} neurons, the recognized diversity of VTA neuronal population, and the emerging interest in information-seeking behavior, points towards a broader role for the VTA network. In particular, the fact that VTA_{glu} neurons code for both rewarding and aversive stimuli (Root et al., 2018), the importance of both dopaminergic and glutamatergic VTA inputs to NAc in behavioral flexibility (Mingote et al., 2019), and the relationship between this region and the hippocampal formation (McNamara et al., 2014), lays the foundation for further studies investigating the role of VTA in exploratory and information-seeking behavior.

1.4 Central hypothesis

Based on prior experimental evidence reviewed in the introductory paragraphs, it is plausible to hypothesize that both MSDB and VTA play a role in exploratory behavior. Previous work showed convincingly that MSDB neurons were an important generator of theta rhythm in the hippocampal formation (Bland and Bland, 1986; Bland et al., 1999; Pignatelli et al., 2012). Theta oscillations are known to play a crucial role in memory and spatial navigation (Buzsáki, 2002). Moreover, hippocampal theta frequency correlated with the speed of locomotion (Bender et al., 2015) and is modulated by septohippocampal efferents including $VGluT2^{+}$ axons and entorhinal cortical projections conveying external sensory inputs (Buzsáki and Moser, 2013). $MSDB_{glu}$ neuronal activity not only provides speed-correlated inputs to the hippocampal formation, but is also sufficient to control movement onset and speed (Fuhrmann et al., 2015; Justus et al., 2017). This indicates that a downstream pathway must exist that links the septal activation to locomotor activity. Based on anatomical evidence (Meibach and Siegel, 1977), the information from the septal area flows through 3 pathways: from the MSDB to the hippocampus via the dorsal fornix fimbria; from the MSDB to the habenular nuclei through the stria medullaris; and via the medial forebrain bundle running ventral into the thalamic and hypothalamic regions, crossing the midbrain and reaching the brainstem. The medial forebrain bundle appears the most promising pathway that can send the information from the MSDB to the long been known diencephalic and mesencephalic locomotor regions. As discussed earlier, the

glutamatergic efferents of the MSDB have specific locomotor behavioral relevance. While the preoptic and hypothalamic regions appear good output candidates, evidence suggest that they mediate innate responses to metabolic state, rather than driving a more general locomotor response aimed at exploring the environment. Since the locomotor activity elicited by $MSDB_{glu}$ neurons includes rearing and exploratory behavior, it is reasonable to look at the VTA as a possible output region. As I laid out before, VTA has been classically linked to locomotor activation, and recent findings were pointing to a multiplexed role of VTA neurons, not only responding to reward-related information but also to the animal's speed and acceleration (Engelhard et al., 2019; Kremer et al., 2020). It stands to reason that VTA could receive the speed and acceleration dependent information from the $MSDB_{glu}$ neurons. Moreover, VTA is involved in responding to environmental changes. It has been shown that VTA induce locomotor responses in naïve animals similar to the behavior elicited by $MSDB_{glu}$ stimulation (Hooks and Kalivas, 1995).

Taken together, the evidence available does not exclude, but is even consistent with a putative circuit linking MSDB and theta rhythm to VTA and locomotor circuits. My key hypothesis is that the septohippocampal network, that is constantly updated on the position of the animal in the environment, is providing glutamatergic excitation to the VTA. The VTA, for its part, is receiving other inputs from several brain regions that signal the valence of the environmental changes. The combination of self-motion related inputs from the septum together with subcortical motivational- and valence-related inputs to the VTA may drive a motivation for the animal to act, and to produce a locomotor response. Thus, the aim of this PhD project is to identify and experimentally confirm a specific role of the glutamatergic MSDB projections to VTA in driving information-seeking and exploratory behavior.

2. Material and methods

2.1 Animals

All *in vivo* experiments were performed in adult wild type mice (C57BL/6.J, Charles River Laboratories, Sulzfeld, Germany)) and VGluT2-Cre mice (Slc17a6 tm2(cre)Lowl/J, The Jackson Laboratory, Bar Harbor, USA; Stock No. 016963) of both sexes. The animals were bred under specific pathogen-free conditions and housed with a 12 hours day-night inverted cycle at 21 °C. Food and water were provided *ad libitum* if not differently stated in the results section. *In vitro* patch clamp experiments were performed in adult male and female VGluT2-Cre mice (Slc17a6tm2(cre)Lowl/J, The Jackson Laboratory, Bar Harbor, USA; Stock No. 028863). Mice aged between 8 and 24 weeks were used. All mice were group-housed with a 12h day-night light cycle at 21°C, with food and water provided *ad libitum*. All experiments were approved by the local authorities.

2.2 Surgical procedures

Prior to surgeries mice were deeply anesthetized with an intraperitoneal injection of ketamine (0.13 mg/g, Pfizer, Germany) and xylazine (0.01 mg/g, Bayer, Germany). Surgeries started when animals became unresponsive to stimuli as toe pinch. During anesthesia, a heating mat (Fine Science Tools, Heidelberg, Germany) set at 36 °C allowed to maintain the animal body at a physiological temperature. The mice were head-fixed using a head holder (MA-6N, Narishige, Tokyo, Japan) and placed into a motorized stereotactic frame (Luigs-Neumann, Ratingen, Germany). Prior to every surgery, a local anesthetic (Xylocain Pump spray, Astra Zeneca) was applied on the mouse head and the eyes covered with ointment (Bepanthen, Bayer). An incision of around 5 mm was made, the periosteum removed and bregma identified. After surgery buprenorphine (0.05 mg/kg) was administered twice daily for 3 days.

2.2.1 Stereotactic injections

Coordinates for injections of adeno-associated viruses (AAV) were determined in relation to bregma and based on Franklin and Paxinos (Paxinos and Franklin, 2019). After the surgical preparation, a 0.5mm hole was drilled through the skull (Ideal micro drill, World Precision Instruments, Berlin, Germany) and using an UltraMicroPump, 34G cannula and Hamilton syringe (World Precision Instruments, Berlin, Germany) the virus was injected. For electrophysiological slice-based studies, 500 nl of channelrhodopsin virus (AAV2/1 EF1a double floxed ChR2 (H134R) EYFP WPRE hGH) was injected into each of the two loci of the MSDB (anterior-posterior: +1 mm, lateral: -0.7, ventral: -4.6 mm and -4.2 mm, relative to bregma with a 10° angle) at 0.1 µl/min in VGluT2-Cre mice. To target VGluT2 neurons, some of the mice were also injected bilaterally in VTA (anterior-posterior: -3.3 mm, lateral: ±0.4, ventral: -4 mm and -4.5 mm, relative to bregma) with 250 nl per side of a red fluorescent reporter for Cre^{+} neurons (AAV1 CAG Flex tdTomato WPRE bGH, CS1241, Penn Vector Core, Philadelphia, USA) at a speed of 0.1 µl/min. For fiber photometry experiments, 500 nl of a genetically encoded calcium indicator (AAV1 Syn Flex GCaMP6s WPRE SV40) was injected into each of the two loci of the MSDB (anterior-posterior: +1 mm, lateral: -0.7, ventral: -4.6 mm and -4.2 mm, relative to bregma with a 10° angle) at a speed of 0.1 µl/min in VGluT2-Cre mice. For optogenetic experiments targeting the MSDB, a total of 200 nl of channelrhodopsin virus or appropriate control virus (AAV1 or AAV9 EF1a DIO eYFP WPRE; or AAV1-EF1a-DIO-eYFP) was injected into the two loci as previously described.

VIRUSES	**SOURCE**	**IDENTIFIER**
AAV1-Syn-Flex-GCaMP6s	Addgene	100838
AAV1-EF1a-dbf-hChR2-eYFP-WPRE	Addgene	20298
AAV9-EF1a-dbf-hChR2-eYFP-WPRE	Addgene	20298
AAV1-EF1a-DIO-eYFP	Addgene	27056
AAV2.1-Ef1a-dbf-hChR2(H134R)-eYFP-WPRE	Addgene	20940

Table 1 – List of viruses

2.2.2 Chronic surgeries

In addition, to the ketamine/xylazine anesthesia, animals undergoing chronic surgeries were also subcutaneously injected with dexamethasone (0.2 mg/kg), caprofen (5 mg/kg) and buprenorphine (0.05 mg/kg) to prevent pain and inflammation. After removal of the scalp and the periosteum, phosphoric acid (Phosphoric Acid Gel Etchant 37.5 %, Kerr Italia, Italy) allowed to etch the skull and create a more adhesive surface for the next steps. A volatile primer solution (OptiBond FL Prime, Kerr Italia, Italy) followed by an adhesive substance (OptiBond FL Adhesive, Kerr Italia, Italy) covering the exposed skull served as foundation for all implants. For head-fixed experiments, a metal-bar (Luigs-Neumann, Ratingen, Germany) was positioned paramedian on the skull. Dental acrylic (Cyano-Veneer fast; Heinrich Schein Dental Depot, Munich, Germany) served to fix all the implants: fluid cannulas, fiber-optic cannulas, or monopolar field potential electrodes. After surgery, mice were treated with buprenorphine (0.05 mg/kg) for 3 days. For fiberphotometry experiments, a fiber-optic cannula (MFC_400/430-0.37_5mm_SM3(P)_FLT, Doric Lenses, Quebec, Canada) was implanted unilaterally on top of VTA (anterior-posterior: -3.3 mm, lateral: -0.4, ventral: -4 mm, relative to bregma). For optogenetic experiments monopolar tungsten electrodes (W558511, Advent Research Materials, Oxford, England) were positioned in the hippocampus (anterior-posterior: -2 mm, lateral: +2, ventral: -1.6 mm, relative to bregma), and a bilateral fiber-optic cannula (DFC_200/245-0.37_5mm_GS1.0_FLT, Doric Lenses, Quebec, Canada) was implanted on top of VTA (anterior-posterior: -3.2, lateral: ±0.5, ventral: -4 mm, relative to bregma). Some animals were also implanted with an infusion cannula (guide: C315GS-5-SP 388834 26GA 5MM PED, CUT 4 mm, dummy: C315DCS-5-SPC SM .008-.2mm, FIT 4mm C315GS-S W0 PROJ, internal: C315IS-5-SPC 33GA FIT 5mm PED GUIDE, FIT 4mm C315GS-5 W 1mm PROJ, P1 Technologies, Virginia, USA) for drug delivery in the MSDB (anterior-posterior: +1 mm, lateral: -0.7, ventral: -3.5, relative to bregma with a 10° angle).

2.3 *In vivo* recordings

Prior to the *in vivo* experiments, all the animals were habituated to the experimenter, the recording environment and the experimental procedure (e.g. head fixation) for at least one week. The experiments were performed either head fixed or freely moving in almost complete darkness with infrared light illumination unless stated otherwise.

2.3.1 Head-fixed experiments

For head-fixed experiments a 3.6 meters linear treadmill was custom built. The animals were positioned on the belt through the implanted metal bar. An infrared sensor tracked the distance run by the animals, while two infrared cameras monitored their face and body movements. For a subset of experiments, a pump and a mechanical sensor guided via a custom-made Python script were connected to a metal sipper tube and delivered a defined amount of milk-based cream (10% fat) while recording the licking attempts done by the animals over the belt. In reward-based experiments, the belt was divided into 6 different regions defined by different textures. All treadmill data were acquired at 10 kHz through an ITC-18 board (NPI, Germany) operated via Igor Pro software (Wavemetrics, Oregon, USA). Patch cord, LFP wiring, and/or infusion cannula were connected to the animal implants prior to the experiment. All mice learned to run on the belt and showed voluntary running behavior.

2.3.2 Freely moving experiments

For the open field exploration task, a circular arena of 50 cm diameter and 50 cm height made of transparent Plexiglas was used and placed on top of a red Plexiglas table. The animals were recorded with a CMOS camera (Basler acA2040-90umNIR) placed centrally below the arena at around 50 cm distance. Four infrared light sources (LIU780A, Thorlabs) were placed on the 4 corners of the red Plexiglas platform to provide a homogeneous illumination of the recording area. A fiber optic rotary joint placed on top of the arena (FRJ_1x1_FC, Doric Lenses, Quebec, Canada) allowed the patch cord to not intertwine. LFP wires and silicon probe cables were supported by a counterweight to avoid excessive torsions. In a subset of experiments chocolate chips, a conspecific or a plastic object were placed in the center of the arena and number of approaches to the different stimuli were quantified. Further experiments were performed in the same settings (infrared light, red Plexiglas surface and bottom camera recording) in which a cartoon arena of 70 cm

diameter and 50 cm high was used for the open field anxiety test. The floor was covered by cardboard and the animals were tracked via a top camera (Basler acA2040-90umNIR). A lux meter (MS 1300, Voltcraft) was used to measure the light intensity in the middle (200 Lux) and at the walls (5 to 10 Lux) of the arena.

2.3.3 Fiber photometry

For fiber photometry experiments, a fiber-optic cannula (MFC_400/430-0.37_5mm_SM3(P)_FLT, Doric Lenses) was implanted unilaterally on top of VTA (coordinates: -3.3 mm anterior-posterior, -0.4mm lateral, -4 mm ventral, relative to bregma). A fiberoptometer (npi electronics) was used to perform the fiber photometry recordings. The 470 nm diode was collimated into a fiber-optic patch-cord (MFP_400/430/1100_0.37_1m_FC_CM3(P), Doric Lenses). The light intensity at the fiber tip was 0.6 to 1.2 mW. The signal was converted into an analog voltage signal, sampled at 10 kHz using an ITC-18 interface (HEKA Elektronik) and recorded with a custom-written Igor Pro 6.3 software (WaveMetrics).

2.3.4 Optogenetic stimulation

For optogenetic experiments in head-fixed and freely moving conditions, a fiber-optic cannula (DFC_200/245-0.37_5mm_GS1.0_FLT, Doric Lenses, Quebec, Canada) was implanted bilaterally on top of VTA (coordinates: -3.3 mm anterior-posterior, -0.4mm lateral, -4 mm ventral, relative to bregma). Half of the animals used in the freely moving experiments had a unilateral fiber-optic cannula as described for the fiber photometry recordings. The light-stimulation was performed with a fiber-coupled 473 nm diode laser (LuxX 473-80, Omicron-Laserage). The square pulse TTL signal at 3, 6, 9, or 12 Hz was generated via a custom-written Igor Pro 6.3 software (WaveMetrics) to modulate the laser output. The square pulse width was adjusted based on the frequency of the stimulation to guarantee a constant total time of illumination: 50 ms at 3 Hz, 25 ms at 6 Hz, 16 ms at 9 Hz, and 12 ms at 12 Hz. The length of each stimulation epoch is of 20s with 20s pre-stimulation and 20s post-stimulation epochs, unless otherwise specified.

2.3.5 Local field potential recordings

To record hippocampal local field potentials a monopolar tungsten electrode (W558511, Advent Research Materials) was positioned in the hippocampus. The coordinates for the tungsten electrode were: -2 mm anterior-posterior, +2 mm lateral, -1.6 mm ventral relative

to bregma. Reference and ground electrodes were placed on top of the cerebellum. The tungsten electrodes LFP was recorded using an extracellular amplifier (EXT-02F/2, npi electronic), sampled at 25 kHz using an ITC-18 interface (HEKA Elektronik) and recorded with a custom-written Igor Pro software (WaveMetrics).

2.3.6 Pharmacology

In the treadmill experiments the animals had initially received a craniotomy on top of the MSDB (+1 mm anterior-posterior, -0.75 mm lateral relative to bregma) sealed with Kwik-Cast (World Precision Instruments). On the day of the experiment the mice were head fixed on the treadmill, the sealant was removed, and the lidocaine was acutely injected with a 34-gauge cannula and Hamilton syringe (World Precision Instruments) using an UltraMicroPump (-4.3 mm ventral relative to bregma with a 10° angle). The UltraMicroPump connected to a plastic tube to the internal cannula was used for drug injection. All mice were injected with 500 nl of lidocaine (40 mg/ml in cortex buffer, SIGMA, L5647-15G) delivered at 100 nl/min. After the injections, the mice were given 15 minutes to recover and to let the drug diffuse in the brain before starting the recordings. The silencing efficiency was evaluated by comparing hippocampal LFP amplitude before and after the perfusion of the drug.

2.4 Slice preparation and *in vitro* electrophysiology

Four to six weeks after the virus injection, mice were deeply anesthetized and decapitated. The preparation of coronal VTA brain slices was performed with a VT-1200S vibratome (Leica Microsystems, Wetzlar, Germany) with standard solutions as described in Fuhrmann et al., (2015). Current-clamp whole cell recordings were performed at 35 °C ± 1 °C (Heated Perfusion Tube, ALA scientific) using a Dagan BVC-700A amplifier and digitalized at 25 kHz using an ITC-18 interface board (HEKA Elektronik) controlled by IgorPro 6.3 software (WaveMetrics). Recording pipettes were pulled with a horizontal puller (DMZ-Universal Puller) to a resistance of 3-6 MΩ. The recording pipettes were filled with standard intracellular solution ([mM]: 140 K-gluconate, 7 KCl, 5 HEPES-acid, 0.5 MgCl2, 5 phosphocreatine, 0.16 EGTA (pH: 7.3, osmolarity: 289 mOsm)). Biocytin (0.4%) was added freshly before the recording to subsequently localize and reconstruct the patched neurons. Whole-cell current-clamp recordings of VTA neurons were performed

and the resting membrane potential was annotated immediately after the whole-cell formation. The series resistance for the cell recordings was between 13 and 55 MΩ (29.9 ± 9.8 mean series resistance ± s.d.). Neuronal membrane potential was kept between -65 and -60 mV. For the electrophysiological characterization, a series of hyperpolarizing and depolarizing step current injections lasting 500 ms each was performed with the following amplitudes: −200 pA, −100 pA, −50pA, −30 pA, −20 pA, −10 pA, +10 pA, +20 pA, +30 pA, +50 pA, +100 pA, +200 pA, +300 pA, +400 pA and +500 pA. Optogenetic stimulation of $VGluT2^{+}$ ChR^{+} MSDB axons was performed with a light fiber coupled 473 nm diode laser (LuxX 473-80, Omicron-Laserage), placed at around 5 mm distance from the slice, and activated at theta-band frequencies (3, 6, 9 and 12 Hz) for 1 s with 3-ms light pulses. If VTA neurons exhibited PSPs in control conditions with ACSF, the same optogenetic stimulation was performed after bath application of TTX (1μM) and 4-AP (100μM) to confirm the monosynaptic nature of the input, followed by NBQX (10μM) and D-AP5 (50μM) application to confirm its glutamatergic origin. After recording, the slices were kept in 4% PFA overnight and then washed and conserved in PBS**.**

CHEMICALS	**SOURCE**	**IDENTIFIER**
TTX	Tocris	1069
4-AP	Sigma	A78403-25G
NBQX	Tocris	0373
DAP5	Tocris	0106
PFA	Sigma	158127-500G
NaCl	Sigma	S3014-1KG
Sucrose	Sigma	S0389-500G
KCl	Sigma	P9541-500G
NaH2PO4	Sigma	S8282-500G
NaHCO3	Sigma	S5761-500G
CaCl2	Sigma	C5670-100G
MgCl2	Sigma	M2670-500G
Glucose	Sigma	G8270-1KG

K-gluconate	Sigma	G4500-100G
HEPES-acid	Sigma	H3375-250G
phosphocreatine	Sigma	P7936-1G
EGTA	Sigma	E3889-10G
Biocytin	Sigma	B4261-25MG
Aqua-Poly/Mount	Polysciences	18606-20
Normal Donkey Serum (NDS)	Jackson	017-000-121
Triton-X-100	Roth	3051.4

Table 2 – List of chemicals

2.4.1 Antibody staining

The 300 µm slices were fixed in a 4% PFA solution overnight and then washed three times in PBS (0.1M) for 10 minutes each. Non-specific antibody binding was prevented by incubating for 1 hour at room temperature with a PBS-based blocking solution of 10% NDS and 1% Triton-X-100. The primary antibody anti-TH (1:500) was incubated for 16 hours at 4°C in PBS with 1% NDS and 0.5% Triton-X-100. After 4 times 5 minutes washing in PBS, the slices were incubated with the secondary antibody (Alexa Fluor 405) and streptavidin (Alexa Fluor 647) in 0.5% Triton X-100 PBS for 2 hours at room temperature. To remove the unbound secondary antibodies, the slices were washed 6 times for 5 minutes each in PBS. Finally, they were mounted with Aqua-Poly/Mount and images were acquired using a confocal microscope (LSM700, Zeiss, Germany) with a 20x objective (Plan-Apochromat 20x/0.8, Zeiss, Germany). The post-hoc validation of virus injection and implants for the *in vivo* experiments followed a similar procedure except that the slice thickness was 100 µm. In some experiments an additional DAPI staining was performed.

ANTIBODIES	**SOURCE**	**IDENTIFIER**
TH (rabbit α tyrosine-hydroxylase)	Millipore	AB152
Alexa Fluor 405 (donkey α-rabbit)	Abcam	ab175649
Streptavidin Alexa Fluor 647	Life technologies	S21374
DAPI	Sigma	D9564

Table 3 – List of antibodies

2.5 Tracing experiment

The surgical procedure and stereotactic coordinates correspond to the one described in paragraph 2.2. The rabies tracing experiment was performed by Dr. Falko Fuhrmann and the viruses were provided by the laboratory of Dr. Martin K. Schwarz. A 2:1 mix of AAV1/2 EF1a DIO RG-IRES-TVA and AAV1/2 EF1a DIO mCherry was injected into the VTA of VGluT2 Cre mice (titer of the AAVs was ~10^{12}/ml). RABV (titer of ~2.5 x 10^{7}/ml) was mixed in a 1:6 ratio with the AAVs for a final volume of ~1000 nl. The virus mix was injected using a WPI injection pump with a speed of 100 nl/min. In addition, 500 nl of AAV1 CAG Flex TdTomato were injected in the MSDB. Nine days after the injection the animal was sacrificed.

2.6 Data analysis

2.6.1 Detection and analysis of movement

To consider a locomotor epoch valid the mouse had to move at a speed of at least 2 cm/s for 2 seconds with 1 second of immobility before. Movement onset is calculated as the first time the speed overcomes 0.5 cm/s on the treadmill experiments. For freely moving data we used the average x and y position of the pose estimation data to calculate distance, mean speed, and max speed and time spent moving.

2.6.2 Treadmill camera recordings analysis

All analyses were performed by Dr. Oliver Barnstedt using either Python or R. Markerless pose estimation (DeepGraphPose/DeepLabCut (Mathis et al., 2018) was used to detect facial and body movements for both types of video. For this, a deep neural network was trained to automatically discriminate 15 markers for videos of the body (paw, tail and head segments) and 13 markers for videos of the face (6 for pupil, eye, nose, mouth, etc). The network was trained on a large variety of lighting conditions and angles until it reached satisfactory performance. Whiskerpad and nose facial regions of interest were automatically segmented using video-averaged marker points of nose tip, the eye's tear duct and the mouth as stable landmarks. Dense optical flow of face regions was calculated using Python-based OpenCV (v4.2) cuda_FarnebackOpticalFlow function and averaging frame-to-frame optical flow magnitude and angle per facial region. Optical flow magnitude

was then Z-scored by subtracting the mean and dividing by the standard deviation from the entire time series.

2.6.3 Fiber photometry analysis

Fiber photometry data were first downsampled to 1 kHz. A third-degree polynomial function was fitted to the original signal. The resulting polynomial values were then subtracted to the signal along the time axes in order to detrend it (detrended signal = d_signal). The ΔF/F was calculated as d_signal/min(d_signal) and smoothed only for visualization purposes. The Z-score was calculated as (ΔF/F)/standard deviation (ΔF/F) in order to compare the signal between animals.

2.6.4 Analysis of hippocampal local field potentials

First, we removed the 50 Hz noise from the hippocampal local field potentials using a notch filter (scipy.signal.iirnotch). Further, we applied a Hilbert function (scipy.signal.hilbert) to calculate the signal envelope and use it to exclude fast, high frequency artifacts with a custom written despike function. The signal was then processed with a butterworth bandpass filter (2 and 15Hz). To calculate the spectrogram we used the Morlet-Wavelet transform over 9 cycles (elephant.signal_processing.wavelet_transform). Welch's method was used to estimate the power spectral density (elephant.spectral.welch_psd) and calculate the maximum power for each frequency in the theta range.

2.6.5 Pose estimation and behavioral quantification

Mice pose estimation from the 40Hz bottom-up view videos was extracted using DeepLabCut (Mathis et al., 2018). 20 frames per video were manually annotated selecting 6 points of the mouse body (nose, right front paw, left front paw, right hindpaw, left hindpaw, tail base). The network (ResNet-50) was trained up to 106 iterations and DeepLabCut pose tracking results were exported to CSV files. VAME (Luxem et al., 2022), a self-supervised method for behavioral quantification, allowed to identify behavioral motifs starting from the DLC CSV files. After training VAME on the freely moving data, we identified the relevant number of motifs by first segmenting the data into 100 motifs and then considering only the motifs that overcome the 1% usage threshold. This resulted in the identification of 35 distinct behavioral motifs. Afterwards, we determined the communities as groups of highly connected motifs by creating a hierarchical tree

representation of the Markovian time series. After visual inspections of the single motif videos and the hierarchical representation, six communities were identified describing well defined behavioral actions. All behavioral quantification analyses were performed together with Kevin Luxem.

2.6.7 Community glossary

VAME is assigning a motif number to each frame that is further categorized into communities. The community behavioral representation was defined by observing the videos (as the one provided in S2 video) and identifying the most prominent actions performed by the mice referring to mousebehavior.org. Our definitions are described below. Motifs 12, 22, 34 were detected in less than 5% of all the videos analyzed with a motifs usage <0.001 thus were not taken into account.

a_Running: rapid locomotion in the center or around the arena (motifs #0, 2, 27, 29, 32)

b_Rearing: weight on hind legs, raise, forelimbs on the ground (motifs #3, 4, 7, 14, 25, 33)

c_walking: slow locomotion, when approaching the walls or before moving to another behavioral action (motifs #11, 17, 19, 20, 23, 28)

d_sniffing: nose held in the air (motifs #1, 5, 10, 18, 24)

e_grooming: sitting position, combination of lick, groom and scratch (motifs #6, 13, 15, 21)

f_resting: immobile sitting (motifs #8, 9, 16, 26, 30, 31)

2.6.8 Analysis of whole-cell recordings

Subthreshold, action potential and after-hyperpolarization properties of the neurons were quantified as in (Justus et al., 2017). Subthreshold properties were calculated based on the hyperpolarizing and depolarizing current injections that could not elicit action potentials (AP). The resting membrane potential was annotated immediately after the whole cell configuration was established. The input resistance was calculated based on the cell response to currents between -30 and +30 pA in 10 pA steps. The IV curve defined as $\Delta_{\text{membrane potential}}$ ($\Delta_{\text{current input}}$) = IR × $\Delta_{\text{current input}}$ was fitted linearly. The membrane time constant (τ) is defined as the time needed to reach 63% of the plateau response after a certain current injection and was averaged for the cell responses between -30 and +30 pA. The sag index is calculated in the traces where the amplitude of the cell response to

hyperpolarizing currents reaches -50 mV. It is the difference between the maximum response amplitude and the stable response amplitude of the cell to the defined current: sag index= ($\Delta_{\text{max response}} - \Delta_{\text{stable response}}$) / $\Delta_{\text{max response}} \times 100$ (Alonso and Klink, 1993). The rebound index is the maximal membrane potential deflection after stimulus offset and is calculated similarly as the sag index: rebound index = $\Delta_{\text{rebound response}}$) / $\Delta_{\text{max response}} \times 100$. Firing properties and after-hyperpolarization properties were calculated based on the depolarizing current injections able to elicit at least one AP, defined as rheobase. AP threshold was calculated as the membrane potential at which the AP reaches the 10% of the maximum peak. The AP amplitude and half width were measured at rheobase. The latency value describes the duration from current injection onset until the first AP threshold is reached. Firing properties were measured from the current injection giving rise to the maximum number of APs. The firing frequency is defined as the mean frequency of AP spiking after depolarizing currents. The firing amplitude is measured for each AP detected and allows to calculate the amplitude adaption index as $\text{Amplitude}_{\text{last AP}}$ / $\text{Amplitude}_{\text{first AP}} \times 100$.

2.6.9 Cluster analysis

The electrophysiological values of the patched cells were transformed into principal components via principal component analysis (PCA). The cumulative variance was calculated and the number of principal components that explain 80% of the variance for the data were identified. This resulted in 11 components that were afterwards used for clustering. Based on the Elbow method we identified 7 as the number of clusters that can optimally segregate our cells. We run both k-means and agglomerative clustering an found that 5 clusters could better explain our cells' features.

SOFTWARES	**SOURCE**	**IDENTIFIER**
Pylon Viewer	Basler	
Custom written MATLAB code for analysis	MATLAB	SCR_001622
IGOR Pro	WaveMetrics	SCR_000325
Prism	GraphPad	SCR_002798
VAME	VAME	
Custom written Python code for analysis	Python	SCR_008394

OpenCV library	OpenCV	SCR_015526
Elephant library	Elephant	SCR_003833
Scipy library	Scipy	SCR_008058
Scikit-learn library	Scikit-learn	SCR_002577
Fiji	NIH	SCR_002285

Table 4 – List of softwares

2.6.10 Statistical analysis

Statistical analysis was performed using Prism 8. Statistical tests are indicated in the figure legends. To evaluate statistical significance, data from Figures 10F, 12C, 13D, and 14C-D were subjected to Student's t-tests. Data from Figures 11C, 12D-H, 15C, 15F, 16C, 17C-F, 18B-G were subjected to repeated measures (RM) one- or two-way ANOVAs followed by Sidak or Tukey post-hoc analysis. Kruskal-Wallis test was used for nonparametric data from Figure 5C and 7A-C with post-hoc Dunn's multiple comparison test. For all analyses data are presented as mean ± SEM unless noted, and the threshold for significance was at $p < 0.05$.

3. Results

The first goal of this work was to investigate whether $MSDB_{glu}$ axons were directly innervating the VTA neuronal population. Building on previous results from our group showing the presence of $MSDB_{glu}$ axons in VTA via anterograde tracing (Fuhrmann et al., 2015), I used mono trans-synaptic rabies tracing and optogenetic-assisted circuit mapping in brain slices to confirm the monosynaptic and glutamatergic nature of those inputs. These anatomical and electrophysiological data have been the foundation of the following *in vivo* studies.

To test the hypothesis of a locomotor circuit linking MSDB to VTA, I combined optogenetics, pharmacology and electrophysiology in head-fixed awake mice. In this way, I could manipulate the activity of the $MSDB_{glu}$ axons locally in the VTA. The observed behavioral output consisted in an increase in locomotor activity upon activation of the $MSDB_{glu}$-VTA projections. The use of high-resolution cameras to record the animals allowed for an in-depth analysis of their face and body movements.

Finally, freely moving experiments provided additional information regarding the motivation for these animals to move (see(Mocellin and Mikulovic, 2021)). Open field, anxiety test, and novel cues were used to identify the driving force behind the optogenetically elicited locomotor effect. A self-supervised machine learning model developed in our research group (Luxem et al., 2022) helped identify behavioral actions in those datasets with sub-second resolution and supported the non-anxiogenic, exploratory nature of the described behavior.

3.1 $MSDB_{glu}$ axons monosynaptically target a heterogeneous VTA population

3.1.1 Retrograde mono trans-synaptic rabies tracing

Rabies viruses (RABV) have the ability to spread retrogradely across the synaptic cleft. However, intact RABV infects cells in a non-specific way and replicate across multiple synapses. To limit the spreading of the virus to only one synapse, the RABV was genetically engineered by deleting the glycoprotein gene (RABVΔG) necessary for the virus replication. In this way, the RABVΔG can infect the cells, but won't be able to replicate and spread unless the infected neurons already present the missing rabies glycoprotein (RG). To limit the infection only to the desired neuronal population, the virus tropism was altered by pseudotyping it with EnvA (envelope protein of the subgroup A avian sarcoma and leukosis virus), thus creating the RABVΔG (EnvA) (Wickersham et al., 2007). EnvA can direct the infection specifically into cells expressing the cognate TVA viral receptor present in avian, but not mammalian cells. This allows for specific targeting of the post-synaptic neurons achieved by the viral injection of an AAV expressing the RG and TVA constructs. Therefore, this approach combining a first injection of an AAV TVA-RG virus to the desired post-synaptic target area, and a subsequent injection of the RABVΔG (EnvA) within the same region, grants for a region-specific monosynaptic retrograde tracing.

We used this transcomplementation strategy to investigate if $MSDB_{glu}$ neurons form monosynaptic contacts with VTA neurons. A 2:1 mix of AAV1/2 EF1a DIO RG-IRES-TVA and AAV1/2 EF1a DIO mCherry was injected into the VTA of VGluT2 Cre mice. Since this technique does not have any specificity for the pre-synaptic neuron type, we injected the same mice with an AAV1 CAG Flex TdTomato in the MSDB. This Cre dependent red fluorescent protein allowed us to visualize post-hoc the $MSDB_{glu}$ neurons. The RABVΔG (EnvA) EGFP was injected in the same VTA coordinates (Figure 4A). Nine days later the animals were sacrificed. As described, the modified rabies virus can enter only VTA neurons previously transfected and actively expressing the TVA receptor and the rabies glycoprotein. Indeed, confocal imaging showed red (TVA^+ and RG^+), green ($RABV\Delta G^+$) and yellow neurons in the VTA (Figure 4B). The latter are defined as "starter cells", meaning that those are the neurons co-expressing both the RG and the RABVΔG, thus

allowing the pseudotyped rabies virus to replicate and retrogradely cross one synapse. Only cells monosynaptically connected with VTA neurons will then express the rabies virus and the EGFP protein. Looking at the MSDB slices with the red fluorescent protein labelling only VGluT2$^+$ neurons, we found yellow cells (RABVΔG$^+$ and VGluT2$^+$). This anatomical data confirms the existence of a monosynaptic glutamatergic MSDB to VTA network.

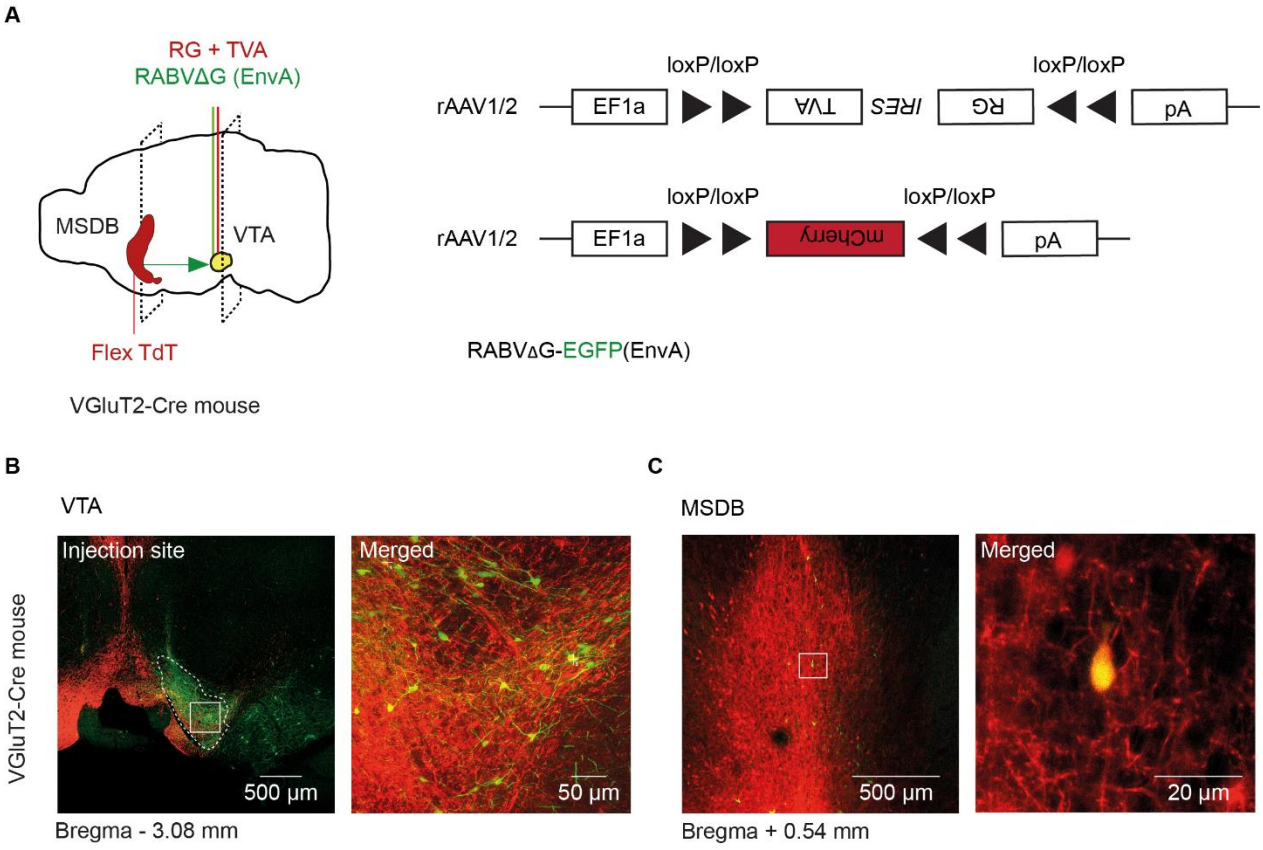

Figure 4 - MSDB neurons send monosynaptic glutamatergic projections to VTA. (A) Scheme of injections sites and viral constructs. (B) Low and high magnification of VTA from a VGluT2 Cre mouse injected with AAV1/2 DIO TVA-RG, AAV1/2 DIO mCherry, and glycoprotein-deleted rabies. Cre$^+$ neurons expressing mCherry in red, Cre$^+$ neurons expressing mCherry, TVA-RG and rabies in yellow, Cre$^+$ neurons expressing TVA-RG and rabies and/or retrogradely labelled neurons in green. (C) Low and high magnification of MSDB from the same VGluT2 Cre mouse injected with AAV1/2 DIO mCherry in MSDB. Cre$^+$ neurons expressing mCherry in red, retrogradely labelled $MSDB_{glu}$ neurons in yellow

3.1.2 Channelrhodopsin assisted circuit mapping

Since my anatomical data did not provide information about the functional relationship between the brain areas, the possibility remained that the synapses detected between neurons were not functional. To rule out this possibility and to further characterize the $MSDB_{glu}$-VTA network, I used patch-clamp recordings to perform channelrhodopsin-guided circuit mapping in VTA slices. VGluT2 Cre mice were injected with AAV2/1 DIO ChR eYFP in MSDB, and VTA neurons were patched in whole-cell configuration (n = 106 patched VTA neurons; Figure 5A). Electrophysiological features of VTA neurons were recorded and photoactivation of $MSDB_{glu}$ fibers in the slice evoked excitatory post-synaptic potentials (EPSPs, 5.520 ± 1.257mV, mean ± s.e.m.) in synaptically connected VTA neurons (n = 16 neurons). To confirm the monosynaptic nature of these projections, tetrodotoxin (TTX, a Na^+ channel blocker) and 4-amynopyridine (4-AP, a K^+ channel blocker) were perfused into the recording chamber. By blocking Na^+ and K^+ channels, only neurons directly innervated by $MSDB_{glu}$ ChR^+ axons can produce an EPSPs, while poly-synaptic connections are silenced. Subsequent application of 2,3-dioxo-6-nitro-7-sulfamoyl-benzo[f]quinoxaline (NBQX, an AMPA receptor antagonist) and D-2-amino-5-phosphonopentanoate (D-AP5, an NMDA receptor antagonist) confirmed the glutamatergic origin of these inputs (Figure 5B). Indeed, EPSPs amplitude was not reduced by TTX and 4-AP application, but was significantly decreased by the presence of glutamate antagonists in the chamber (n = 16 cells, Kruskal-Wallis test, $p<0.0001$; Dunn's multiple comparison test **<0.001, ****<0.0001; Figure 5C). Overall, 15% of the patched neurons received monosynaptic glutamatergic inputs from MSDB (n = 16 connected neurons out of 106 patched cells; Figure 5D), consistent with the small and sparse MSDB projections to the VTA reported in previous studies (Beier et al., 2019; Geisler and Wise, 2008; Geisler et al., 2007). Interestingly, VTA neurons excited by $MSDB_{glu}$ inputs were found throughout the anterior-posterior and medio-lateral axis of the VTA region (Figure 5D).

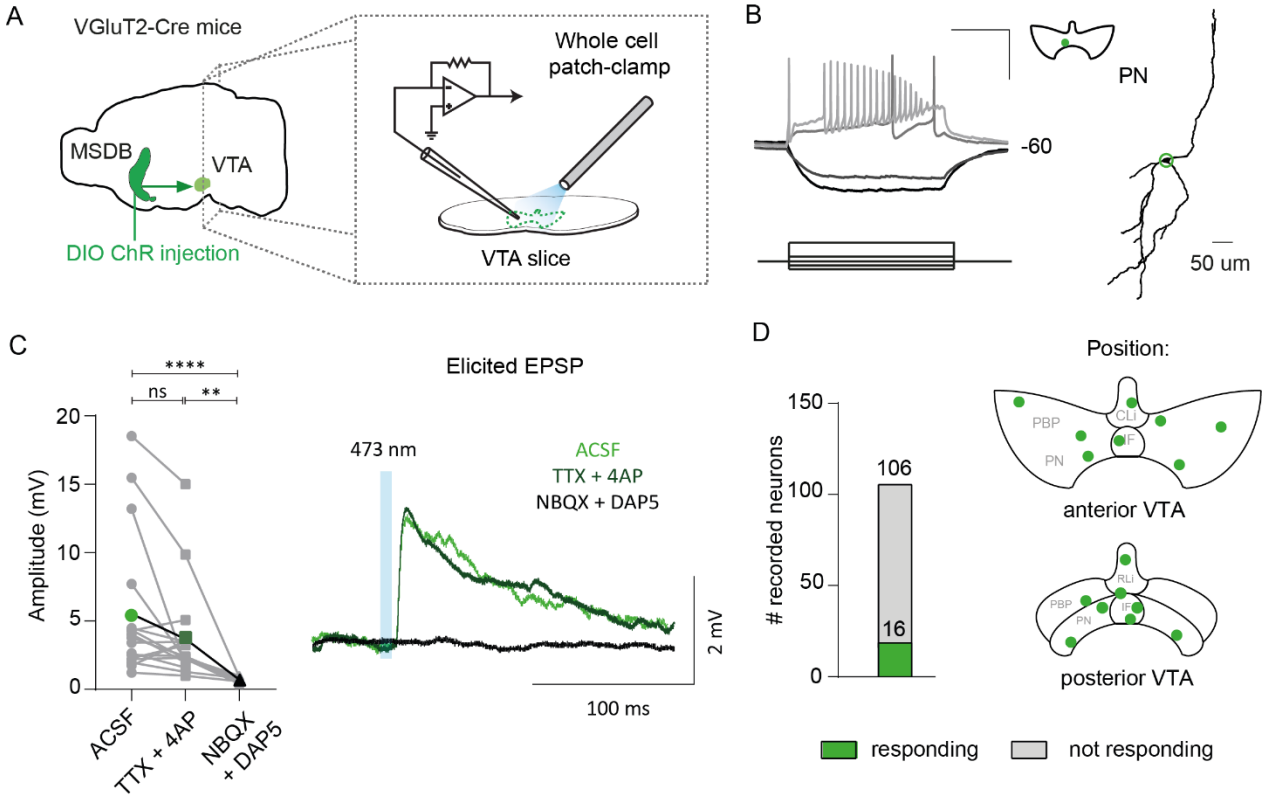

Figure 5 – Optogenetic activation of MSDB$_{glu}$ axons elicits EPSPs in VTA neurons. (A) Scheme of injection site and experimental setup. (B) Representative example of whole-cell recorded VTA neuron. Left: response to 500 ms current injections. Right: cell position in VTA and cell morphology after reconstruction. (C) Left: EPSP amplitude quantification (n=16 cells, in gray single cell values, in bold colors mean values, Kruskal-Wallis test, p<0.0001; Dunn's multiple comparison test **<0.001, ****<0.0001) EPSP in response to light stimulation of ChR$^+$ MSDB$_{glu}$ neurons. Light green: ACSF/control condition. Dark green: bath application of TTX and 4-AP. Black: bath application of NBQX and D-AP5. (D) Percentage and localization of VTA neurons receiving monosynaptic MSDB$_{glu}$ inputs (total number of neurons patched: 106 of which 16 receiving monosynaptic inputs from MSDB$_{glu}$ neurons).

3.1.3 Characterization of VTA patched neurons

I further characterized the diversity of $MSDB_{glu}$ target by electrophysiological properties and neurotransmitter release. Therefore, I performed hierarchical cluster analysis over the electrophysiological features of all the VTA neurons I have recorded (n = 145; Figure 6A). The principal component number was selected as the one explaining 80% of the variance of the data, resulting in the 11 components that we used for the clustering. Five clusters emerged, as confirmed also by the K-Means clustering approach (Figure 6B). When looking at the electrophysiological profiles of exemplary neurons in each cluster, clear differences appeared (Figure 6C).

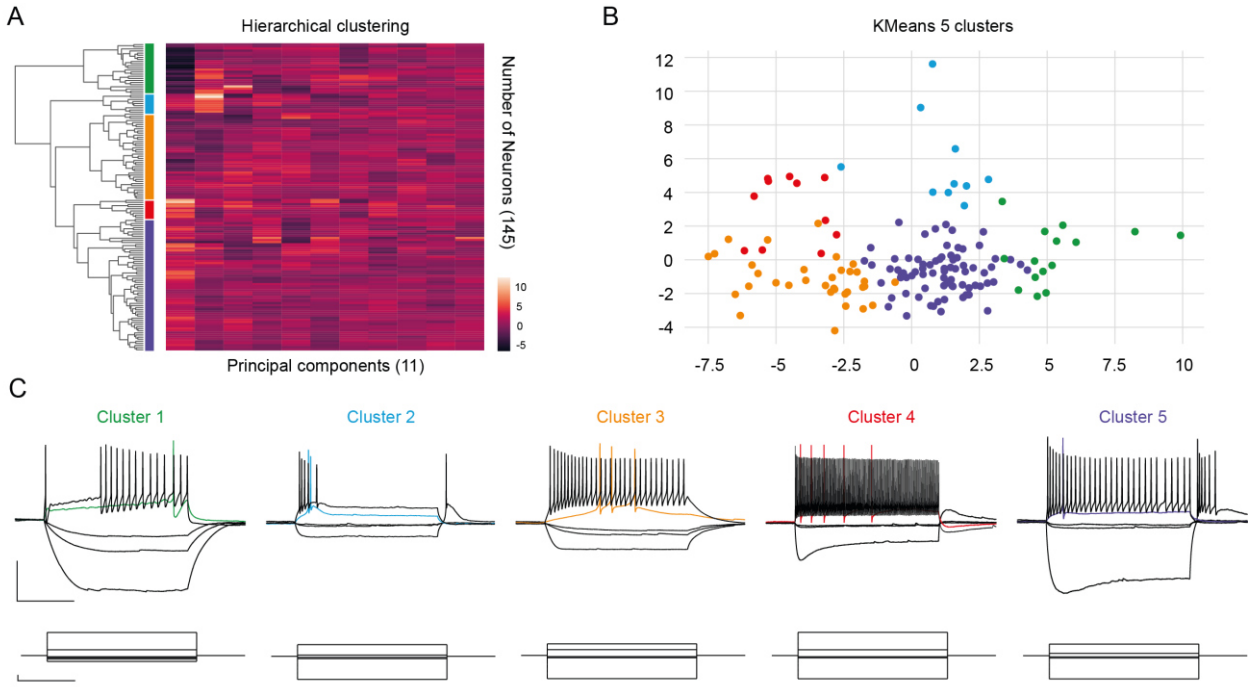

Figure 6 – Patched VTA neurons form 5 clusters based on their electrophysiological properties. (A) Dendrogram and heat map of the hierarchical clustering based on VTA neurons electrophysiological properties (n=145 cells). (B) Kmeans clustering of the same dataset. (C) Responses to hyperpolarizing and depolarizing current injection from representative VTA neurons belonging to each cluster (upper panel) and current injections (lower panel). Scale bar indicates 200 ms and 100 pA.

To inspect the quality of this method, the neurons in the different clusters were compared based on classically used electrophysiological parameters for passive and active properties. In particular, rheobase, input resistance, tau, sag index, rebound index, AP latency, AP threshold, AP half width, firing duration and mean firing frequency were taken into consideration (Figure 7).

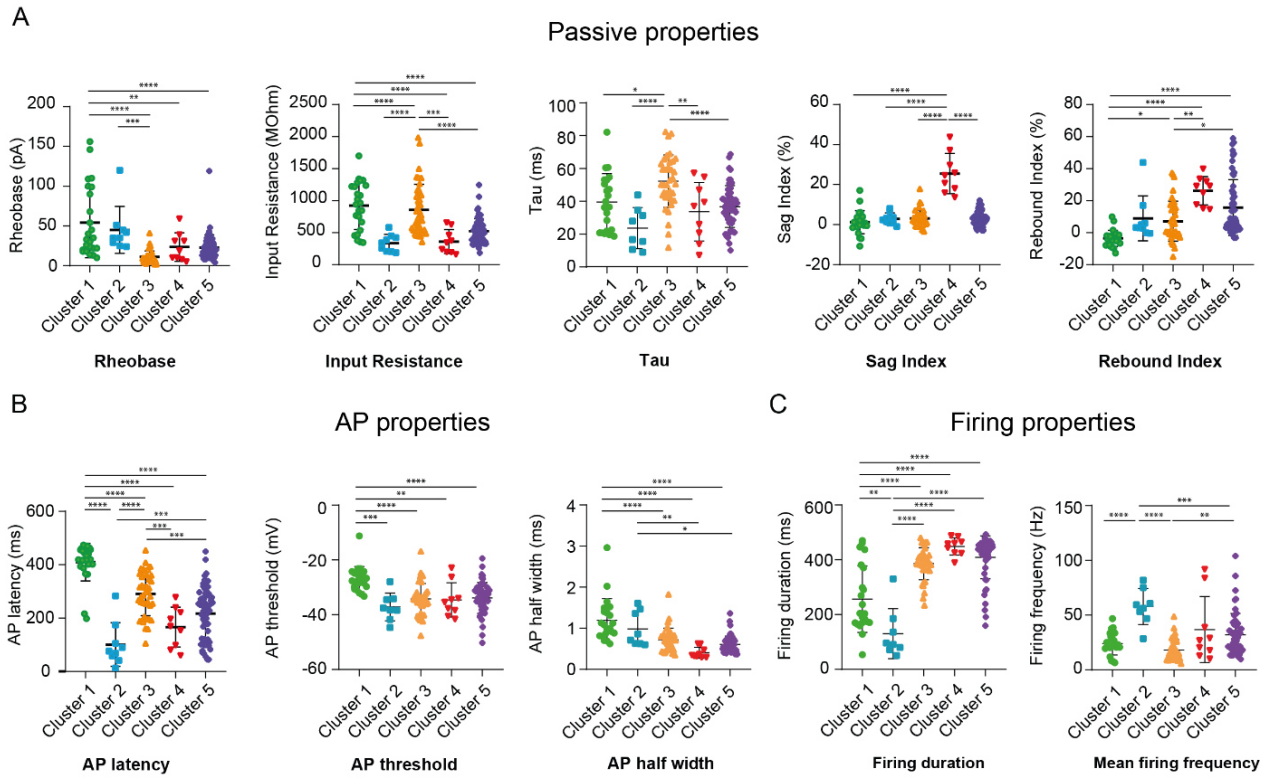

Figure 7 – Distinct electrophysiological features of the 5 VTA clusters. (A) Passive properties of neurons in different clusters (n = 146 neurons in 5 clusters): rheobase ($p<0.0001$), input resistance ($p<0.0001$), tau ($p<0.0001$), sag index ($p<0.0001$), rebound index ($p<0.0001$). (B) Action potential properties of neurons in different clusters (n = 146 neurons in 5 clusters): AP latency ($p<0.0001$), AP threshold ($p<0.0001$), and AP half width ($p<0.0001$). (C) Firing properties of neurons in different clusters (n = 146 neurons in 5 clusters): firing duration ($p<0.0001$), and firing frequency ($p<0.0001$). All n = 146 neurons in 5 clusters; Kruskal-Wallis non parametric test with Dunn's multiple comparison test. All data are presented as mean ± SEM. *$p<0.05$, **$p<0.01$, ***$p<0.001$, ****$p<0.0001$.

The five identified clusters showed significant differences in the compared properties. For example, cluster one cells are characterized by a high rheobase, a high input resistance, and a very high AP latency. While cluster four neurons present a high sag index, small AP half-width, and high firing duration. These results are in agreement with other studies reporting similar electrophysiological properties in VTA neurons (see (Steffensen et al.,

1998; Koyama and Appel, 2006; Zhang et al., 2010; Liu et al., 2014; Tracy et al., 2018); in particular: (Miranda-Barrientos et al., 2021) for cluster one; (Ferris et al., 2014) for cluster two). As discussed in paragraph 1.3, VTA neurons nature cannot be assessed solely based on their electrophysiological properties. Thus, using AAV1 Flox TdTomato injection in the VTA of a sub-set of mice (n = 5 VGluT2 Cre mice) and TH immunostaining, it was possible to determine whether there is a correspondence between the identified clusters and the protein expression for VTA markers labelling putative glutamatergic (VGluT2/TdTomato$^+$) and putative dopaminergic (TH$^+$) cells, respectively. Among the recorded neurons, it was possible to detect TH$^+$ (Figure 8A), VGluT2$^+$ (Figure 8B) and co-labelled neurons positive for both TH and VGluT2 (Figure 8C). When inspecting the clusters, there was no clear differentiation (Figure 8D). TH$^+$ neurons were found in each cluster apart from number four, and VGluT2$^+$ neurons were represented in all clusters. Only co-labelled TH$^+$/VGluT2$^+$ neurons were specific for cluster one that interestingly shares the same electrophysiological features of the VGluT2$^+$/GAD$^+$ VTA cell population (as reported by(Miranda-Barrientos et al., 2021)).

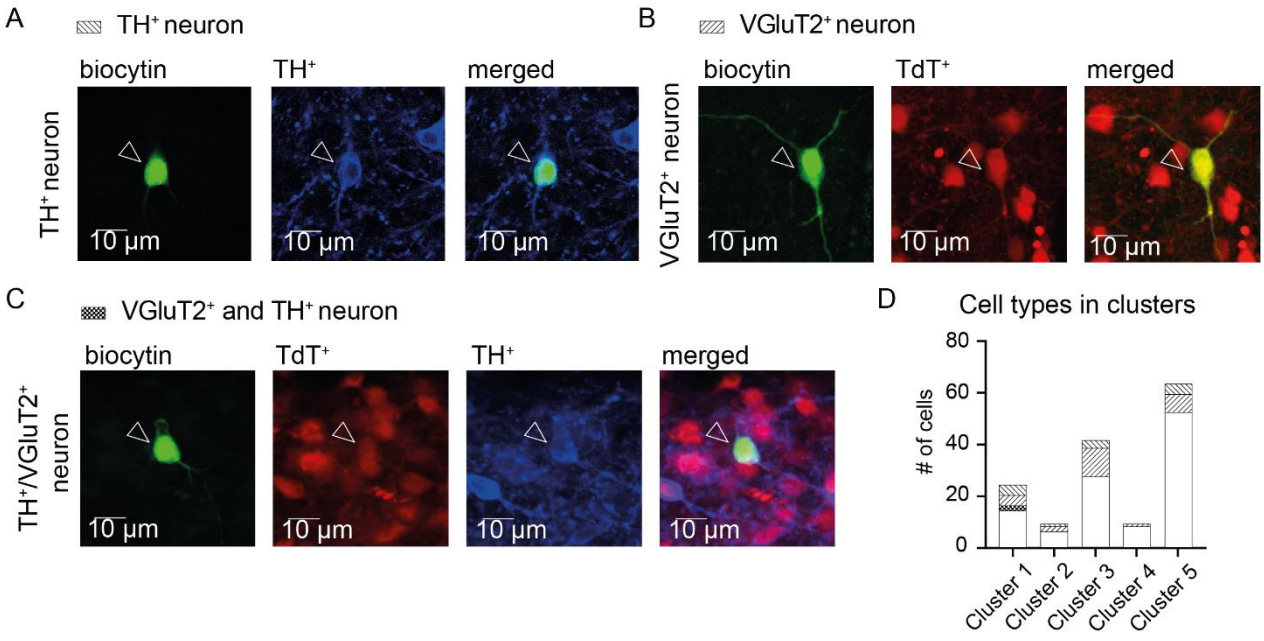

Figure 8 – Immunohistochemical properties of patched VTA neurons. (A) Representative co-localization of biocytin and TH, (B) of biocytin and TdTomato, (C) of biocytin, TdTomato and TH in recorded VTA neurons. (D) Number of neurons belonging to the different clusters and their immunohistochemical features (left striped = TH$^+$, right striped = VGluT2$^+$, chess = VGluT2$^+$ and TH$^+$, white = not identified).

3.4.3 Properties of VTA neurons receiving MSDB$_{glu}$ inputs

Finally, after analysing the electrophysiological profiles of all the recorded cells and recovering the immunohistochemical features for some of them, I could further inspect and analyse the properties of the VTA neurons receiving monosynaptic inputs from the MSDB$_{glu}$ axons. No clear pattern emerged. When calculating the percentage of responding cells over the total number of cells for each cluster, I found that 31.3% are in cluster one, 20% in cluster two, 10.3% in cluster three, 11.1% in cluster four and 12.8% in cluster five. Moreover, cluster one and cluster five present responding neurons that are TH$^+$; cluster one, three, and five have VGluT2$^+$ responding neurons; and cluster one present 6.26% of responding neurons that are co-labelled by both TH and VGluT2 (Figure 9A). Looking at the evoked EPSPs of representative neurons in each cluster, differences in the amplitude and kinetics of the response can be observed (Figure 9B).

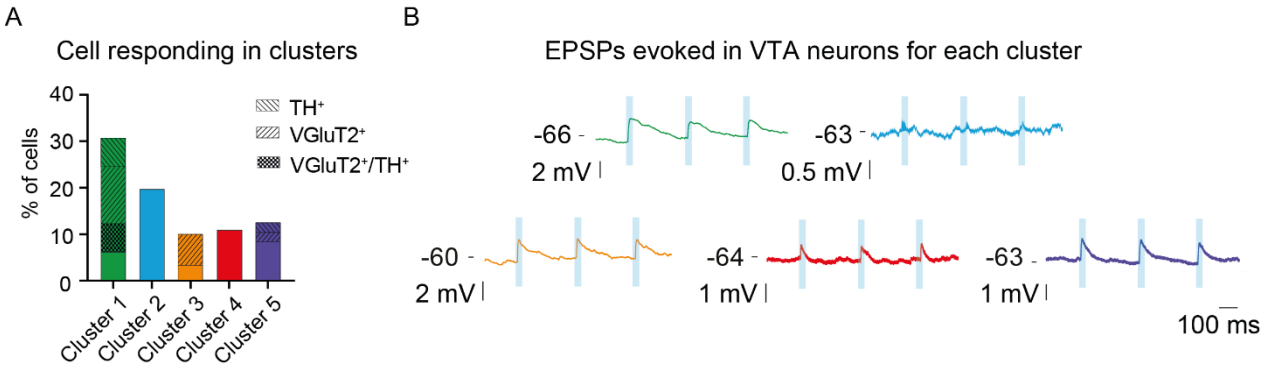

Figure 9 – MSDB$_{glu}$ neurons target a heterogeneous VTA population. (A) Percentage of responding neurons in each cluster and the recovered immunohistochemical features (left striped = TH$^+$, right striped = VGluT2$^+$, chess = VGluT2$^+$ and TH$^+$). (B) EPSPs evoked by 3 Hz optogenetic stimulation after bath application of TTX and 4-AP in representative neurons for each cluster.

Taken together, these data provide anatomical (Figure 4) and functional (Figure 5) evidence for a monosynaptic glutamatergic projection from MSDB to VTA. They also highlight the heterogeneity of VTA neurons regarding both their electrophysiological (Figure 6 and 7) and immunohistochemical (Figure 8) properties. This heterogeneity is also reflected in the VTA neurons receiving MSDB$_{glu}$ inputs that not only are located throughout the medio-lateral and rostro-caudal axis of this brain area (Figure 5D), but also show non-unique electrophysiological and immunohistochemical properties (Figure 9).

3.2 The $MSDB_{glu}$-VTA network mediates locomotion

3.1.1 Fiber photometry recordings

The *in vitro* data confirmed the monosynaptic and glutamatergic nature of the MSDB to VTA projections. Next, I wanted to determine the function of this network *in vivo*. Since it is known that the $MSDB_{glu}$ neuronal population i) is active during locomotor activity (Fuhrmann et al., 2015; Justus et al., 2017) and ii) its optogenetic stimulation reliably initiates locomotion (Fuhrmann et al., 2015; Korvasová et al., 2021), I here tested if the VTA-projecting $MSDB_{glu}$ subpopulation exhibited an increase in its activity upon locomotion when the animal had volitional control over weather rest or run on a treadmill. To do so, I injected AAV1 Syn Flex GCaMP6s into the MSDB of VGluT2 Cre mice and implanted an optic fiber above the VTA region (Figure 10A-C).

Genetically encoded calcium indicators (GECI) are a family of sensors used to detect fluctuations of intracellular calcium activity as a proxy for neuronal activity. In particular, GCaMP sensors consists of a calmodulin (CaM) domain and a green fluorescent protein (GFP) domain. At low Ca^{2+} concentrations the GFP chromophore exists in a protonated state, thus emitting just a minimal fluorescence. Upon Ca^{2+} binding, the CaM domain undergoes conformational changes that prevent water to get in contact with the GFP domain, thus leading to its deprotonation and increase in fluorescence. Since in neurons AP firing induces Ca^{2+} influx, increased GFP fluorescence is classically interpreted as an increase of neuronal activity. To measure the change in fluorescence the ΔF/F is calculated ((F(t)-F0)/F0). I used optic fibers to visualize the changes of GFP fluorescence and measure the bulk activity of the neurons expressing the GCaMP sensor.

Using fiber photometry, I monitored the activity-dependent Ca^{2+} dynamics of the $MSDB_{glu}$ axons in VTA while simultaneously recording the behavior of the mice. The axonal ΔF/F was calculated and its changes were analyzed in combination with the voluntary locomotor activity of the animals on the belt (Figure 10D-E). A consistent increase in $MSDB_{glu}$ axonal fluorescence was detected in VTA every time the animals initiated a locomotor activity

(Figure 10F). Thus, these data show a correlation between locomotion and $MSDB_{glu}$ activity in VTA, supporting a role of the network during movement.

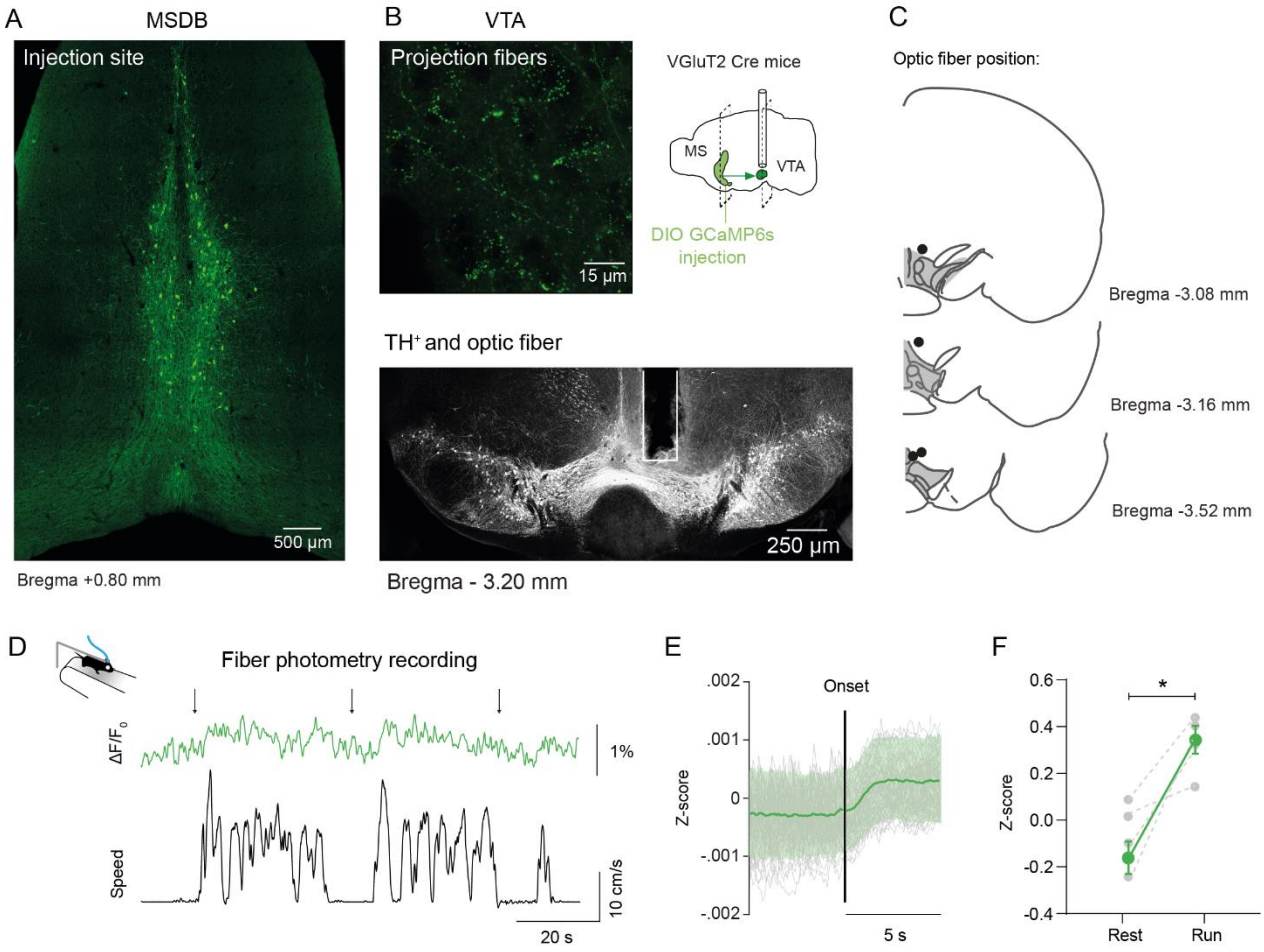

Figure 10 – $MSDB_{glu}$ axons increase activity in VTA during running. (A) Representative example of Flex GCaMP6s expression in the MSDB of a VGluT2 Cre mouse. (B) Upper panel left: MSDB Flex GCaMP6s axons in VTA at higher magnification. Upper panel right: scheme of injection site and implant. Lower panel: example optic fiber placement directly dorsal to VTA (stained with TH in gray), square indicates the magnified upper panel position on the slice. (C) Diagram of coronal VTA sections outlined in gray and placement of the unilateral optic fiber tip (black circles). (D) Representative example of GCaMP6s fluorescence of $MSDB_{glu}$-VTA axons in different locomotion episodes in a head-fixed mouse on a treadmill. Arrows indicate the time of movement onset. Upper trace: ΔF/F signal recorded in $MSDB_{glu}$-VTA axons. Lower trace: corresponding speed trace. (E) Overall Z-score for one mouse over 90 movement onsets. Gray represents single trials, green average across trials. (F) Difference in Z-score between running and resting phases (n = 4 GCaMP6s mice, average across all trials; paired t-test).

3.1.2 Head-fixed optogenetic activation

To confirm the causal role of this circuit during locomotion and to investigate if the locomotor effect described after $MSDB_{glu}$ stimulation (Fuhrmann et al., 2015) was mediated by its VTA inputs, I specifically activated these projections using an excitatory opsin.

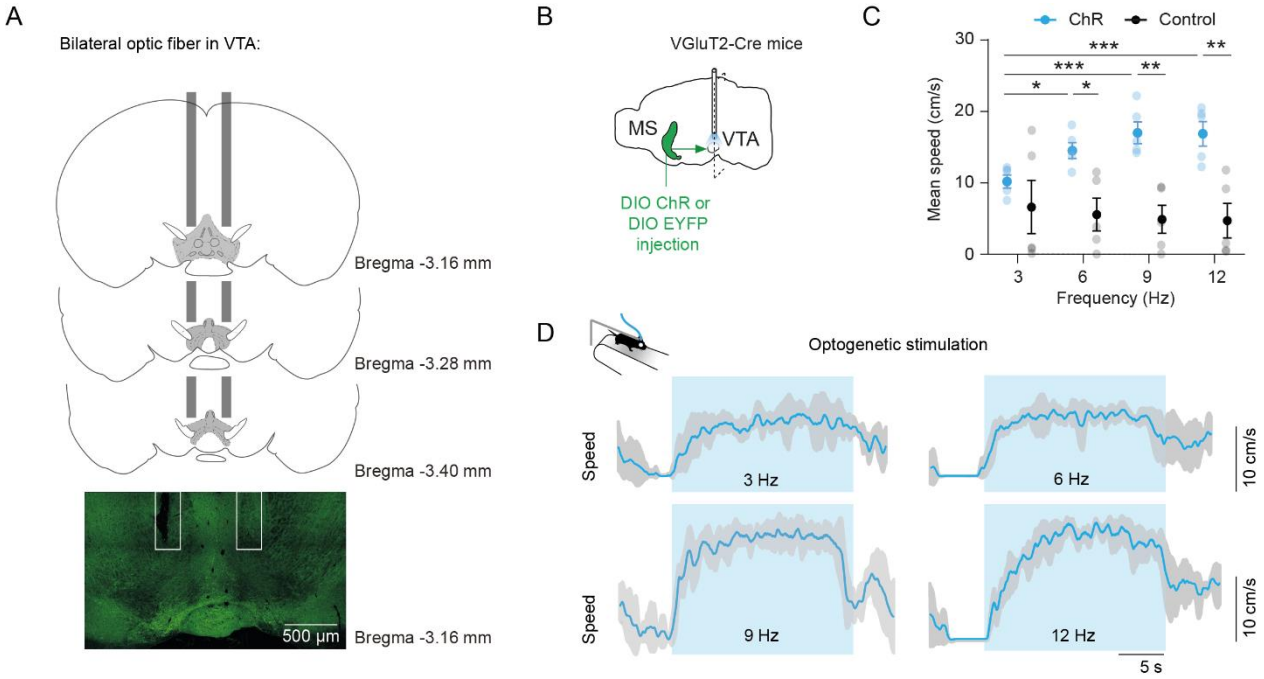

Figure 11 – Optogenetic stimulation of $MSDB_{glu}$-VTA axons elicits locomotion. (A) Upper panel: diagram of coronal VTA sections outlined in gray and placement of the bilateral optic fibers in dark gray. Bottom panel: histology with fiber position. (B) Scheme of injection site and implant. (C) Mean locomotor speed at different stimulation frequencies (n = 5 ChR mice, n = 5 Ctrl mice; RM two-way ANOVA: group x frequency interaction, frequency (3,24) = 3.13, p = 0.0445; Sidak's multiple comparison test. Data shown as mean ± SEM. n.s. = non-significant, *p < 0.05, **p < 0.01.). (D) Representative example of 20s optogenetic stimulation at different frequencies in the same animal. 5 repetitions, mean and s.d. displayed.

Mice were injected with either channelrhodopsin (AAV1 EF1a DIO ChR eYFP) or a control construct (AAV1 EF1a DIO eYFP) in the MSDB and bilaterally optic fibers were implanted in the VTA to deliver 473 nm laser light (Figure 11A-B). As for the fiber photometry experiment, the animals were tested head-fixed on a linear treadmill to reduce the variability of the observed behavior to the locomotor effect. Four different stimulation frequencies in the theta frequency range were applied (3, 6, 9 and 12 Hz) based on previous literature showing the most reliable effect on $MSDB_{glu}$ neurons activation using

stimulation protocols in the theta frequency range (Fuhrmann et al., 2015; Robinson et al., 2016). Optogenetic stimulation in VTA reliably initiated locomotion in all channelrhodopsin (ChR^+) injected animals while it did not have an effect in the control mice (Ctrl) (n = 5 ChR mice, n = 5 Ctrl mice; RM two-way ANOVA: group x frequency interaction, F(3,24) = 9.363, p = 0.0003; Sidak's multiple comparison test; Figure 11 C-D). Moreover, in ChR^+ mice the speed of locomotion was significantly modulated by the frequency of the optogenetic activation (RM two-way ANOVA: frequency (3,24) = 3.13, p = 0.0445; Sidak's multiple comparison test; Figure 11C).

Given these results, I concluded that the optogenetic activation of the $MSDB_{glu}$-VTA axons is sufficient to induce and maintain locomotor activity in mice in a frequency-modulated manner.

3.1.3 Pharmacological silencing of $MSDB_{glu}$ neurons

The optogenetic stimulation of axons, and the subsequent depolarization and calcium influx in the terminals, could lead to the initiation of backpropagating action potentials (bAPs) (Sheffield et al., 2013). To make sure that the stimulation paradigm and the observed behavior was not dependent on bAPs, I prevented AP generation in the MSDB region with the sodium channel blocker lidocaine while optogenetically driving the activation of the $MSDB_{glu}$ axons in VTA. I selected lidocaine because it allows a faster recovery of the network (30 minutes to one hour) compared to muscimol (Martin and Ghez, 1999; Gallo, n.d.). As previously reported (Koenig et al., 2011) lidocaine in MSDB significantly reduced hippocampal theta amplitude and frequency. Thus, I also performed HPC local field potential (LFP) recordings in the tested animals that served as a readout for effective silencing of the septal neurons (Figure 12A). Indeed, lidocaine injection in the MSDB significantly reduced hippocampal theta amplitude (Figure 12B-C, n = 4, 2 ChR mice and 2 Ctrl; paired t-test). However, as expected upon silencing of the MSDB, optogenetic stimulation of $MSDB_{glu}$ axons in VTA was still sufficient to induce locomotion and did not display statistically significant differences in the mean and maximal speed, in the latency to locomotion onset, and in the reliability of locomotion initiation (Figure 12D-G; n = 5 ChR mice mice before and after lidocaine injection; RM two-way ANOVA: group x frequency interaction (D) F(3,24) = 0.3060, p = 0.8208; (E) F(3,24) = 0.7076, p = 0.5569; (F) F(3,24) = 0.08191, p = 0.9692; (G) F(3,24) = 0.5165, p = 0.6749. All post-hoc analysis done via Sidak's multiple comparison test). Taken together, the pharmacological silencing

of the MSDB shows that VTA is a direct downstream target for the locomotor-initiated activity of the $MSDB_{glu}$ neurons, as its optogenetic activation is sufficient to induce movement despite the MSDB soma inactivation.

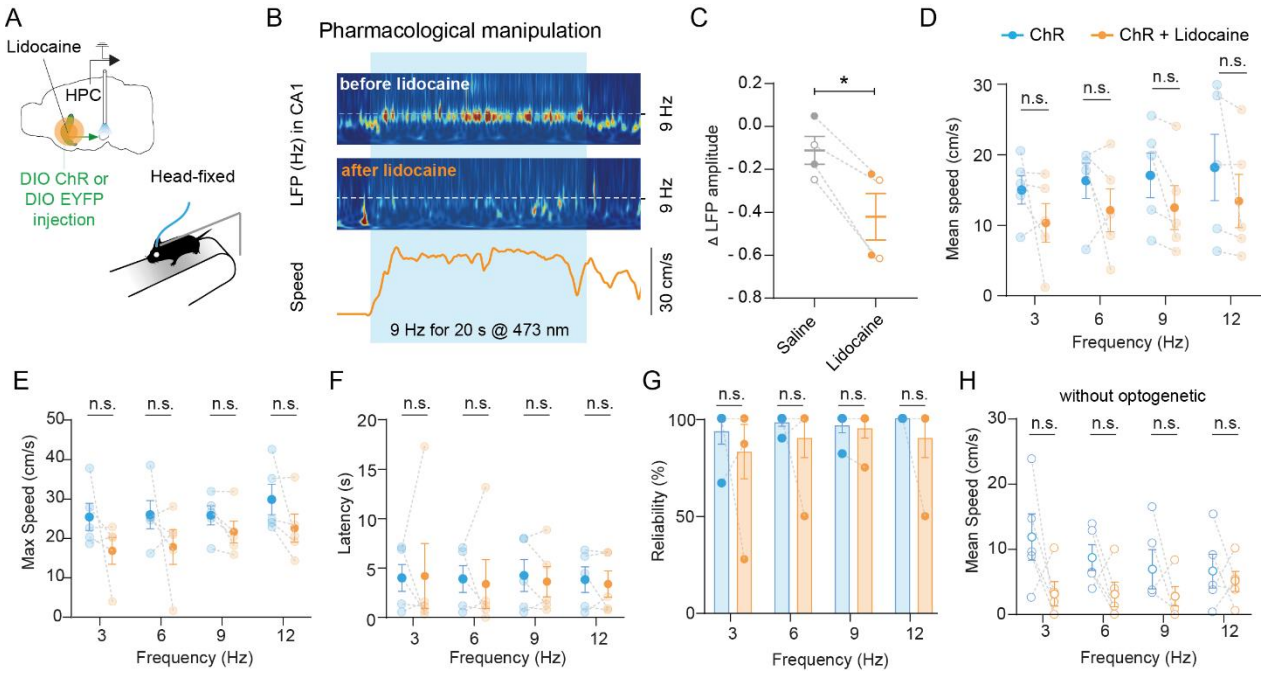

Figure 12 – Optogenetically evoked locomotion in VTA persists despite MSDB silencing. (A) Scheme of injection site and experimental setup. (B) Representative spectrogram of CA1 LFP. Upper panel: spectrogram before lidocaine injection. Middle panel: spectrogram after lidocaine injection. Lower panel: corresponding speed trace after lidocaine injection. (C) LFP amplitude difference before and after saline or lidocaine injection. (n = 4, 2 ChR mice (filled circles) and 2 Ctrl (open circles); paired t-test). (D) Mean locomotor speed (n = 5 ChR mice before and after lidocaine injection; RM two-way ANOVA: group x frequency interaction, $F(3,24) = 0.3060$, $p = 0.8208$; Sidak's multiple comparison test). (E) Maximum locomotor speed (n = 5 ChR mice before and after lidocaine injection; RM two-way ANOVA: group x frequency interaction, $F(3,24) = 0.7076$, $p = 0.5569$; Sidak's multiple comparison test). (F) Latency before movement onset (n = 5 ChR mice before and after lidocaine injection; RM two-way ANOVA: group x frequency interaction, $F(3,24) = 0.08191$, $p = 0.9692$; Sidak's multiple comparison test). (G) Locomotion reliability (n = 5 ChR mice before and after lidocaine injection; RM two-way ANOVA: group x frequency interaction, $F(3,24) = 0.5165$, $p = 0.6749$; Sidak's multiple comparison test). (H) Mean locomotor speed without optogenetics (n = 5 ChR mice before and after lidocaine injection; RM two-way ANOVA: group x frequency interaction, $F(3,24) = 0.3060$, $p = 0.820$; Tukey's multiple comparison test). All data are presented as mean ± SEM. n.s. = non-significant, *$p < 0.05$, **$p < 0.01$.

3.1.4 Optical Flow detection of facial dynamics

When mice are running on a treadmill, it is possible to reduce their behavior to a locomotion/no locomotion dichotomy.

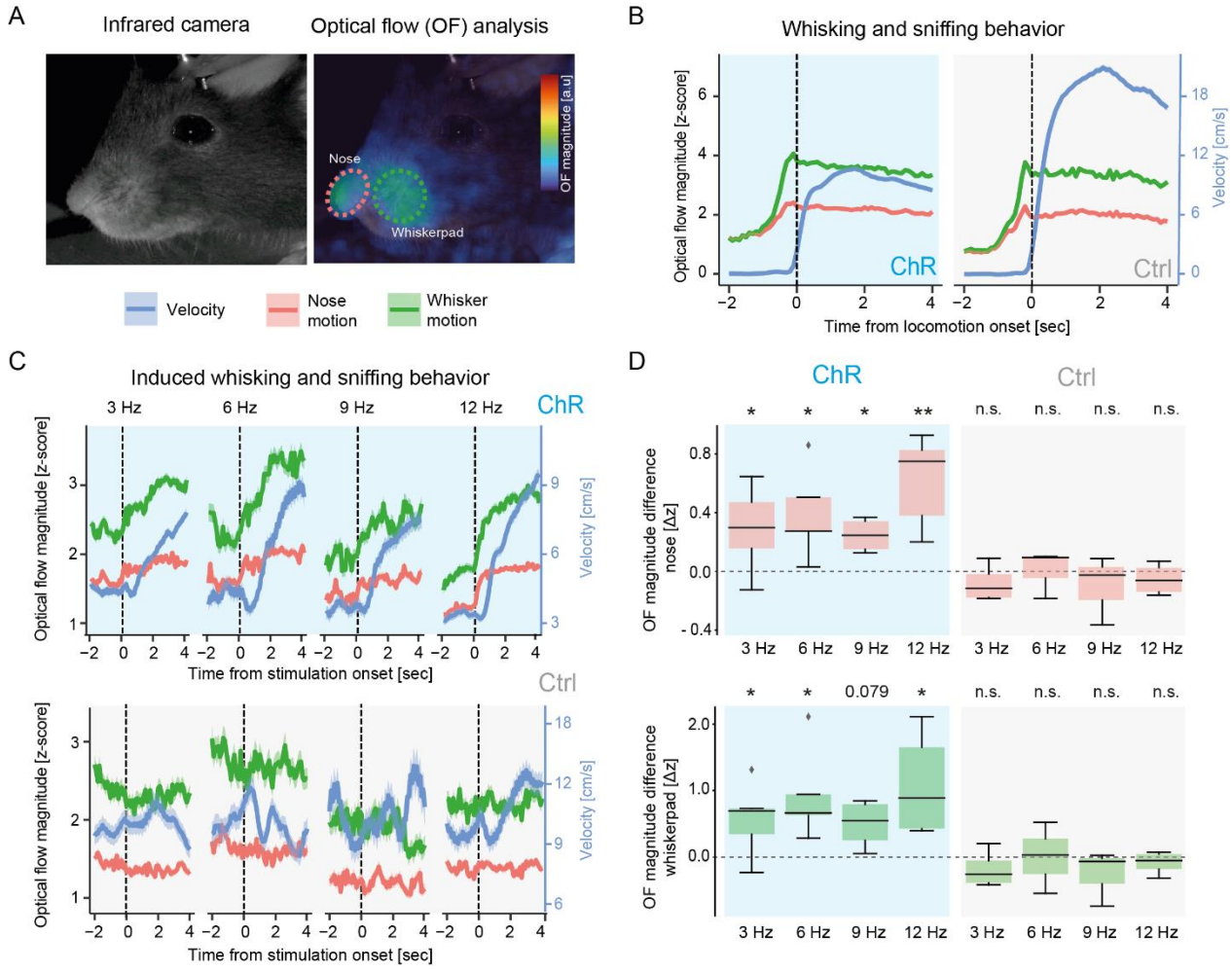

Figure 13 – Increase of whisking and sniffing behavior prior to evoked locomotion. (A) Representative frame from infrared camera recording (left) and superimposed optical flow analysis (right). Dotted lines represent automatically detected nose (red) and whisker pad (green) areas. (B) Representative trace showing sniffing (red) and whisking (green) behavior elicited by optogenetic stimulation (bright blue dashed line) preceding locomotion (blue). (C) Average velocity (blue), sniffing (red) and whisking (green) z-score magnitude in relation to different optogenetic stimulation frequencies (n = 5 ChR mice, n = 5 Ctrl mice). (D) Optical flow magnitude difference (post-pre stimulation) between optogenetically induced sniffing (upper panel) and whisking (lower panel) in ChR (left) and Ctrl (right) mice at different stimulation frequencies (n = 3-6 mice, average across all trials; one-sample t-test against a difference of 0). The data presented in this figure were analyzed by Dr. Oliver Barnstedt.

While this makes the quantification of the time spent running and resting easier, it also limits the repertoire of actions the mouse can perform. With the emergence of high-speed cameras to track animal behavior, and machine learning approaches to analyse those recordings, the neuroscientific community gained new insights into animals' state based solely on their facial expression (Dolensek et al., 2020). Taking advantage of this, we monitored the animal face throughout the head-fixed experiments and used a combination of DeepLabCut (DLC,(Mathis et al., 2018)) and Optical Flow (OF) to gain additional behavioral information. DLC is a method for markerless pose estimation based on machine learning. This deep neural network was pretrained on ImageNet, an open database containing millions of images, and then the architecture was optimized for the estimation of human and animals poses. In order to use it, the experimenter must label a small number of frames to mark the body parts of interest. Based on that, the deep learning algorithm will identify the same points in all the video frames using not only the trained dataset but also mechanical constraints relatively to the distance and spatial location of the body parts. The result is a time series containing the (x,y) position of each marked body part over time. In our dataset, we marked the nose and whisker pad regions of the mouse face. Once these two regions were defined for all the frames, we quantified the average movement magnitude using OF. OF is defined as the motion of objects between the consecutive frames of the sequence, caused by the relative motion between the camera and the object of interest (docs.opencv.org). For our analysis, OF quantification of the nose and whisker pad region were used as proxies for the animal sniffing and whisking activity (Figure 13A).

We found that both ChR and Ctrl mice were increasing sniffing and whisking behavior prior to spontaneous locomotion onsets (Figure 13B). This behavior is classically associated to sensory exploration of the environment as it allows the animal to collect sensory cues like odours and textures of the surroundings (Deschênes et al., 2012). When aligning the whisking and sniffing activity with the optogenetic stimulation at each given frequency (3, 6, 9, and 12 Hz) we observed an immediate sniffing and whisking behavior in ChR mice preceding locomotion onset by about 0.5 seconds, while no correlation between optogenetic stimulation and facial activity was found in the Ctrl animals (Figure 13C-D). To confirm that this behavior is elicited by the $MSDB_{glu}$-VTA pathway specifically,

and not depend on collateral projections from the MSDB to other brain regions, the same analysis was repeated after lidocaine administration in the MSDB. The animals were recorded 15 minutes after the pharmacological manipulation to ensure a full diffusion of the drug into the brain (Figure 14A). We found that the increase in facial movement upon optogenetic stimulation of the $MSDB_{glu}$ axons in VTA was unaffected by lidocaine injection (Figure 14B) both in terms of sniffing (Figure 14C) and whisking (Figure 14D) activity.

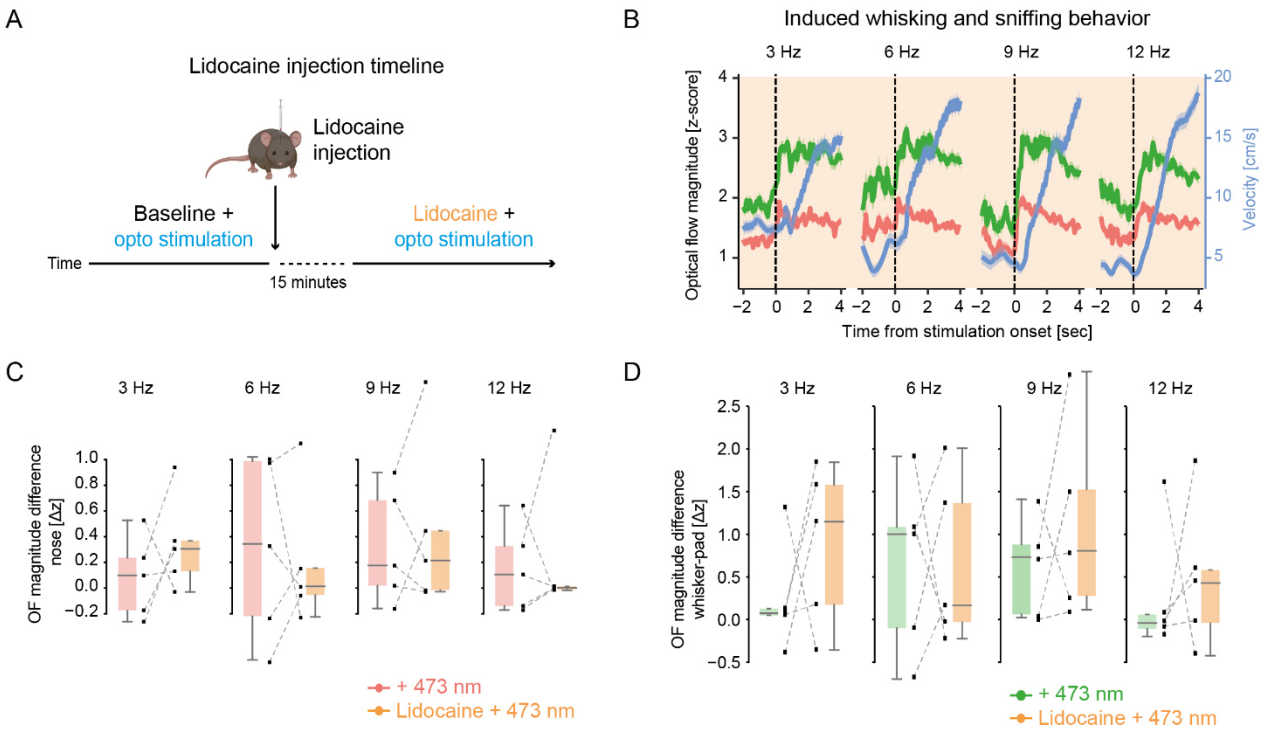

Figure 14 – MSDB silencing do not reduce elicited whisking and sniffing behavior. (A) Scheme of lidocaine injection timeline (B) Average velocity (blue), sniffing (red) and whisking (green) z-score magnitude in relation to different optogenetic stimulation frequencies after lidocaine injection (n = 5 ChR mice). (C-D) Optical flow magnitude difference (post-pre stimulation) between optogenetically induced sniffing (C) and whisking (D) in ChR mice before (blue) and after (orange) lidocaine injection at different stimulation frequencies (n = 5 mice, average across all trials; pairwise t-tests with Bonferroni correction). All data are presented as mean ± SEM. n.s. = non-significant, *p < 0.05, **p < 0.01. The data presented in this figure were analyzed by Dr. Oliver Barnstedt.

Thus, these data support a role for the $MSDB_{glu}$-VTA network during locomotion (Figure 10), showing that its activation is sufficient to initiate and maintain movement (Figure 11) specifically via its VTA projections (Figure 12). It also demonstrates its role in activities related to the exploration of the environment like sniffing and whisking (Figure 13 and 14).

3.3 $MSDB_{glu}$-VTA network increases exploratory actions

3.3.1 Freely moving optogenetic stimulation

To explore the full behavioral repertoire of the ChR injected mice, I decided to test the animals also freely moving in an open field arena (Figure 15A). The stimulation protocol consisted of a 20 second optogenetic activation at 9 Hz and a 20 second epoch before and after the laser stimulation, the entire protocol was repeated 10 times for a total of a 10 minutes recording (Figure 15B). The animals mean speed reliably increased upon activation of the $MSDB_{glu}$-VTA pathway (Figure 15C, n=5 ChR mice, RM one-way ANOVA, pre-, stim and post-optogenetic stimulation epochs, $F(1.014,5.072) = 12.04$, $p=0.0173$; Tukey's multiple comparisons), consistent with the locomotor effect already observed in the head-fixed condition (Figure 11). The local injection of lidocaine into the MSDB resulted in a reduction of the animal activity in the open field as observed by the lower occupancy of the arena. Optogenetic stimulation of the $MSDB_{glu}$ axons in VTA was capable to increase the animal activity and occupancy (Figure 15D). Indeed, the excitation of the pathway was sufficient to reliably increase the speed of locomotion despite septal soma silencing (Figure 15E). When compared to the control condition before lidocaine injection, a statistically significant increase in speed was observed between the stimulated and non-stimulated conditions (Figure 15F, 2 way ANOVA, optogenetic stimulation $F(1,2) = 36.14$, $p=0.0266$; Sidak's multiple comparisons test *<0.05). No difference in mean speed could be detected between the optogenetically induced activity before and after lidocaine, supporting the hypothesis that the locomotor effect is driven locally by the $MSDB_{glu}$ inputs to VTA and not systemically by the MSDB activity per se or by other collaterals. Finally, no significant difference was observed in the non-stimulated condition before and after lidocaine, but a trend towards a reduction of mean speed after lidocaine injection is present. Thus, freely moving optogenetic stimulation of the $MSDB_{glu}$-VTA pathway confirmed its role in driving a locomotor response, increasing the mean speed, and being dependent on the local glutamatergic projections from the MSDB to the VTA.

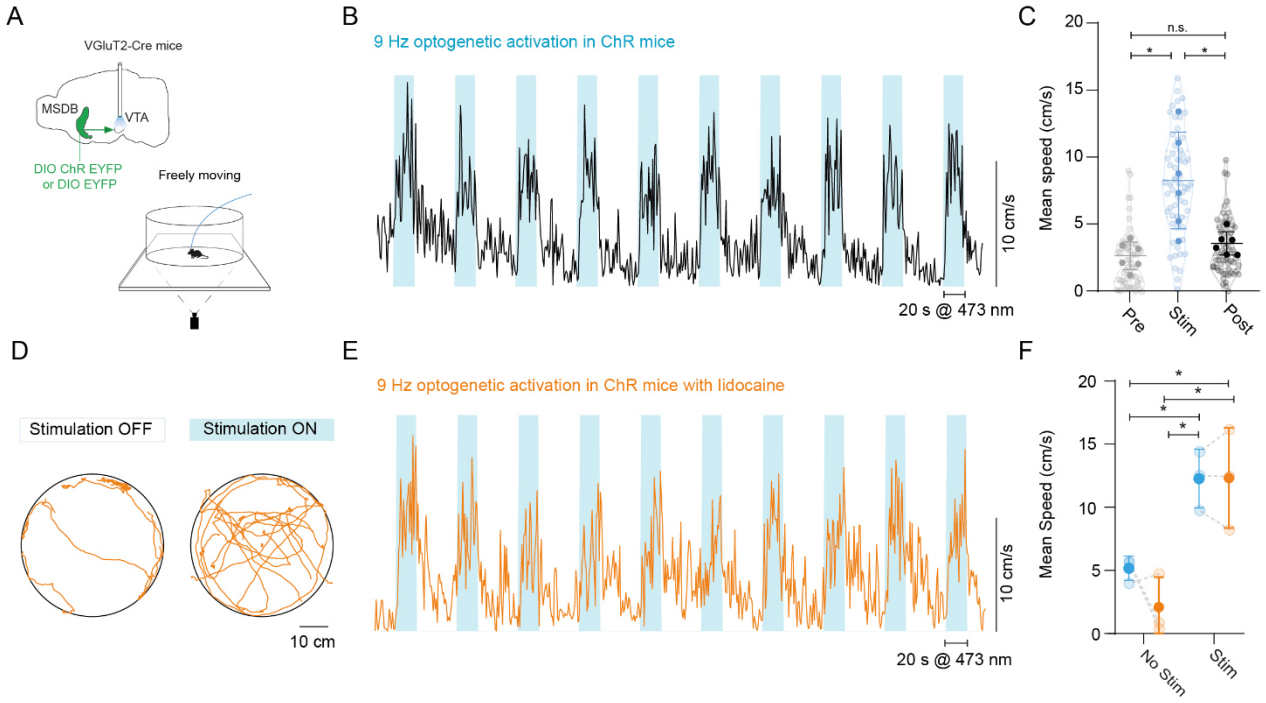

Figure 15 – Locomotion is reliably elicited also in freely moving settings. (A) Scheme of injection site and experimental setup. (B) Representative example of speed modulation upon optogenetic stimulation in an open field arena (20s pre stimulation epoch, 20s stimulation epoch, 20s post stimulation epoch, 10 repetitions, mean ± s.d., 9 Hz optogenetic stimulation). (C) Mean locomotor speed (n = 5 ChR mice, 10 repetitions per mouse; RM one-way ANOVA, pre-, stim and post-optogenetic stimulation epochs, $F(1.014,5.072) = 12.04$, $p=0.0173$; Tukey's multiple comparisons *<0.05). (D) Open field arena occupancy of one exemplary ChR mouse after lidocaine injection without (left panel) and with (right panel) optogenetic stimulation. (E) As in (B) but after lidocaine injection. (F) Mean locomotor speed (n = 3 ChR mice, 2 way ANOVA, optogenetic stimulation $F(1,2) = 36.14$, $p=0.0266$; Sidak's multiple comparisons test *<0.05)

3.3.2 VAME quantification of behavioral motifs

Locomotion and speed are only a fraction of the multifaceted behavior that an animal can express in the open field. However, the quantification of other types of behavioral responses represents a challenge in systems neuroscience, given the wide variety of movements that an animal can perform and the high inter-animal variability. In order to detect animals' actions, several tools have been developed in the past years. Two main classes of tools exist: supervised and unsupervised methods. The first rely on human annotations and classify the animals' actions into user-defined behaviors (like DeepEthogram (Bohnslav et al., 2021)). The latter is based on machine learning models that autonomously discover the animals' actions without any a priori human-based

classification (like Motion Sequencing, B-SOiD, or Motion Mapper (Berman et al., 2014; Wiltschko et al., 2015; Hsu and Yttri, 2021)). In our research group, we developed our own unsupervised machine-learning method to quantify animal behavior (VAME, (Luxem et al., 2022)). VAME input data consist of DLC annotation of the mouse in the open field arena recorded via a bottom camera. Six body parts are labelled: the nose, the four paws, and the tail. Those point are detected for each video frame and egocentrically aligned in order to have the nose and tail position always in the same orientation relative to the Y axis. The (x,y) position of each point during time defines the input time series with which the VAME model, consistent of an encoder, is trained. After training, VAME is capable of inferring which frames are more similar to each other, thus classifying them as part of the same behavioral motif. Finally, using a hidden Markov model (HMM), the probability of each motif to be preceded or followed by another motif is calculated. In this way, similar motifs will be closer to each other in the hierarchical representation of the animal's behavior, and will form a so called "community".

We applied VAME to investigate the behavioral responses elicited by the optogenetic stimulation of the $MSDB_{glu}$-VTA circuit. In the open field arena VAME identified 35 motifs that were hierarchically organized into 3 stationary (sniff, groom, rest) and 3 non-stationary communities (run, walk, rear) (Figure 16A). For each motif, it was possible to inspect the respective video captures and assign the corresponding behavioral action (Figure 16B). Stationary motifs were defined every time the animal was performing a static action without displacement in the environment. Instead, non-stationary motifs reflected a movement of the animals body in space, be it on the x,y axis like walking or running; or in the z axis as in the rearing episodes. As in the kinematic analysis, the increase in locomotion was observed also through the VAME motifs distribution and reflected by an increase in the walking motifs during the stimulation period (motifs number 0, 2, 27,29, 32). Interestingly, also the rearing motifs were more expressed during stimulation (motifs number 33, 7, 3), while sniffing (motifs number 24, 10, 18, 5) and resting motifs (motifs number 16, 30, 31, 9, 8, 26) were almost absent (Figure 16C). Walking and rearing are classical actions associated with exploration. The overall comparable usage of the motifs during stimulation and non-stimulation epochs supports the hypothesis that the elicited behavior belongs to the realm of exploratory actions rather than to stress or fear response (no freezing or jumping behavior was detected during the recorded sessions).

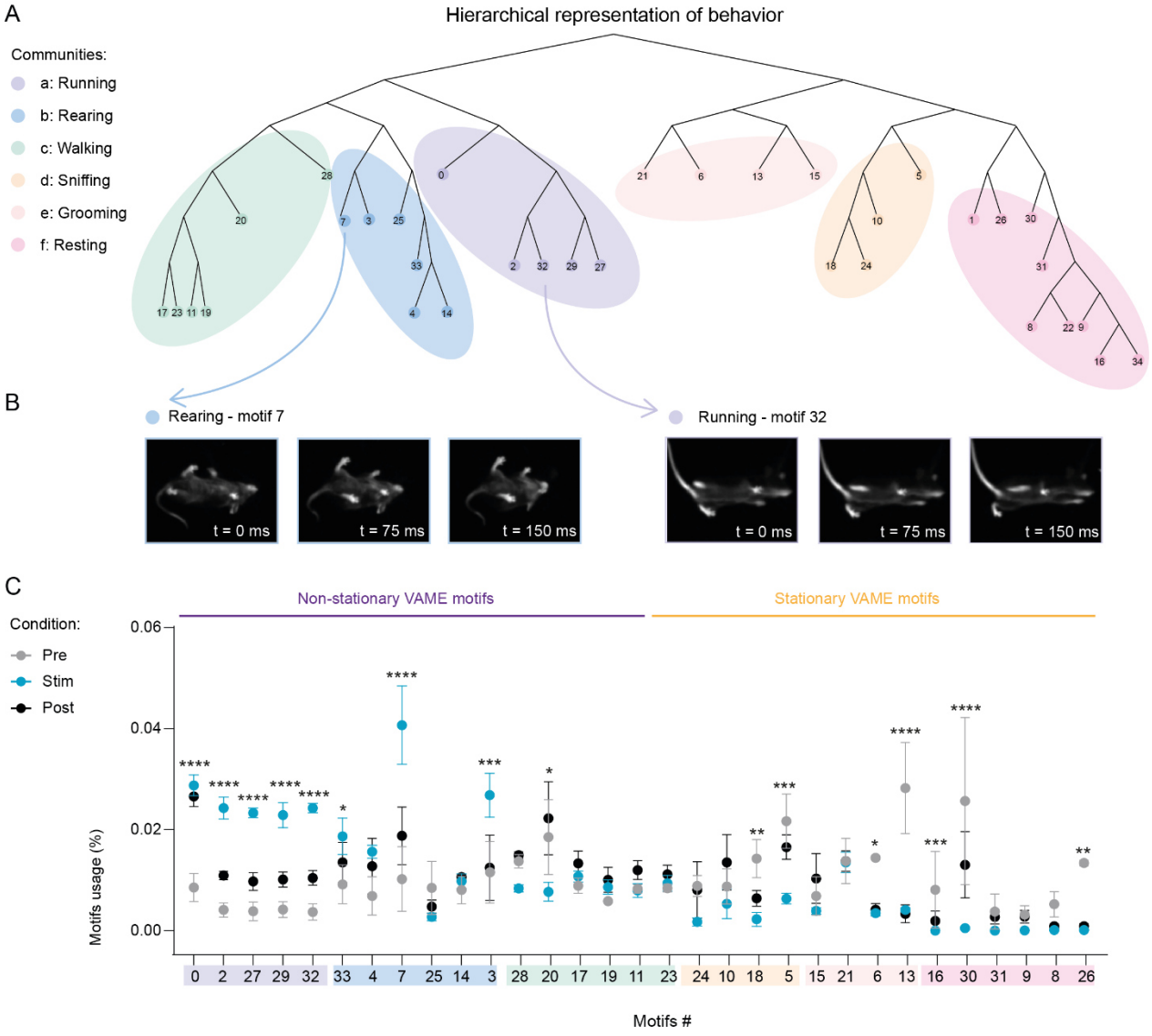

Figure 16 – Optogenetic stimulation increases running and rearing behavioral motifs. (A) Hierarchical representation of the 35 identified behavioral motifs divided into the 6 communities after the HMM classification. (B) Representative examples of video frame segmented by VAME for the motif number 32 and 7. (C) VAME motif usage during pre-, stim, and post-stimulation epochs (n = 3 ChR mice, RM two-way ANOVA: motifs x pre-stim-post interaction, $F(68, 136) = 6.936$, $p < 0.0001$; Sidak's multiple comparison test, mean ± SEM. *p < 0.05, **p < 0.01, ***p<0.001, ****p<0.0001). The data presented in this figure were analyzed by Kevin Luxem.

3.3.3 Open field anxiety test

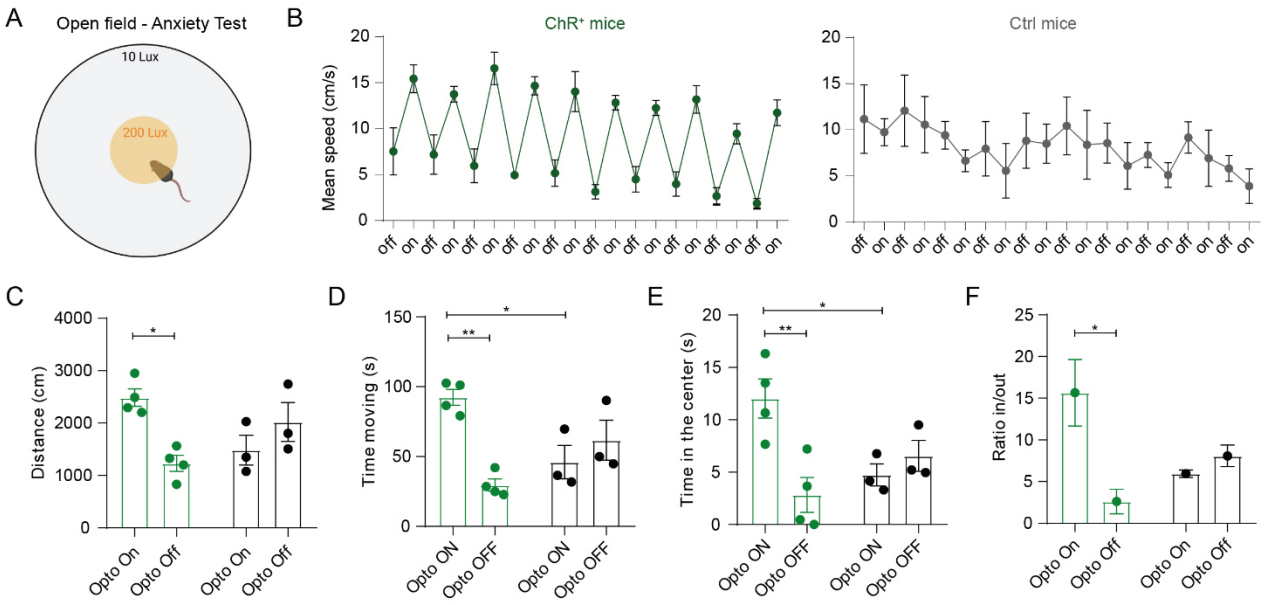

Figure 17 – Increased center crossing upon MSDB$_{glu}$-VTA stimulation in the anxiety test. (A) Experimental setup of the open field anxiety test. (B) Mean locomotor speed in ChR and Ctrl mice during stimulation and non-stimulation periods. (C) Distance travelled (group x stimulation interaction, $F(1,10) = 14.26$, $p = 0.036$). (D) Time spent moving (group x stimulation interaction, $F(1,10) = 19.57$, $p = 0.0013$). (E) Time spent in the center (group x stimulation interaction, $F(1,10) = 11.01$, $p = 0.0078$). (F) Ratio of the time spent in the center and the time spent in the periphery of the arena (group x stimulation interaction, $F(1,10) = 8.686$, $p = 0.0146$). All $n = 4$ ChR mice (green), $n = 3$ Ctrl mice (black); two-way ANOVA with Tukey's multiple comparison test. All data are presented as mean ± SEM. *$p < 0.05$, **$p < 0.01$.

To exclude that the described behavior was elicited by stress or anxiety responses, I tested the animals in an open field anxiety test. The open field anxiety test is considered an approach to assess anxiety. The animals were placed in a novel arena, larger in size and made of a different material, with an intense bright light in the middle. The intensity of the light was of 200 Lux in the center and of 5 to 10 Lux close to the wall (Figure 17A). Even in this condition the MSDB$_{glu}$-VTA optogenetic stimulation reliably increased the mean locomotor speed in ChR mice, while the Ctrl animals exhibited a reduction of mean speed over the 10 minutes time recorded (Figure 17B). The innate response of rodents to this environment is to avoid the center and spend most of the time close to the walls, also referred to as thigmotaxis. Entering the bright lighted center may be interpreted as a dangerous action, given that it can expose them to predators and unknown dangers. However, the environment being novel, there is also an intrinsic drive for the animals to

explore areas they have never visited before (Berlyne, 1955, 1966). Upon stimulation of the network, not only did the animals move for longer distances (Figure 17C, two-way ANOVA: group x stimulation interaction, $F(1,10) = 14.26$, $p = 0.036$) and longer time (Figure 17D, two-way ANOVA: group x stimulation interaction, $F(1,10) = 19.57$, $p = 0.0013$); but they also spent more time in the center (Figure 17E, two-way ANOVA: group x stimulation interaction, $F(1,10) = 11.01$, $p = 0.0078$) compared to the time spent close to the wall (Figure 17F, two-way ANOVA: group x stimulation interaction, $F(1,10) = 8.686$, $p = 0.0146$). Thus, the locomotor activity that the $MSDB_{glu}$-VTA network is promoting appears not to be related to anxiety, as in that case more time spent close to the wall would have been expected. On the contrary, the increased time spent in the middle of the arena, in the presence of an intense bright light, suggests a motivation for the animal to explore the environment, despite the risk of encountering potential dangers.

3.3.4 Novel cues test in the open field

Since the MSDB and VTA regions are both involved in detecting saliency, I tested if the presence of novel stimuli modifies the locomotor behavior previously described. Thus, a novel object, novel food, or a novel conspecific with matched age and sex, were positioned in the middle of the arena. Each day the tested animals were exposed to one of the stimuli and the mean speed and occupancy were analyzed (Figure 18A). The first observation was that the overall mean distance (Figure 18B, RM one-way ANOVA: novel stimuli $F(1, 2) = 0.4485$, $p = 0.578$) and mean speed (Figure 18C, RM one-way ANOVA: novel stimuli $F(1, 2) = 0.084$, $p = 0.798$) was not differing between stimuli. The optogenetic stimulation significantly increased the mean speed (Figure 18D, RM two-way ANOVA: stimulation x stimulus interaction, $F(2,8) = 0.5459$, $p = 0.0320$) and the maximum speed (Figure 18E, RM two-way ANOVA: stimulation x stimulus interaction, $F(2,8) = 3.313$, $p = 0.0895$) of the mice only in the presence of a novel object, while no statistically significant differences were detected for the novel food and the novel conspecific test. The time spent moving did not differ between conditions (Figure 18F, RM two-way ANOVA: stimulation x stimulus interaction, $F(2,8) = 1.362$, $p = 0.3097$) and no significant difference was observed regarding the time spent approaching the novel stimuli with and without stimulation (Figure 18G, RM two-way ANOVA: stimulation x stimulus interaction, $F(2,8) = 1.324$, $p = 0.3187$). Thus, in the presence of novel and salient stimuli the optogenetic stimulation did not impair the animal's attention level, as the time spent investigating the novel cues did not differ.

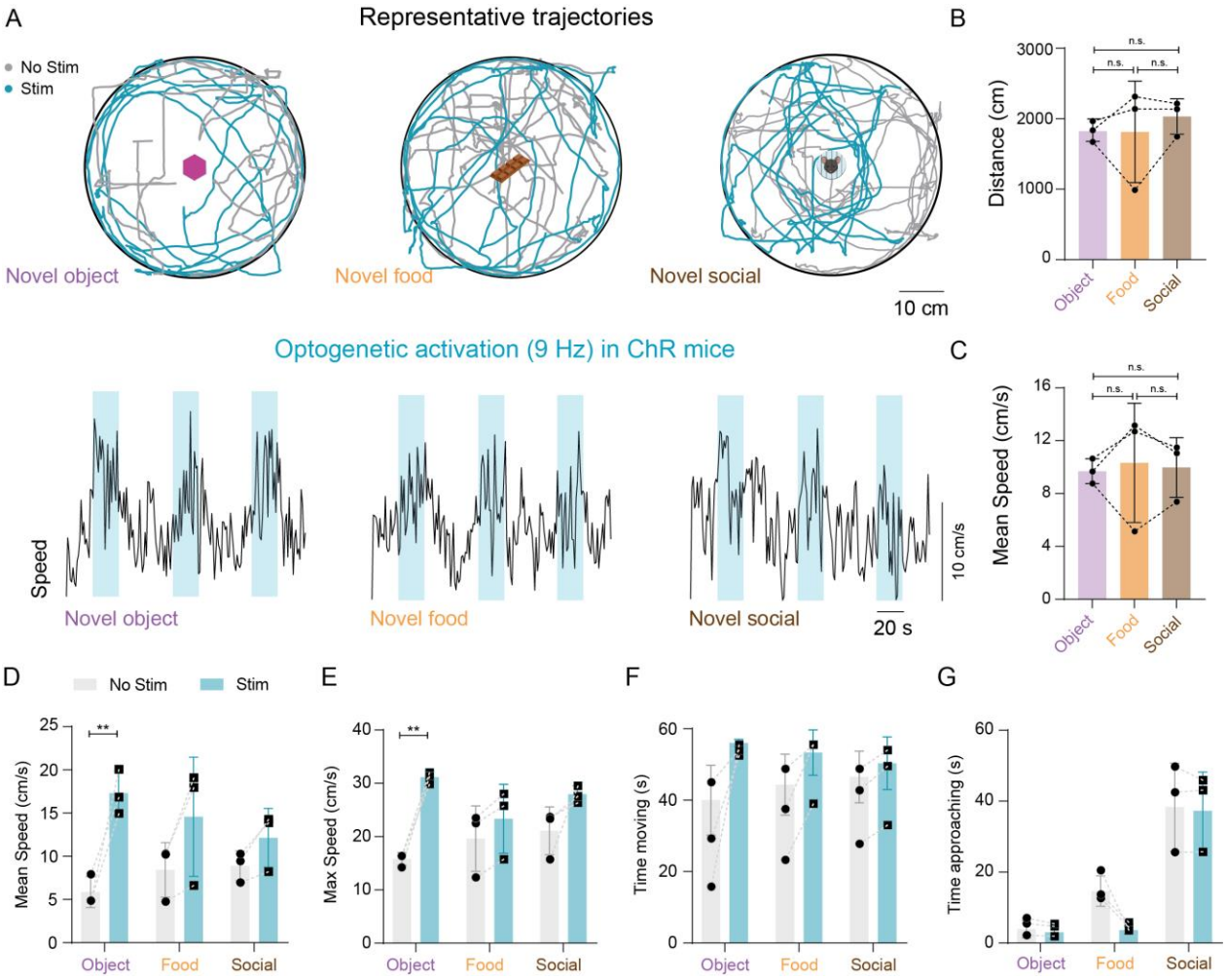

Figure 18 – Novel stimuli do not influence the elicited locomotor effect. (A) Upper panel: experimental setup with a circular arena and a novel object (left), novel food (middle), or novel conspecific (left) overlapped with the arena occupancy of one exemplary ChR mouse with and without optogenetic stimulation for each condition. Lower panel: speed modulation upon optogenetic stimulation in the three conditions (*n* = 3 ChR mice, mean ± s.d., 9 Hz optogenetic stimulation). (B) Overall distance travelled for each condition (*n* = 3 ChR mice; RM one-way ANOVA: novel stimuli F(1, 2) = 0.4485, p = 0.578; Tukey's multiple comparison test). (C) Overall mean speed for each condition (*n* = 3 ChR mice; RM one-way ANOVA: novel stimuli F(1, 2) = 0.084, p = 0.798; Tukey's multiple comparison test). (D) Mean speed (*n* = 3 ChR mice; RM two-way ANOVA: stimulation x stimulus interaction, F(2,8) = 0.5459, p = 0.0320; Sidak's multiple comparison test). (E) Max speed (*n* = 3 ChR mice; RM two-way ANOVA: stimulation x stimulus interaction, F(2,8) = 3.313, p = 0.0895; Sidak's multiple comparison test). (F) Time spent moving (*n* = 3 ChR mice, RM two-way ANOVA: stimulation x stimulus interaction, F(2,8) = 1.362, p = 0.3097; Sidak's multiple comparison test). (G) Time spent approaching the center (*n* = 3 ChR mice, RM two-way ANOVA: stimulation x stimulus interaction, F(2,8) = 1.324, p = 0.3187; Sidak's multiple comparison test). (All data are presented as mean ± SEM., *p < 0.05, **p < 0.01, ***p< 0.001.

Overall, these data point to a broader role of the $MSDB_{glu}$-VTA network. It appears to be not limited to locomotor activity. Indeed, in the freely moving condition the increased speed of locomotion (Figure 15) was accompanied by a complementary increase in the rearing behavioral motifs (Figure 16). Rearing is classically associated with exploratory behavior and the need for an animal to collect more spatial information and reach distant environmental cues. To exclude the possibility of a rearing action oriented towards escaping behavior, the open field anxiety test was performed. In this condition, the optogenetic activation of the circuit not only increased the mean speed of locomotion but also the time spent in the center of the arena (Figure 17). Thus, the elicited locomotor behavior was not anxiogenic and led the animal to explore the environment even in situations that may be perceived riskier, as in the bright light in the center of the open field anxiety test. This drive to explore was not directed towards a specific stimulus, as the presence of a novel object, a novel food, or a novel conspecific did not differentially impact the locomotor behavior or the time spent investigating the novel cue (Figure 18).

Taken together, I provide strong experimental evidence for the presence and functional relevance of a monosynaptic glutamatergic network linking the MSDB and the VTA (3.1). This network reliably induced locomotion when optogenetically stimulated and increased sniffing and whisking behavior on a head-fixed condition (3.2). Freely moving, the increase in locomotion was accompanied by an increase of rearing motifs, an increase of center crossings, and an unaffected valence of the novel stimuli (3.3). The in-depth analysis of the behavioral responses indicated a role for the $MSDB_{glu}$-VTA pathway in information-seeking behavior, defined as the exploratory behavior driven by the interest of the animal to gain access to environmental information (sniffing, whisking, rearing), rather than directed towards a specific goal or reward (food, object, conspecific).

4. Discussion

Animals move for different reasons and their movement in the environment is characterized by a series of actions including, but not limited to walking, running, galloping, digging, rearing, leaning, and jumping. The complex coordination of these diverse movements engages the entire brain, and our comprehension of the circuits responsible for generating single or multiple patterns of actions remains incomplete.
In the present work, I investigated the $MSDB_{glu}$ neurons and their projections to VTA and unveil a new role for this subcortical network in promoting exploratory behavior. In particular,

1) I demonstrated the existence of a functional monosynaptic glutamatergic projection from MSDB to VTA;

2) I showed that the locomotor output described upon stimulation of the $MSDB_{glu}$ neurons is mediated by their projections to VTA;

3) I revealed that the activation of $MSDB_{glu}$ axonal projections to VTA elicits exploratory and information-seeking behavior.

4.1 A functional monosynaptic glutamatergic circuit linking MSDB and VTA

Septal glutamatergic neurons account for 25% of the overall MSDB cell population (Colom et al., 2005). Given their recent discovery (Sotty et al., 2003), small cell size (Colom et al., 2005), and electrophysiological heterogeneity (Huh et al., 2010), their precise functions both within and outside of the MSDB remain incompletely understood. The use of genetic mouse lines, such as VGluT2 Cre, allows an easier access to the manipulation and visualization of these neurons. By injecting Cre-dependent viruses into the MSDB, it is possible to specifically label the $MSDB_{glu}$ population, to study its projections targets outside the MSDB, and to identify new monosynaptic pathways.

Taking advantage of the modified rabies virus tracing strategy, retrogradely labelled neurons from the VTA into the MSDB were detected. Among these cells, $MSDB_{glu}$ neurons co-expressing the RABVΔG and a Cre-dependent injected fluorophore were identified

(Figure 3). However, the anatomical confirmation of the monosynaptic glutamatergic pathway between MSDB and VTA has some limitations. First of all, the amount of TVA expressing cells in the target region constitutes the limiting factor for the transduction and spreading of the rabies virus. The use of a two-virus labelling strategy in the present study, with the co-injection of AAV1/2 DIO TVA-RG and AAV1/2 DIO mCherry, makes it difficult to precisely quantify the number of starting cells in the VTA, as some neurons may have incorporated the TVA-RG plasmid but not the mCherry one. Thus, only a qualitative, but not quantitative, evaluation of those monosynaptic projections was possible. Moreover, the existence of a synaptic contact between two neurons does not necessarily indicate that the synapse is active and leading to a post-synaptic response (Atwood and Wojtowicz, 1999). Finally, depending on the cell type and the AAV serotype, different transduction efficiency has been reported (Aschauer et al., 2013), meaning that some neurons are more likely to be transduced and express the viral transgene than others. Despite these methodological constraints, the retrograde rabies tracing results presented in this work are consistent with previous studies that reported 1) pan-neuronal MSDB inputs to the VTA by using the cTRIO approach (Beier et al., 2015, 2019); 2) specific $MSDB_{glu}$ projections to the VTA via retrograde (Faget et al., 2016) and anterograde tracing (Kesner et al., 2021).

Only a functional characterization of the system can demonstrate that action potentials generated in the $MSDB_{glu}$ neurons are translated into post-synaptic receptor currents in the VTA. The use of optogenetic-assisted circuit mapping together with pharmacological intervention in brain slices allowed me to demonstrate that in addition to an anatomical connection, a functional one also exists (Figure 5). The recorded PSPs were excitatory, still present after blocking voltage-gated Na^+ and K^+ channels, and completely abolished by the bath perfusion of AMPA and NMDA receptor antagonists, confirming the monosynaptic and glutamatergic nature of the MSDB to VTA pathway. Overall, 15% of the recorded VTA cells received direct inputs from the $MSDB_{glu}$ neurons. Previous anatomical studies characterized the percentage of MSDB inputs reaching the VTA over the total number of glutamatergic projections from the whole brain. $MSDB_{glu}$ -VTA inputs ranged between 0.8% (Faget et al., 2016) and 5% (Geisler et al., 2007b). As discussed, tracing experiments have several limitations including cell tropism, injection site, and

volume of transduced cells. Moreover, while the anatomical results highlight the relatively sparse innervation of $MSDB_{glu}$ fibers in VTA, it is not possible to infer how many VTA neurons are contacted by a single $MSDB_{glu}$ axon solely based on retro-tracing data. In this work, using a combination of optogenetic-assisted circuit mapping and pharmacology, I found that 15% of VTA neurons receive direct functional inputs from the $MSDB_{glu}$ axons, reflecting a sparse, but possibly powerful, glutamatergic innervation of the VTA by the $MSDB_{glu}$ projections.

The amplitude of the elicited EPSPs varied between 2 and 20 mV. The broad difference in the responses can be explained by a) the different number of transfected cells in the MSDB, b) the distance of the light fiber from the slices, c) the density of the ChR^+ $MSDB_{glu}$ fibers around the patched cell, and d) the different intrinsic electrophysiological properties of the VTA neurons. Indeed, VTA cell types are known to display a high variability with regard to electrophysiological features, neurotransmitter release and co-release, and immunohistochemistry (Margolis et al., 2006; Hnasko et al., 2012; Morales and Margolis, 2017). Among the recorded VTA neurons, a high heterogeneity in terms of active and passive electrophysiological properties (Figure 6 and 7) as well as immunohistochemical features (Figure 8) was observed. A similar pattern holds true when focusing only on the monosynaptically connected VTA neurons (Figure 9) that were found in each of the five clusters and were labelled for TH, VGluT2, or both. These results are coherent with recent tracing studies showing that VTA subpopulations of excitatory, inhibitory, and neuro-modulatory neurons receive qualitatively similar, though quantitatively different, inputs (Faget et al., 2016).

The electrophysiological properties of the five clusters can offer insights into their putative neurotransmitter release. Indeed, cluster two neurons, characterized by burst activity and after hyperpolarization spiking, resemble the phasic spiking activity reported in both VTA and SN dopaminergic neurons (Overton and Clark, 1997; Blythe et al., 2009). Cluster three, showing AP firing adaptation, high input resistance and low rheobase, presents similarities with identified GABAergic neurons in the VTA, also positive for SST (Nagaeva et al., 2020). Cluster four could also be considered a classic example of GABAergic neurons, given their high firing frequency largely reported in the VTA literature (Steffensen

et al., 1998; Nagaeva et al., 2020; Miranda-Barrientos et al., 2021). Cluster five, on the other hand, could be considered an example of a classical dopaminergic neuron, presenting the typical Ih sag, and firing adaptation over time (Zhang et al., 2010).
Interestingly, the connected neurons in cluster one displayed highly overlapping features with a previously identified Glu-GABA co-releasing population (Miranda-Barrientos et al., 2021). This cell type is characterized by a high input resistance and AP threshold (Miranda-Barrientos et al., 2021). It is conceivable that, as shown for the glutamatergic population in VTA (Morales and Margolis, 2017; Barbano et al., 2020) , also this sub-group of Glu-GABA co-releasing neurons receives multiple excitatory inputs from subcortical areas. The data provided here show that $MSDB_{glu}$ projections are directly targeting those cells and one could speculate that they constitute (one of) the excitatory inputs that those neurons need in order to discharge (Miranda-Barrientos et al., 2021). In addition, given that VTA_{glu} neurons are strongly implicated in locomotion, behavioral flexibility and reinforcing behavior (Wang et al., 2015; Root et al., 2018, 2020; McGovern et al., 2020; Zell et al., 2020), they represent a potential candidate for $MSDB_{glu}$ inputs. While VTA DA neurons have been largely studied for their role in goal-directed and rewarding actions (Schultz, 2016), the biophysical and behavioral features of VTA_{glu} neurons could place them in a relevant position for mediating locomotor actions.

Thus, the data presented here provide experimental evidence of a $MSDB_{glu}$ excitatory input targeting a heterogeneous population of VTA neurons, among which the VTA_{glu} cluster appears to be of particular interest in the context of locomotion and exploration.

4.2 Locomotor pathways originating in the MSDB

Previous work showed that the stimulation of $MSDB_{glu}$ neurons elicits locomotion and hippocampal theta generation prior to locomotion onset (Fuhrmann et al., 2015). In particular, it was shown that $MSDB_{glu}$ neurons send speed-dependent input to the hippocampal formation and entorhinal cortex (Fuhrmann et al., 2015; Justus et al., 2017), targeted preferentially the hippocampal interneurons in the hippocampal stratum oriens (Fuhrmann et al., 2015), and control the animal's speed in a frequency-dependent manner (Fuhrmann et al., 2015). When the $MSDB_{glu}$ network was selectively blocked, a reduction in theta rhythm and in theta-speed coupling was observed (Fuhrmann et al., 2015).

However, the decoupling of the MSDB and the hippocampal network, achieved by pharmacological intervention, did not impair the ability of the $MSDB_{glu}$ neurons to induce locomotion (Korvasová et al., 2021). Thus, the $MSDB_{glu}$ neuronal subpopulation represent a key player in movement execution's control. In particular, the present work highlights the role of the $MSDB_{glu}$ projections to VTA in initiating and maintaining locomotor actions.

Fiber photometry is a method for gathering information on neuronal activity at the axonal level, especially in deeper regions of the brain otherwise not accessible through two-photon imaging. By implanting an optic fiber above the VTA and expressing GCaMP6s specifically in $MSDB_{glu}$ neurons, I could monitor the axons activity during resting and running periods. I found that locomotion episodes were accompanied by an increase in the axonal fluorescence (Figure 10), thus supporting the hypothesis of a downstream locomotor circuit extending from the basal forebrain to the midbrain areas. It was previously shown that a similar increase in $MSDB_{glu}$ axonal fluorescence, linked to the animal's locomotor activity, was also occurring in the entorhinal cortex and in the hippocampal CA1 region (Fuhrmann et al., 2015; Justus et al., 2017). It stands to reason that the excitatory population of the MSDB codes for locomotion and sends movement-related information to its downstream structures via both the septo-hippocampal pathway and the basal forebrain bundle. Although fiber photometry is considered the state-of-the-art method to visualize axons in deep regions, there are still some limitations in this technique. In particular, the kinetics of the GCaMP sensor, slight variations in the distance of the implanted optic fiber, as well as the low signal to noise ratio, do not allow for a precise temporal resolution. In fact, fiber photometry signals are the result of the bulk fluorescence in the region of interest, and do not provide any information about single axons activity. For this reason, a high number of projections must be simultaneously active to detect the signal. This is especially the case when the innervation is sparse as in the $MSDB_{glu}$-VTA pathway, thus compromising the ability to resolve the precise onset time of the signal. It is still particularly challenging to visualize axons in deep brain structure like the VTA. The use of gradient-index (GRIN) lenses, combined with single photon or two photon microscopy, enables progress towards *in vivo* recordings of axonal activity in deep regions. However, the small field of view given by the lenses, the movement artifacts, and the complexity of the implant yields only a modest success rate. Taken together, fiber

photometry is currently the best approach to investigate projection-specific activity in deep brain structures, and demonstrated that $MSDB_{glu}$ axons in the VTA are active during voluntary locomotor episodes.

To clarify if the increase of $MSDB_{glu}$ calcium activity in the VTA is causally linked to the detected running events, I have activated the projection using optogenetics. This technique allows both spatial and temporal control over the circuit, thus guaranteeing that only the axons of interest are activated and this exclusively happens during the timeframes in which the laser is on. The optogenetic activation of the $MSDB_{glu}$-VTA pathway reliably induced locomotion, corroborating the fiber photometry data (Figure 11). The circuit was excited at four different frequencies (3, 6, 9, and 12 Hz) in the theta range. Previous studies showed a positive correlation between the frequency of the $MSDB_{glu}$ neuronal stimulation and the animal's running speed (Fuhrmann et al., 2015). In line with these observations, the speed of the channelrhodopsin injected mice was significantly positively modulated by the stimulation frequency applied to VTA terminals. This effect, resembling the manipulation at the level of the $MSDB_{glu}$ somata (Fuhrmann et al., 2015), indicates a causal link between MSDB-elicited locomotion and its downstream projections to VTA. However, light-evoked neurotransmitter release at the axonal level may cause APs propagation travelling antidromically to the soma and inducing transmitter release from other collaterals (Britt et al., 2012; Lee et al., 2020). To exclude this possibility, one option is to block antidromic APs at the soma by injecting lidocaine, a voltage-gated Na^+ channel blocker (Stuber et al., 2011; Rost et al., 2022). By pharmacologically silencing the $MSDB_{glu}$ somata with lidocaine, while optogenetically activating their axons in VTA, I demonstrated that VTA constitutes a downstream target of the locomotor circuit initiated by the $MSDB_{glu}$ neurons. To further confirm the effect of the lidocaine injection in the MSDB, I simultaneously recorded hippocampal LFP activity. MSDB inputs to the HPC are key players in the generation of rhythmic oscillations (Smythe et al., 1992; Vertes and Kocsis, 1997; Vinogradova et al., 1998) and inhibition of MSDB neurons reliably suppresses theta activity (Winson, 1978; Brandon et al., 2011; Koenig et al., 2011; Pignatelli et al., 2012). Lidocaine infusion caused two main effects: 1) a significant reduction in theta amplitude, as expected upon pharmacological inhibition of the MSDB; 2) a flattening of the mean

running speed around 10 cm/s at all stimulation frequencies, thus reducing the speed-frequency modulation previously described (Figure 12).

Early studies suggested that variations in the hippocampal theta frequency are linked to locomotor speed and sensorimotor integration (Bland and Oddie, 2001; Wyble et al., 2004; Sinnamon, 2006). Indeed, HPC firing is altered by the change of the animal's running velocity (Markus et al., 1995; Góis and Tort, 2018), indicating that HPC neurons receive and encode information about speed. The speed signal is in turn modulating hippocampal place cell activity, guaranteeing a constant encoding of the distance travelled and the animal position in space (Geisler et al., 2007a). Finally, HPC output projections to the LS can adjust ongoing locomotor speed (Bender et al., 2015). Based on these data, it is reasonable to speculate that the pharmacological inhibition of the MSDB, and the consequent reduction in movement related type 1 hippocampal theta activity, are compromising the animal's ability to navigate through space and adjust its running velocity. The specific activation of the $MSDB_{glu}$-VTA network proves that the motor circuits necessary to initiate the locomotor action are independent from the septo-hippocampal network. However, the mismatch between the artificially induced stimulation in the VTA, and the lack of an on-line readout of the animal speed in the HPC, may cause the observed flattening in the speed of locomotion.

Interestingly, stimulating another downstream projection from $MSDB_{glu}$ neurons results in a similar behavioral effect (Zhang et al., 2018a). The $MSDB_{glu}$-POA pathway elicits locomotion when optogenetically activated even when the MSDB network is silenced. However, the aforementioned study does not provide any evidence of a monosynaptic projection from MSDB to POA, with the possibility that the network manipulation was targeting septal fibers en passant through the preoptic region, possibly reaching the VTA via the basal forebrain bundle. Behaviorally, the $MSDB_{glu}$ projections to POA and VTA m may derive from embryonically distinct clusters (Magno et al., 2022) and encode for different behavioral repertoires linked to locomotion (Mocellin and Mikulovic, 2021). In particular, POA activity is associated with social and homeostatic functions, including arousal, parental and social interactions (Wu et al., 2014; Scott et al., 2015; Allen et al.,

2017; McHenry et al., 2017); while VTA is linked to reinforcement, motivation, and exploratory behavior (Mohebi et al., 2019; Zell et al., 2020; Mishra et al., 2021).

In fact, upon activation of the $MSDB_{glu}$-VTA pathway, the animals not only moved more, but also showed a remarkable increase of exploratory actions. In the head-fixed configuration, orofacial movements preceding locomotion were detected (Figure 13) even after lidocaine infusion (Figure 14). Mice started whisking and sniffing 500 ms prior to the optogenetically driven locomotion onset, similarly to the behavioral pattern recorded prior to natural locomotor episodes. All the mice were trained on a cued belt with 6 different textures. In a head-fixed condition, it is conceivable that whisking and sniffing represented the only possible motor actions mice could perform to detect changes in the environment. Indeed, it is known that rodents move their nose and vibrissae in order to explore their peripersonal space (Kurnikova et al., 2017) and sniffing has been classically associated with motivated behavior (Clarke and Trowill, 1971). It has also been observed that during bouts of exploration, whisking and sniffing are phase-locked within the theta frequency range (Ranade et al., 2013). Indeed, the frequency of sniffing and whisking oscillates between 4 and 12 Hz in a 1:1 ratio (one sniffing cycle corresponds to one whisking cycle)(Ranade et al., 2013). This phase-locking could facilitate cross-modal linking of smell and touch, and could enable the temporal alignment of multimodal sensory stream during exploration. As the MSDB is a key player in theta rhythm generation, its position at the interface between the hippocampal formation, the motivational systems, and the motor outputs could be essential to synchronize the animal behavior (locomotion, sniffing, whisking) with the underlying cognitive processes.

4.3 MSDB and VTA in information seeking behavior

To investigate a broader repertoire of the behaviors that can be elicited by the $MSDB_{glu}$-VTA pathway, I tested freely moving mice in an open field arena. Similar to what was observed on the treadmill, the optogenetic stimulation of the network increased the mean and maximum speed of locomotion. Moreover, I confirmed that the locomotor effect relies on downstream VTA projections, since the infusion of lidocaine in the MSDB did not affect the behavioral outcome elicited by network activation (Figure 15). The coherence between head-fixed and freely moving results corroborate the key role of this circuit in locomotor

activity. However, when moving in an environment, mice can exhibit a way richer behavioral repertoire that can be analyzed and quantified. The systematic quantification of naturalistic behavior represents a challenge in circuit neuroscience given the wide variety of movements, the inter-animal variability, and the different recording setups used. To overcome these challenges, several unsupervised machine learning methods have been recently developed. They allow the creation of benchmark datasets that can be compared between laboratories and experimental tasks, thus reducing the scientists' subjective biases during behavioral quantification. In particular, our group developed VAME (Luxem et al., 2022), a method based on a recurrent neural network in a variational autoencoder setting that enables the analysis of freely moving behavioral data with sub-second resolution. Applying VAME on my data confirmed the increase in running motifs and the near-complete absence of resting motifs during the optogenetic stimulation of the $MSDB_{glu}$-VTA pathway (Figure 16). The detailed analysis of the animal's actions also uncovered an increase in 3 out of 6 rearing motifs during stimulation, while 2 out of 4 sniffing motifs increased when the optogenetics stimulation turned off. VAME is detecting the overall motifs usage in each condition (before, during, and after stimulation). It is plausible that the sniffing motifs over the 20 seconds stimulation epochs are less pronounced when compared to the time intervals without the stimulation, as the animals spend most of their time running and rearing. Indeed, the treadmill data showed an increase in sniffing and whisking time-locked to the onset of the stimulation around 500 ms prior to movement (corresponding to 1/40 of the total time the animal is subjected to the circuit manipulation). On the other side the increase in rearing and running behavioral motifs together with a decrease in the majority of the stationary motifs support a general increase in attention and alert.

Rearing is classically considered a way for an animal to sample environmental information, especially when cues are distant and otherwise not accessible (Barth et al., 2018). However, recent studies have also discussed rearing as a sign of distress reflecting the need for the animal to escape an unpleasant situation (Sturman et al., 2018; Hughes et al., 2020). If that was the case, an increase in thigmotaxis during the open field anxiety test would be expected, as this behavior is naturally evoked by novel and potentially dangerous environments (Simon et al., 1994). Instead, stimulation of the $MSDB_{glu}$-VTA

circuit not only reliably increased locomotion, but it also increased the time spent in the center of the arena (Figure 17). It is broadly known that rodent locomotor activity is reduced in bright environments (Blizard, 1971), and an increase in center crossings is associated with lower anxiety levels and higher exploratory activity (Belzung, 1999). Thus, the locomotion and rearing actions observed in these experiments seem not to be dependent on anxiety or stress, but they were more likely to be associated with curiosity and exploration.

To test if the exploratory drive elicited by the network is oriented towards specific rewards, the animals were exposed to novel cues in the form of an object, food, or another mouse with matched age and sex. Surprisingly, in the presence of those novel stimuli there was no significant increase of approaches compared to the non-stimulated periods, while the locomotor effect was once again confirmed (Figure 18). This could be explained by the fact that the network response to novelty is already saturated when the animal encounters a novel stimulus for the first time. Thus, the optogenetic stimulation cannot increase these behavioral actions any further. When looking at specific stimuli, novelty evoked by an object, food, or conspecific did not show significant inter-stimulus differences in terms of speed and time moving during stimulation. However, an increase in the time spent approaching the other mouse was detected compared to the time spent exploring the object or the food under both control and optogenetic stimulation conditions. The increased interest of an animal for a conspecific is not surprising and supports the idea that the optogenetic manipulation is not over-writing the animal's attention level and physiological interests. Rather, it seems that apart from concentrating on the novel cues, the stimulated animals maintain a higher level of locomotor activity and tend to move more throughout the environment. These results reinforce previous observations supporting a role of the $MSDB_{glu}$-VTA network in exploratory and information-seeking behavior, rather than goal-directed actions (Kesner et al., 2021). Indeed, Kesner and colleagues hypothesized that the $MSDB_{glu}$-VTA circuit may constitute the neural substrate linking memory, navigation, and novelty detection, with environmental salience, motivation, and locomotor activity (Kesner et al., 2022) (Figure 19).

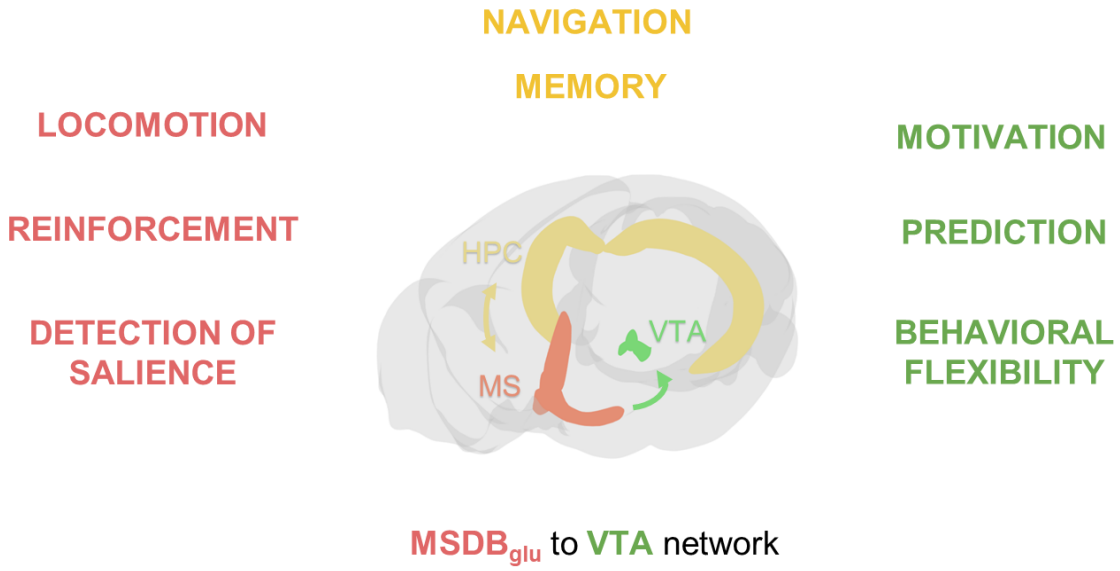

Figure 19 – The $MSDB_{glu}$-VTA network role in exploration and information-seeking behavior. Overview of the septo-hippocampal and MSDB-VTA pathway. Highlighted are the relevant behavioral outcomes related to exploration and encoded by the different parts of the network.

4.4 Conclusions and future directions

Environments are replete with cues, such as objects, light, or obstacles, that demarcate the space. Animals possess an innate drive to collect information about their surroundings, even in the absence of an immediate goal or reward (Tolman, 1948; Butler, 1953). It can be hypothesized that this intrinsic inclination towards novelty or salient stimuli has profound evolutionary relevance: knowledge of the environment confers an advantage for future goal-oriented navigation, when needed. This is especially crucial for wild animals, where unpredictability regarding forthcoming events poses a major threat to survival. Thus, identifying sources of food or water, shelters to hide, or paths to escape from a predator, is critical for their well-being. To achieve this, cognitive and behavioral processes need to be coordinated by the interaction of different brain circuits.

In this scenario, the MSDB stands at the crucial interface between memory and navigational hippocampal networks on the one hand, and reinforcing, locomotor, and rewarding limbic and midbrain circuits on the other. MSDB dense projections to the HPC formation are necessary and sufficient to induce theta oscillations, that are prominent during environmental interaction (Buzsáki, 2002) and support the formation of episodic

memories (Eichenbaum, 2017) and cognitive maps (O'Keefe and Nadel, 1978). Moreover, the HPC has long been considered a "comparator" (Vinogradova, 2001), detecting mismatches between current and past experiences, making it an essential component of a network that aims to build a representation of the environment and to detect its salient features. MSDB, and in particular its glutamatergic subpopulation, not only regulates hippocampal theta activity (Kocsis et al., 2022), but can also detect salient stimuli (Zhang et al., 2018a, 2018b) and elicit locomotion (Fuhrmann et al., 2015), observable actions underlying the neural mechanisms for exploratory and information-seeking behaviors.

Seeking behaviors, be they reward- or information- driven, require motivation. A key network involved in motivated behaviors is the VTA. My work shows that an excitatory pathway from the MSDB to the VTA exists and drives locomotor activity. The elicited movement is associated with an increase in whisking, sniffing, and rearing, all of which are part of the exploratory behavioral repertoire of rodents (Lever et al., 2006; Barth et al., 2018) Moreover, the $MSDB_{glu}$ axons target a heterogeneous VTA network, including glutamatergic, dopaminergic, and putative co-releasing neurons positive for both VGluT2 and TH immunostaining. VTA_{glu} neurons are of particular interest in the context of information-seeking behavior: both DA and non-DA neurons receive glutamatergic inputs from local VTA_{glu} axons (Dobi et al., 2010; Wang et al., 2015), thus suggesting that the excitatory MSDB inputs to VTA_{glu} neurons may play a critical role in the intra-VTA network modulation. Moreover, VTA_{glu} neurons are active during both reward and aversion (Wang et al., 2015; Root et al., 2018; McGovern et al., 2020) and signal violations in reward expectations (Root et al., 2020). It stands to reason that this population codes for saliency *per se*, without showing preferential activity for positive or negative cues. In addition, VTA_{glu} neurons activation *in vivo* results in the firing of DA neurons that innervate the NAc (Wang et al., 2015), a key region involved in behavioral flexibility and action switching upon environmental changes (Haluk and Floresco, 2009).

While exploring, animals must balance their adversity to risk with the curiosity of navigating a new environment. It stands to reason that the circuit I here described is part of a broader glutamatergic network. The MSDB, with its sparse but widespread glutamatergic projections modulating the intra- and extra- septal circuits, may play a critical role in synchronizing hippocampal activity, aimed at the formation of memories and

spatial maps, with the motivational and locomotor drive necessary for the animal to explore the environment. Future work is needed to understand which VTA downstream pathways elicit this behavior, and the contribution of the striatum, a relay station for emotional and sensory processing resulting in motor outputs. Finally, VTA neurons are also sending direct inputs to the hippocampal formation and have been proposed to be necessary for the formation of long-term memory (Lisman and Grace, 2005). Further studies should clarify the contribution of these projections in the context of exploration, but it is plausible that DA release in the HPC may be necessary to link salient stimuli detected by the VTA network, with their spatial location encoded by the HPC.

Taken together, my work investigated both *in vitro* and *in vivo* the $MSDB_{glu}$-VTA network, critically positioned at the interface of septo-hippocampal and VTA-striatal circuits. This pathway increases locomotion, sniffing, whisking, and rearing, revealing a novel role for the $MSDB_{glu}$-VTA circuit in exploration and information-seeking behavior.

5. Abstract

Locomotion is a fundamental behavior that comprises different specialized neuronal networks. In the basal forebrain, the glutamatergic neurons of the medial septum and diagonal band of Broca ($MSDB_{glu}$) can initiate locomotion and control its speed when optogenetically stimulated. $MSDB_{glu}$ neuronal activity is also linked to hippocampal theta oscillations and codes for aversive salient stimuli. This work aims at investigating the downstream target of the $MSDB_{glu}$ neurons responsible for the locomotor effect, and the underlying motivation that brings animals to move upon the activation of this circuit. Tracing studies identified the ventral tegmental area (VTA) as a candidate region receiving $MSDB_{glu}$ inputs. Combining retrograde tracing, slice electrophysiology, *in vivo* fiberphotometry, pharmacology, and optogenetics, my aim was to understand the role of $MSDB_{glu}$ projections to VTA during rodents' behavior in both head-fixed and freely moving tasks. Unsupervised machine learning methods allowed me to extract the animal's pose dynamics and quantify the effect of the network manipulation on behavior at a sub-second time scale.

Tracing and *in vitro* patch-clamp data confirmed the existence of a monosynaptic glutamatergic connection between MSDB and VTA, and highlighted how $MSDB_{glu}$ inputs target a heterogeneous population of VTA neurons. Optogenetic activation of $MSDB_{glu}$ axons in VTA was sufficient to induce locomotion and to control its speed in a frequency-dependent manner. Lidocaine infusion in the MSDB did not affect the results of the optogenetic stimulation, thus identifying the VTA as a downstream region in the locomotor circuit initiated in the MSDB. These findings were further supported by the increase in calcium signals of $MSDB_{glu}$ axons in VTA when animals were spontaneously moving. I found that $MSDB_{glu}$-VTA circuit activation causes an increase of sniffing and whisking prior to locomotion initiation on the treadmill, and leads to a higher representation of rearing motifs in the open field, all actions classically linked to exploration.

Taken together, in the present work I investigated the $MSDB_{glu}$ neurons and their projections to VTA, and unveiled a new role for this subcortical network in promoting exploratory and information-seeking behavior.

6. List of figures

7. List of tables

8. References

Adhikari, A., Topiwala, M. A., and Gordon, J. A. (2010). Synchronized Activity between the Ventral Hippocampus and the Medial Prefrontal Cortex during Anxiety. *Neuron* 65, 257–269. doi: 10.1016/j.neuron.2009.12.002.

Aggleton, J. P., Hunt, P. R., and Rawlins, J. N. P. (1986). The effects of hippocampal lesions upon spatial and non-spatial tests of working memory. *Behavioural Brain Research* 19, 133–146. doi: 10.1016/0166-4328(86)90011-2.

Agostinelli, L. J., Geerling, J. C., and Scammell, T. E. (2019). Basal forebrain subcortical projections. *Brain Struct Funct* 224, 1097–1117. doi: 10.1007/s00429-018-01820-6.

Allen, W. E., DeNardo, L. A., Chen, M. Z., Liu, C. D., Loh, K. M., Fenno, L. E., et al. (2017). Thirst-associated preoptic neurons encode an aversive motivational drive. *Science* 357, 1149–1155. doi: 10.1126/science.aan6747.

Alonso, A., and Klink, R. (1993). Differential electroresponsiveness of stellate and pyramidal-like cells of medial entorhinal cortex layer II. *J Neurophysiol* 70, 128–143. doi: 10.1152/jn.1993.70.1.128.

Aransay, A., Rodríguez-López, C., García-Amado, M., Clascá, F., and Prensa, L. (2015). Long-range projection neurons of the mouse ventral tegmental area: a single-cell axon tracing analysis. *Frontiers in Neuroanatomy* 9. Available at: https://www.frontiersin.org/articles/10.3389/fnana.2015.00059 [Accessed February 18, 2023].

Arnt, J., and Scheel-Krüger, J. (1979b). GABA in the ventral tegmental area: Differential regional effects on locomotion, aggression and food intake after microinjection of GABA agonists and antagonists. *Life Sciences* 25, 1351–1360. doi: 10.1016/0024-3205(79)90402-8.

Aschauer, D. F., Kreuz, S., and Rumpel, S. (2013). Analysis of Transduction Efficiency, Tropism and Axonal Transport of AAV Serotypes 1, 2, 5, 6, 8 and 9 in the Mouse Brain. *PLoS ONE* 8, e76310. doi: 10.1371/journal.pone.0076310.

Atwood, H. L., and Wojtowicz, J. M. (1999). Silent Synapses in Neural Plasticity: Current Evidence. *Learn. Mem.* 6, 542–571.

Barbano, M. F., Wang, H.-L., Zhang, S., Miranda-Barrientos, J., Estrin, D. J., Figueroa-González, A., et al. (2020). VTA Glutamatergic Neurons Mediate Innate Defensive Behaviors. *Neuron* 107, 368-382.e8. doi: 10.1016/j.neuron.2020.04.024.

Barth, A. M., Domonkos, A., Fernandez-Ruiz, A., Freund, T. F., and Varga, V. (2018). Hippocampal Network Dynamics during Rearing Episodes. *Cell Reports* 23, 1706–1715. doi: 10.1016/j.celrep.2018.04.021.

Beier, K. T., Gao, X. J., Xie, S., DeLoach, K. E., Malenka, R. C., and Luo, L. (2019). Topological Organization of Ventral Tegmental Area Connectivity Revealed by Viral-Genetic Dissection of Input-Output Relations. *Cell Reports* 26, 159-167.e6. doi: 10.1016/j.celrep.2018.12.040.

Beier, K. T., Steinberg, E. E., DeLoach, K. E., Xie, S., Miyamichi, K., Schwarz, L., et al. (2015). Circuit Architecture of VTA Dopamine Neurons Revealed by Systematic Input-Output Mapping. *Cell* 162, 622–634. doi: 10.1016/j.cell.2015.07.015.

Belzung, C. (1999). “Chapter 4.11 Measuring rodent exploratory behavior,” in *Techniques in the Behavioral and Neural Sciences* (Elsevier), 738–749. doi: 10.1016/S0921-0709(99)80057-1.

Bender, F., Gorbati, M., Cadavieco, M. C., Denisova, N., Gao, X., Holman, C., et al. (2015). Theta oscillations regulate the speed of locomotion via a hippocampus to lateral septum pathway. *Nat Commun* 6, 8521. doi: 10.1038/ncomms9521.

Berlyne, D. E. (1955). The arousal and satiation of perceptual curiosity in the rat. *Journal of Comparative and Physiological Psychology* 48, 238–246. doi: 10.1037/h0042968.

Berlyne, D. E. (1966). Curiosity and exploration. *Science* 153, 25–33. doi: 10.1126/science.153.3731.25.

Berman, G. J., Choi, D. M., Bialek, W., and Shaevitz, J. W. (2014). Mapping the stereotyped behaviour of freely moving fruit flies. *Journal of The Royal Society Interface* 11, 20140672. doi: 10.1098/rsif.2014.0672.

Bland, B. H., and Oddie, S. D. (2001). Theta band oscillation and synchrony in the hippocampal formation and associated structures: the case for its role in sensorimotor integration. *Behavioural Brain Research* 127, 119–136. doi: 10.1016/S0166-4328(01)00358-8.

Bland, B. H., Oddie, S. D., and Colom, L. V. (1999). Mechanisms of Neural Synchrony in the Septohippocampal Pathways Underlying Hippocampal Theta Generation. *J. Neurosci.* 19, 3223–3237. doi: 10.1523/JNEUROSCI.19-08-03223.1999.

Bland, B. H., Seto, M. G., Sinclair, B. R., and Fraser, S. M. (1984). The pharmacology of hippocampal theta cells: Evidence that the sensory processing correlate is cholinergic. *Brain Research* 299, 121–131. doi: 10.1016/0006-8993(84)90794-7.

Bland, S. K., and Bland, B. H. (1986). Medial septal modulation of hippocampal theta cell discharges. *Brain Research* 375, 102–116. doi: 10.1016/0006-8993(86)90963-7.

Blizard, D. A. (1971). Situational Determinants of Open-Field Behaviour in Mus Musculus. *British Journal of Psychology* 62, 245–252. doi: 10.1111/j.2044-8295.1971.tb02034.x.

Blythe, S. N., Wokosin, D., Atherton, J. F., and Bevan, M. D. (2009). Cellular Mechanisms Underlying Burst Firing in Substantia Nigra Dopamine Neurons. *J. Neurosci.* 29, 15531–15541. doi: 10.1523/JNEUROSCI.2961-09.2009.

Bocklisch, C., Pascoli, V., Wong, J. C. Y., House, D. R. C., Yvon, C., de Roo, M., et al. (2013). Cocaine Disinhibits Dopamine Neurons by Potentiation of GABA Transmission in the Ventral Tegmental Area. *Science* 341, 1521–1525. doi: 10.1126/science.1237059.

Bohnslav, J. P., Wimalasena, N. K., Clausing, K. J., Dai, Y. Y., Yarmolinsky, D. A., Cruz, T., et al. (2021). DeepEthogram, a machine learning pipeline for supervised behavior classification from raw pixels. *eLife* 10, e63377. doi: 10.7554/eLife.63377.

Brandon, M. P., Bogaard, A. R., Libby, C. P., Connerney, M. A., Gupta, K., and Hasselmo, M. E. (2011). Reduction of Theta Rhythm Dissociates Grid Cell Spatial Periodicity from Directional Tuning. *Science* 332, 595–599. doi: 10.1126/science.1201652.

Britt, J. P., McDevitt, R. A., and Bonci, A. (2012). Use of Channelrhodopsin for Activation of CNS Neurons. *Current Protocols in Neuroscience* 58, 2.16.1-2.16.19. doi: 10.1002/0471142301.ns0216s58.

Bromberg-Martin, E. S., Matsumoto, M., and Hikosaka, O. (2010). Dopamine in Motivational Control: Rewarding, Aversive, and Alerting. *Neuron* 68, 815–834. doi: 10.1016/j.neuron.2010.11.022.

Butler, R. A. (1953). Discrimination learning by rhesus monkeys to visual-exploration motivation. *Journal of Comparative and Physiological Psychology* 46, 95–98. doi: 10.1037/h0061616.

Buzsáki, G. (2002). Theta Oscillations in the Hippocampus. *Neuron* 33, 325–340. doi: 10.1016/S0896-6273(02)00586-X.

Buzsáki, G., and Moser, E. I. (2013). Memory, navigation and theta rhythm in the hippocampal-entorhinal system. *Nat Neurosci* 16, 130–138. doi: 10.1038/nn.3304.

Cador, M., Marco, N., Stinus, L., and Simonnet, G. (2002). Interaction between neuropeptide FF and opioids in the ventral tegmental area in the behavioral response to novelty. *Neuroscience* 110, 309–318. doi: 10.1016/S0306-4522(01)00587-5.

Caggiano, V., Leiras, R., Goñi-Erro, H., Masini, D., Bellardita, C., Bouvier, J., et al. (2018). Midbrain circuits that set locomotor speed and gait selection. *Nature* 553, 455–460. doi: 10.1038/nature25448.

Capelli, P., Pivetta, C., Soledad Esposito, M., and Arber, S. (2017). Locomotor speed control circuits in the caudal brainstem. *Nature* 551, 373–377. doi: 10.1038/nature24064.

Carlsson, A., Falck, B., Fuxe, K., and Hillarp, N.-Å. (1964). Cellular Localization of Monoamines in the Spinal Cord. *Acta Physiologica Scandinavica* 60, 112–119. doi: 10.1111/j.1748-1716.1964.tb02874.x.

Carr, D. B., and Sesack, S. R. (2000). Projections from the Rat Prefrontal Cortex to the Ventral Tegmental Area: Target Specificity in the Synaptic Associations with Mesoaccumbens and Mesocortical Neurons. *J. Neurosci.* 20, 3864–3873. doi: 10.1523/JNEUROSCI.20-10-03864.2000.

Carr, M. F., Jadhav, S. P., and Frank, L. M. (2011). Hippocampal replay in the awake state: a potential substrate for memory consolidation and retrieval. *Nat Neurosci* 14, 147–153. doi: 10.1038/nn.2732.

Castaldi, L. (1923). Studi sulla struttura e sullo sviluppo del mesencefalo. *Arch. Ital. Anat. Embriol* 20, 23–225.

Cazala, P., Galey, D., and Durkin, T. (1988). Electrical self-stimulation in the medial and lateral septum as compared to the lateral hypothalamus: Differential intervention of reward and learning processes? *Physiology & Behavior* 44, 53–59. doi: 10.1016/0031-9384(88)90345-9.

Charara, A., Smith, Y., and Parent, A. (1996). Glutamatergic inputs from the pedunculopontine nucleus to midbrain dopaminergic neurons in primates: Phaseolus vulgaris-leucoagglutinin anterograde labeling combined with postembedding glutamate and GABA immunohistochemistry. *Journal of Comparative Neurology* 364, 254–266. doi: 10.1002/(SICI)1096-9861(19960108)364:2<254::AID-CNE5>3.0.CO;2-4.

Chieng, B., Azriel, Y., Mohammadi, S., and Christie, M. J. (2011). Distinct cellular properties of identified dopaminergic and GABAergic neurons in the mouse ventral tegmental area: GABA and dopamine neurons in VTA. *The Journal of Physiology* 589, 3775–3787. doi: 10.1113/jphysiol.2011.210807.

Choi, K., Lee, Y., Lee, C., Hong, S., Lee, S., Kang, S. J., et al. (2016). Optogenetic activation of septal GABAergic afferents entrains neuronal firing in the medial habenula. *Sci Rep* 6, 34800. doi: 10.1038/srep34800.

Chrobak, J. J., Stackman, R. W., and Walsh, T. J. (1989). Intraseptal administration of muscimol produces dose-dependent memory impairments in the rat. *Behavioral and Neural Biology* 52, 357–369. doi: 10.1016/S0163-1047(89)90472-X.

Clarke, S., and Trowill, J. A. (1971). Sniffing and motivated behavior in the rat. *Physiology & Behavior* 6, 49–52. doi: 10.1016/0031-9384(71)90013-8.

Cohen, J. Y., Haesler, S., Vong, L., Lowell, B. B., and Uchida, N. (2012). Neuron-type-specific signals for reward and punishment in the ventral tegmental area. *Nature* 482, 85–88. doi: 10.1038/nature10754.

Colom, L. V., Castaneda, M. T., Reyna, T., Hernandez, S., and Garrido-sanabria, E. (2005). Characterization of medial septal glutamatergic neurons and their projection to the hippocampus. *Synapse* 58, 151–164. doi: 10.1002/syn.20184.

Creed, M. C., Ntamati, N. R., and Tan, K. R. (2014). VTA GABA neurons modulate specific learning behaviors through the control of dopamine and cholinergic systems. *Front. Behav. Neurosci.* 8. doi: 10.3389/fnbeh.2014.00008.

Decker, M. W., Radek, R. J., Majchrzak, M. J., and Anderson, D. J. (1992). Differential effects of medial septal lesions on spatial-memory tasks. *Psychobiology* 20, 9–17. doi: 10.3758/BF03327154.

Delle Donne, K. T., Sesack, S. R., and Pickel, V. M. (1997). Ultrastructural immunocytochemical localization of the dopamine D2 receptor within GABAergic neurons of the rat striatum. *Brain Research* 746, 239–255. doi: 10.1016/S0006-8993(96)01226-7.

Deschênes, M., Moore, J., and Kleinfeld, D. (2012). Sniffing and whisking in rodents. *Current Opinion in Neurobiology* 22, 243–250. doi: 10.1016/j.conb.2011.11.013.

Dobi, A., Margolis, E. B., Wang, H.-L., Harvey, B. K., and Morales, M. (2010). Glutamatergic and Nonglutamatergic Neurons of the Ventral Tegmental Area Establish Local Synaptic Contacts with Dopaminergic and Nondopaminergic Neurons. *Journal of Neuroscience* 30, 218–229. doi: 10.1523/JNEUROSCI.3884-09.2010.

Dolensek, N., Gehrlach, D. A., Klein, A. S., and Gogolla, N. (2020). Facial expressions of emotion states and their neuronal correlates in mice. *Science* 368, 89–94. doi: 10.1126/science.aaz9468.

Eichenbaum, H. (2017). Prefrontal-hippocampal interactions in episodic memory. *Nat Rev Neurosci* 18, 547–558. doi: 10.1038/nrn.2017.74.

Engelhard, B., Finkelstein, J., Cox, J., Fleming, W., Jang, H. J., Ornelas, S., et al. (2019). Specialized coding of sensory, motor and cognitive variables in VTA dopamine neurons. *Nature* 570, 509–513. doi: 10.1038/s41586-019-1261-9.

Espinosa, N., Alonso, A., Lara-Vasquez, A., and Fuentealba, P. (2019). Basal forebrain somatostatin cells differentially regulate local gamma oscillations and functionally segregate motor and cognitive circuits. *Sci Rep* 9, 2570. doi: 10.1038/s41598-019-39203-4.

Faget, L., Osakada, F., Duan, J., Ressler, R., Johnson, A. B., Proudfoot, J. A., et al. (2016). Afferent Inputs to Neurotransmitter-Defined Cell Types in the Ventral Tegmental Area. *Cell Reports* 15, 2796–2808. doi: 10.1016/j.celrep.2016.05.057.

Ferreira-Pinto, M. J., Ruder, L., Capelli, P., and Arber, S. (2018). Connecting Circuits for Supraspinal Control of Locomotion. *Neuron* 100, 361–374. doi: 10.1016/j.neuron.2018.09.015.

Ferris, M. J., Milenkovic, M., Liu, S., Mielnik, C. A., Beerepoot, P., John, C. E., et al. (2014). Sustained *N* -methyl- D -aspartate receptor hypofunction remodels the dopamine system and impairs phasic signaling. *Eur J Neurosci* 40, 2255–2263. doi: 10.1111/ejn.12594.

Fields, H. L., Hjelmstad, G. O., Margolis, E. B., and Nicola, S. M. (2007). Ventral Tegmental Area Neurons in Learned Appetitive Behavior and Positive Reinforcement. *Annu. Rev. Neurosci.* 30, 289–316. doi: 10.1146/annurev.neuro.30.051606.094341.

Fink, J. S., and Smith, G. P. (1979). Decreased locomotor and investigatory exploration after denervation of catecholamine terminal fields in the forebrain of rats. *Journal of Comparative and Physiological Psychology* 93, 34–65. doi: 10.1037/h0077587.

Fraser, K. A., Poucet, B., Partlow, G., and Herrmann, T. (1991). Role of the medial and lateral septum in a variable goal spatial problem solving task. *Physiology & Behavior* 50, 739–744. doi: 10.1016/0031-9384(91)90011-C.

Fuhrmann, F., Justus, D., Sosulina, L., Kaneko, H., Beutel, T., Friedrichs, D., et al. (2015). Locomotion, Theta Oscillations, and the Speed-Correlated Firing of Hippocampal Neurons Are Controlled by a Medial Septal Glutamatergic Circuit. *Neuron* 86, 1253–1264. doi: 10.1016/j.neuron.2015.05.001.

Fuxe, K. (1965). Evidence for the existence of monoamine neurons in the central nervous system. *Zeitschrift für Zellforschung* 65, 573–596. doi: 10.1007/BF00337069.

Gallo, M. (n.d.). Chapter 8 Reversible Inactivation of Brain Circuits in Learning and Memory Research.

Geisler, C., Robbe, D., Zugaro, M., Sirota, A., and Buzsáki, G. (2007a). Hippocampal place cell assemblies are speed-controlled oscillators. *Proceedings of the National Academy of Sciences* 104, 8149–8154. doi: 10.1073/pnas.0610121104.

Geisler, S., Derst, C., Veh, R. W., and Zahm, D. S. (2007b). Glutamatergic Afferents of the Ventral Tegmental Area in the Rat. *Journal of Neuroscience* 27, 5730–5743. doi: 10.1523/JNEUROSCI.0012-07.2007.

Geisler, S., and Zahm, D. S. (2006). On the retention of neurotensin in the ventral tegmental area (VTA) despite destruction of the main neurotensinergic afferents of the VTA — Implications for the organization of forebrain projections to the VTA. *Brain Research* 1087, 87–104. doi: 10.1016/j.brainres.2006.02.108.

Georges, F., and Aston-Jones, G. (2001). Potent Regulation of Midbrain Dopamine Neurons by the Bed Nucleus of the Stria Terminalis. *J. Neurosci.* 21, RC160–RC160. doi: 10.1523/JNEUROSCI.21-16-j0003.2001.

Gillies, G. E., Virdee, K., McArthur, S., and Dalley, J. W. (2014). Sex-dependent diversity in ventral tegmental dopaminergic neurons and developmental programing: A molecular, cellular and behavioral analysis. *Neuroscience* 282, 69–85. doi: 10.1016/j.neuroscience.2014.05.033.

Góis, Z. H. T. D., and Tort, A. B. L. (2018). Characterizing Speed Cells in the Rat Hippocampus. *Cell Reports* 25, 1872-1884.e4. doi: 10.1016/j.celrep.2018.10.054.

Gordon, F. J., and Johnson, A. K. (1981). Electrical stimulation of the septal area in the rat: Prolonged suppression of water intake and correlation with self-stimulation. *Brain Research* 206, 421–430. doi: 10.1016/0006-8993(81)90542-4.

Grace, A. A., Floresco, S. B., Goto, Y., and Lodge, D. J. (2007). Regulation of firing of dopaminergic neurons and control of goal-directed behaviors. *Trends in Neurosciences* 30, 220–227. doi: 10.1016/j.tins.2007.03.003.

Griffith, W. H., and Matthews, R. T. (1986). Electrophysiology of AChE-positive neurons in basal forebrain slices. *Neuroscience Letters* 71, 169–174. doi: 10.1016/0304-3940(86)90553-7.

Haluk, D. M., and Floresco, S. B. (2009). Ventral striatal dopamine modulation of different forms of behavioral flexibility. *Neuropsychopharmacology* 34, 2041–2052. doi: 10.1038/npp.2009.21.

Hangya, B., Borhegyi, Z., Szilágyi, N., Freund, T. F., and Varga, V. (2009). GABAergic Neurons of the Medial Septum Lead the Hippocampal Network during Theta Activity. *J Neurosci* 29, 8094–8102. doi: 10.1523/JNEUROSCI.5665-08.2009.

Hasselmo, M. E., and McGaughy, J. (2004). “High acetylcholine levels set circuit dynamics for attention and encoding and low acetylcholine levels set dynamics for consolidation,” in *Progress in Brain Research* (Elsevier), 207–231. doi: 10.1016/S0079-6123(03)45015-2.

Hjelmstad, G. O., Xia, Y., Margolis, E. B., and Fields, H. L. (2013). Opioid Modulation of Ventral Pallidal Afferents to Ventral Tegmental Area Neurons. *J. Neurosci.* 33, 6454–6459. doi: 10.1523/JNEUROSCI.0178-13.2013.

Hnasko, T. S., Chuhma, N., Zhang, H., Goh, G. Y., Sulzer, D., Palmiter, R. D., et al. (2010). Vesicular Glutamate Transport Promotes Dopamine Storage and Glutamate Corelease In Vivo. *Neuron* 65, 643–656. doi: 10.1016/j.neuron.2010.02.012.

Hnasko, T. S., Hjelmstad, G. O., Fields, H. L., and Edwards, R. H. (2012). Ventral Tegmental Area Glutamate Neurons: Electrophysiological Properties and Projections. *Journal of Neuroscience* 32, 15076–15085. doi: 10.1523/JNEUROSCI.3128-12.2012.

Hollup, S. A., Kjelstrup, K. G., Hoff, J., Moser, M.-B., and Moser, E. I. (2001). Impaired Recognition of the Goal Location during Spatial Navigation in Rats with Hippocampal Lesions. *J. Neurosci.* 21, 4505–4513. doi: 10.1523/JNEUROSCI.21-12-04505.2001.

Hooks, M. S., and Kalivas, P. W. (1995). The role of mesoaccumbens-pallidal circuitry in novelty-induced behavioral activation. *Neuroscience* 64, 587–597. doi: 10.1016/0306-4522(94)00409-X.

Horvitz, J. C. (2000). Mesolimbocortical and nigrostriatal dopamine responses to salient non-reward events. *Neuroscience* 96, 651–656. doi: 10.1016/S0306-4522(00)00019-1.

Hosp, J. A., Pekanovic, A., Rioult-Pedotti, M. S., and Luft, A. R. (2011). Dopaminergic Projections from Midbrain to Primary Motor Cortex Mediate Motor Skill Learning. *Journal of Neuroscience* 31, 2481–2487. doi: 10.1523/JNEUROSCI.5411-10.2011.

Howe, M. W., and Dombeck, D. A. (2016). Rapid signalling in distinct dopaminergic axons during locomotion and reward. *Nature* 535, 505–510. doi: 10.1038/nature18942.

Hsu, A. I., and Yttri, E. A. (2021). B-SOiD, an open-source unsupervised algorithm for identification and fast prediction of behaviors. *Nat Commun* 12, 5188. doi: 10.1038/s41467-021-25420-x.

Hughes, R. N., Bakhurin, K. I., Petter, E. A., Watson, G. D. R., Kim, N., Friedman, A. D., et al. (2020). Ventral Tegmental Dopamine Neurons Control the Impulse Vector during Motivated Behavior. *Current Biology* 30, 2681-2694.e5. doi: 10.1016/j.cub.2020.05.003.

Huh, C. Y. L., Goutagny, R., and Williams, S. (2010). Glutamatergic Neurons of the Mouse Medial Septum and Diagonal Band of Broca Synaptically Drive Hippocampal Pyramidal Cells: Relevance for Hippocampal Theta Rhythm. *Journal of Neuroscience* 30, 15951–15961. doi: 10.1523/JNEUROSCI.3663-10.2010.

Ikemoto, S. (2007). Dopamine reward circuitry: Two projection systems from the ventral midbrain to the nucleus accumbens–olfactory tubercle complex. *Brain Research Reviews* 56, 27–78. doi: 10.1016/j.brainresrev.2007.05.004.

Ikemoto, S., and Bonci, A. (2014). Neurocircuitry of drug reward. *Neuropharmacology* 76, 329–341. doi: 10.1016/j.neuropharm.2013.04.031.

Inoue, T., Ota, M., Ogawa, M., Mikoshiba, K., and Aruga, J. (2007). Zic1 and Zic3 Regulate Medial Forebrain Development through Expansion of Neuronal Progenitors. *J. Neurosci.* 27, 5461–5473. doi: 10.1523/JNEUROSCI.4046-06.2007.

Jarrard, L. E. (1993). On the role of the hippocampus in learning and memory in the rat. *Behavioral and Neural Biology* 60, 9–26. doi: 10.1016/0163-1047(93)90664-4.

Jiang, Y.-Y., Zhang, Y., Cui, S., Liu, F.-Y., Yi, M., and Wan, Y. (2018). Cholinergic neurons in medial septum maintain anxiety-like behaviors induced by chronic inflammatory pain. *Neuroscience Letters* 671, 7–12. doi: 10.1016/j.neulet.2018.01.041.

Joo, H. R., and Frank, L. M. (2018). The hippocampal sharp wave–ripple in memory retrieval for immediate use and consolidation. *Nat Rev Neurosci* 19, 744–757. doi: 10.1038/s41583-018-0077-1.

Justus, D., Dalügge, D., Bothe, S., Fuhrmann, F., Hannes, C., Kaneko, H., et al. (2017). Glutamatergic synaptic integration of locomotion speed via septoentorhinal projections. *Nat Neurosci* 20, 16–19. doi: 10.1038/nn.4447.

Kalivas, P. W. (1993). Neurotransmitter regulation of dopamine neurons in the ventral tegmental area. *Brain Research Reviews* 18, 75–113. doi: 10.1016/0165-0173(93)90008-N.

Kalivas, P. W., Burgess, S. K., Nemeroff, C. B., and Prange, A. J. (1983). Behavioral and neurochemical effects of neurotensin microinjection into the ventral tegmental area of the rat. *Neuroscience* 8, 495–505. doi: 10.1016/0306-4522(83)90195-1.

Kawano, M., Kawasaki, A., Sakata-Haga, H., Fukui, Y., Kawano, H., Nogami, H., et al. (2006). Particular subpopulations of midbrain and hypothalamic dopamine neurons express vesicular glutamate transporter 2 in the rat brain. *J. Comp. Neurol.* 498, 581–592. doi: 10.1002/cne.21054.

Kempadoo, K. A., Tourino, C., Cho, S. L., Magnani, F., Leinninger, G.-M., Stuber, G. D., et al. (2013). Hypothalamic Neurotensin Projections Promote Reward by Enhancing Glutamate Transmission in the VTA. *Journal of Neuroscience* 33, 7618–7626. doi: 10.1523/JNEUROSCI.2588-12.2013.

Kesner, A. J., Calva, C. B., and Ikemoto, S. (2022). Seeking motivation and reward: Roles of dopamine, hippocampus, and supramammillo-septal pathway. *Progress in Neurobiology* 212, 102252. doi: 10.1016/j.pneurobio.2022.102252.

Kesner, A. J., Shin, R., Calva, C. B., Don, R. F., Junn, S., Potter, C. T., et al. (2021). Supramammillary neurons projecting to the septum regulate dopamine and motivation for environmental interaction in mice. *Nat Commun* 12, 2811. doi: 10.1038/s41467-021-23040-z.

Kocsis, B., Martínez-Bellver, S., Fiáth, R., Domonkos, A., Sviatkó, K., Schlingloff, D., et al. (2022). Huygens synchronization of medial septal pacemaker neurons generates hippocampal theta oscillation. *Cell Rep* 40, 111149. doi: 10.1016/j.celrep.2022.111149.

Koenig, J., Linder, A. N., Leutgeb, J. K., and Leutgeb, S. (2011). The Spatial Periodicity of Grid Cells Is Not Sustained During Reduced Theta Oscillations. *Science* 332, 592–595. doi: 10.1126/science.1201685.

Korvasová, K., Ludwig, F., Kaneko, H., Sosulina, L., Tetzlaff, T., Remy, S., et al. (2021). Locomotion induced by medial septal glutamatergic neurons is linked to intrinsically generated persistent firing. 2021.04.23.441122. doi: 10.1101/2021.04.23.441122.

Koyama, S., and Appel, S. B. (2006). A-type K^+ Current of Dopamine and GABA Neurons in the Ventral Tegmental Area. *Journal of Neurophysiology* 96, 544–554. doi: 10.1152/jn.01318.2005.

Kramis, R., Vanderwolf, C. H., and Bland, B. H. (1975). Two types of hippocampal rhythmical slow activity in both the rabbit and the rat: Relations to behavior and effects of atropine, diethyl ether, urethane, and pentobarbital. *Experimental Neurology* 49, 58–85. doi: 10.1016/0014-4886(75)90195-8.

Kremer, Y., Flakowski, J., Rohner, C., and Lüscher, C. (2020). Context-Dependent Multiplexing by Individual VTA Dopamine Neurons. *J. Neurosci.* 40, 7489–7509. doi: 10.1523/JNEUROSCI.0502-20.2020.

Kudo, T., Uchigashima, M., Miyazaki, T., Konno, K., Yamasaki, M., Yanagawa, Y., et al. (2012). Three Types of Neurochemical Projection from the Bed Nucleus of the Stria Terminalis to the Ventral Tegmental Area in Adult Mice. *J. Neurosci.* 32, 18035–18046. doi: 10.1523/JNEUROSCI.4057-12.2012.

Kurnikova, A., Moore, J. D., Liao, S.-M., Deschênes, M., and Kleinfeld, D. (2017). Coordination of Orofacial Motor Actions into Exploratory Behavior by Rat. *Current Biology* 27, 688–696. doi: 10.1016/j.cub.2017.01.013.

Lammel, S., Hetzel, A., Häckel, O., Jones, I., Liss, B., and Roeper, J. (2008). Unique Properties of Mesoprefrontal Neurons within a Dual Mesocorticolimbic Dopamine System. *Neuron* 57, 760–773. doi: 10.1016/j.neuron.2008.01.022.

Lanuza, E., and Martínez-García, F. (2009). “Evolution of Septal Nuclei,” in *Encyclopedia of Neuroscience*, eds. M. D. Binder, N. Hirokawa, and U. Windhorst (Berlin, Heidelberg: Springer), 1270–1278. doi: 10.1007/978-3-540-29678-2_3139.

Lee, C., Lavoie, A., Liu, J., Chen, S. X., and Liu, B. (2020). Light Up the Brain: The Application of Optogenetics in Cell-Type Specific Dissection of Mouse Brain Circuits. *Frontiers in Neural Circuits* 14. Available at: https://www.frontiersin.org/articles/10.3389/fncir.2020.00018 [Accessed March 2, 2023].

Lee, E. H. Y., Lin, Y. P., and Yin, T. H. (1988). Effects of lateral and medial septal lesions on various activity and reactivity measures in rats. *Physiology & Behavior* 42, 97–102. doi: 10.1016/0031-9384(88)90267-3.

Lever, C., Burton, S., and O’Keefe, J. (2006). Rearing on hind legs, environmental novelty, and the hippocampal formation. *Rev Neurosci* 17, 111–133. doi: 10.1515/revneuro.2006.17.1-2.111.

Lisman, J. E., and Grace, A. A. (2005). The Hippocampal-VTA Loop: Controlling the Entry of Information into Long-Term Memory. *Neuron* 46, 703–713. doi: 10.1016/j.neuron.2005.05.002.

Liu, Y., Harding, M., Pittman, A., Dore, J., Striessnig, J., Rajadhyaksha, A., et al. (2014). Ca $_{v}$ 1.2 and Ca $_{v}$ 1.3 L-type calcium channels regulate dopaminergic firing activity in the mouse ventral tegmental area. *Journal of Neurophysiology* 112, 1119–1130. doi: 10.1152/jn.00757.2013.

Luxem, K., Mocellin, P., Fuhrmann, F., Kürsch, J., Miller, S. R., Palop, J. J., et al. (2022). Identifying behavioral structure from deep variational embeddings of animal motion. *Commun Biol* 5, 1267. doi: 10.1038/s42003-022-04080-7.

Magno, L., Asgarian, Z., Apanaviciute, M., Milner, Y., Bengoa-Vergniory, N., Rubin, A. N., et al. (2022). Fate mapping reveals mixed embryonic origin and unique developmental codes of mouse forebrain septal neurons. *Commun Biol* 5, 1137. doi: 10.1038/s42003-022-04066-5.

Magno, L., Barry, C., Schmidt-Hieber, C., Theodotou, P., Häusser, M., and Kessaris, N. (2017). NKX2-1 Is Required in the Embryonic Septum for Cholinergic System Development, Learning, and Memory. *Cell Reports* 20, 1572–1584. doi: 10.1016/j.celrep.2017.07.053.

Manseau, F., Danik, M., and Williams, S. (2005). A functional glutamatergic neurone network in the medial septum and diagonal band area: Local glutamatergic network in the medial septum. *The Journal of Physiology* 566, 865–884. doi: 10.1113/jphysiol.2005.089664.

Margolis, E. B., Coker, A. R., Driscoll, J. R., Lemaître, A.-I., and Fields, H. L. (2010). Reliability in the Identification of Midbrain Dopamine Neurons. *PLOS ONE* 5, e15222. doi: 10.1371/journal.pone.0015222.

Margolis, E. B., Lock, H., Hjelmstad, G. O., and Fields, H. L. (2006). The ventral tegmental area revisited: is there an electrophysiological marker for dopaminergic neurons?:

Electrophysiological properties of VTA neurons. *The Journal of Physiology* 577, 907–924. doi: 10.1113/jphysiol.2006.117069.

Margolis, E. B., Toy, B., Himmels, P., Morales, M., and Fields, H. L. (2012). Identification of Rat Ventral Tegmental Area GABAergic Neurons. *PLoS ONE* 7, e42365. doi: 10.1371/journal.pone.0042365.

Markus, E., Qin, Y., Leonard, B., Skaggs, W., McNaughton, B., and Barnes, C. (1995). Interactions between location and task affect the spatial and directional firing of hippocampal neurons. *J. Neurosci.* 15, 7079–7094. doi: 10.1523/JNEUROSCI.15-11-07079.1995.

Martin, J. H., and Ghez, C. (1999). Pharmacological inactivation in the analysis of the central control of movement. *Journal of Neuroscience Methods* 86, 145–159. doi: 10.1016/S0165-0270(98)00163-0.

Mathis, A., Mamidanna, P., Cury, K. M., Abe, T., Murthy, V. N., Mathis, M. W., et al. (2018). DeepLabCut: markerless pose estimation of user-defined body parts with deep learning. *Nat Neurosci* 21, 1281–1289. doi: 10.1038/s41593-018-0209-y.

Matthews, G. A., and Tye, K. M. (2019). Neural mechanisms of social homeostasis. *Annals of the New York Academy of Sciences* 1457, 5–25. doi: 10.1111/nyas.14016.

McGovern, D. J., Polter, A. M., and Root, D. H. (2020). Neurochemical signaling of reward and aversion by ventral tegmental area glutamate neurons. Neuroscience doi: 10.1101/2020.05.18.103234.

McHenry, J. A., Otis, J. M., Rossi, M. A., Robinson, J. E., Kosyk, O., Miller, N. W., et al. (2017). Hormonal gain control of a medial preoptic area social reward circuit. *Nat Neurosci* 20, 449–458. doi: 10.1038/nn.4487.

McNamara, C. G., Tejero-Cantero, Á., Trouche, S., Campo-Urriza, N., and Dupret, D. (2014). Dopaminergic neurons promote hippocampal reactivation and spatial memory persistence. *Nat Neurosci* 17, 1658–1660. doi: 10.1038/nn.3843.

Meibach, R. C., and Siegel, A. (1977). Efferent connections of the septal area in the rat: An analysis utilizing retrograde and anterograde transport methods. *Brain Research* 119, 1–20. doi: 10.1016/0006-8993(77)90088-9.

Melzer, S., Michael, M., Caputi, A., Eliava, M., Fuchs, E. C., Whittington, M. A., et al. (2012). Long-range-projecting GABAergic neurons modulate inhibition in hippocampus and entorhinal cortex. *Science* 335, 1506–1510. doi: 10.1126/science.1217139.

Meye, F. J., and Adan, R. A. H. (2014). Feelings about food: the ventral tegmental area in food reward and emotional eating. *Trends in Pharmacological Sciences* 35, 31–40. doi: 10.1016/j.tips.2013.11.003.

Mikulovic, S., Restrepo, C. E., Siwani, S., Bauer, P., Pupe, S., Tort, A. B. L., et al. (2018). Ventral hippocampal OLM cells control type 2 theta oscillations and response to predator odor. *Nat Commun* 9, 3638. doi: 10.1038/s41467-018-05907-w.

Mingote, S., Amsellem, A., Kempf, A., Rayport, S., and Chuhma, N. (2019). Dopamine-glutamate neuron projections to the nucleus accumbens medial shell and behavioral switching. *Neurochemistry International* 129, 104482. doi: 10.1016/j.neuint.2019.104482.

Miranda-Barrientos, J., Chambers, I., Mongia, S., Liu, B., Wang, H., Mateo-Semidey, G. E., et al. (2021). Ventral tegmental area GABA, glutamate, and glutamate-GABA neurons are heterogeneous in their electrophysiological and pharmacological properties. *Eur J Neurosci* 54, 4061–4084. doi: 10.1111/ejn.15156.

Mirenowicz, J., and Schultz, W. (1994). Importance of unpredictability for reward responses in primate dopamine neurons. *Journal of Neurophysiology* 72, 1024–1027. doi: 10.1152/jn.1994.72.2.1024.

Mishra, A., Marzban, N., Cohen, M. X., and Englitz, B. (2021). Dynamics of Neural Microstates in the VTA–Striatal–Prefrontal Loop during Novelty Exploration in the Rat. *J. Neurosci.* 41, 6864–6877. doi: 10.1523/JNEUROSCI.2256-20.2021.

Mocellin, P., and Mikulovic, S. (2021). The Role of the Medial Septum—Associated Networks in Controlling Locomotion and Motivation to Move. *Front. Neural Circuits* 15, 699798. doi: 10.3389/fncir.2021.699798.

Mogenson, G. J., and Huang, Y. H. (1973). The neurobiology of motivated behavior. *Progress in Neurobiology* 1, 53–83. doi: 10.1016/0301-0082(73)90056-7.

Mogenson, G. J., Wu, M., and Jones, D. L. (1980a). Locomotor activity elicited by injections of picrotoxin into the ventral tegmental area is attenuated by injections of GABA into the globus pallidus. *Brain Research* 191, 569–571. doi: 10.1016/0006-8993(80)91308-6.

Mogenson, G., Jones, D., and Yim, C. (1980b). From motivation to action: Functional interface between the limbic system and the motor system. *Progress in Neurobiology* 14, 69–97. doi: 10.1016/0301-0082(80)90018-0.

Mohebi, A., Pettibone, J. R., Hamid, A. A., Wong, J.-M. T., Vinson, L. T., Patriarchi, T., et al. (2019). Dissociable dopamine dynamics for learning and motivation. *Nature* 570, 65–70. doi: 10.1038/s41586-019-1235-y.

Morales, M., and Margolis, E. B. (2017). Ventral tegmental area: cellular heterogeneity, connectivity and behaviour. *Nat Rev Neurosci* 18, 73–85. doi: 10.1038/nrn.2016.165.

Morrens, J., Aydin, Ç., Janse van Rensburg, A., Esquivelzeta Rabell, J., and Haesler, S. (2020). Cue-Evoked Dopamine Promotes Conditioned Responding during Learning. *Neuron* 106, 142-153.e7. doi: 10.1016/j.neuron.2020.01.012.

Nagaeva, E., Zubarev, I., Bengtsson Gonzales, C., Forss, M., Nikouei, K., de Miguel, E., et al. (2020). Heterogeneous somatostatin-expressing neuron population in mouse ventral tegmental area. *eLife* 9, e59328. doi: 10.7554/eLife.59328.

Nagahara, A. H., and McGaugh, J. L. (1992). Muscimol infused into the medial septal area impairs long-term memory but not short-term memory in inhibitory avoidance, water maze place learning and rewarded alternation tasks. *Brain Research* 591, 54–61. doi: 10.1016/0006-8993(92)90977-H.

Nair-Roberts, R. G., Chatelain-Badie, S. D., Benson, E., White-Cooper, H., Bolam, J. P., and Ungless, M. A. (2008). Stereological estimates of dopaminergic, GABAergic and glutamatergic neurons in the ventral tegmental area, substantia nigra and retrorubral field in the rat. *Neuroscience* 152, 1024–1031. doi: 10.1016/j.neuroscience.2008.01.046.

Nauta, W. J. (1958). Hippocampal projections and related neural pathways to the midbrain in the cat. *Brain* 81, 319–340. doi: 10.1093/brain/81.3.319.

Nestler, E. J., and Carlezon, W. A. (2006). The Mesolimbic Dopamine Reward Circuit in Depression. *Biological Psychiatry* 59, 1151–1159. doi: 10.1016/j.biopsych.2005.09.018.

Nieh, E. H., Vander Weele, C. M., Matthews, G. A., Presbrey, K. N., Wichmann, R., Leppla, C. A., et al. (2016). Inhibitory Input from the Lateral Hypothalamus to the Ventral Tegmental Area Disinhibits Dopamine Neurons and Promotes Behavioral Activation. *Neuron* 90, 1286–1298. doi: 10.1016/j.neuron.2016.04.035.

Ntamati, N. R., and Lüscher, C. (2016). VTA Projection Neurons Releasing GABA and Glutamate in the Dentate Gyrus. *eneuro* 3, ENEURO.0137-16.2016. doi: 10.1523/ENEURO.0137-16.2016.

Oades, R. D., and Halliday, G. M. (1987). Ventral tegmental (A10) system: neurobiology. 1. Anatomy and connectivity. *Brain Res* 434, 117–165. doi: 10.1016/0165-0173(87)90011-7.

O'Keefe, J., and Nadel, L. (1978). *The Hippocampus as a Cognitive Map*. Oxford, UK: Oxford University Press Available at: http://www.cognitivemap.net/ [Accessed March 2, 2023].

Olds, J., and Milner, P. (1954). Positive reinforcement produced by electrical stimulation of septal area and other regions of rat brain. *Journal of Comparative and Physiological Psychology* 47, 419–427. doi: 10.1037/h0058775.

Olpe, H.-R., Koella, W. P., Wolf, P., and Haas, H. L. (1977). The action of Baclofen on neurons of the substantia nigra and of the ventral tegmental area. *Brain Research* 134, 577–580. doi: 10.1016/0006-8993(77)90834-4.

Olson, V. G. (2005). Regulation of Drug Reward by cAMP Response Element-Binding Protein: Evidence for Two Functionally Distinct Subregions of the Ventral Tegmental Area. *Journal of Neuroscience* 25, 5553–5562. doi: 10.1523/JNEUROSCI.0345-05.2005.

Olson, V. G., and Nestler, E. J. (2007). Topographical organization of GABAergic neurons within the ventral tegmental area of the rat. *Synapse* 61, 87–95. doi: 10.1002/syn.20345.

Omelchenko, N., Bell, R., and Sesack, S. R. (2009). Lateral habenula projections to dopamine and GABA neurons in the rat ventral tegmental area. *European Journal of Neuroscience* 30, 1239–1250. doi: 10.1111/j.1460-9568.2009.06924.x.

Omelchenko, N., and Sesack, S. R. (2005). Laterodorsal tegmental projections to identified cell populations in the rat ventral tegmental area. *Journal of Comparative Neurology* 483, 217–235. doi: 10.1002/cne.20417.

Omelchenko, N., and Sesack, S. R. (2007). Glutamate synaptic inputs to ventral tegmental area neurons in the rat derive primarily from subcortical sources. *Neuroscience* 146, 1259–1274. doi: 10.1016/j.neuroscience.2007.02.016.

Omelchenko, N., and Sesack, S. R. (2010). Periaqueductal gray afferents synapse onto dopamine and GABA neurons in the rat ventral tegmental area. *Journal of Neuroscience Research* 88, 981–991. doi: 10.1002/jnr.22265.

Orzeł-Gryglewska, J., Jurkowlaniec, E., and Trojniar, W. (2006). Microinjection of procaine and electrolytic lesion in the ventral tegmental area suppresses hippocampal theta rhythm in urethane-anesthetized rats. *Brain Research Bulletin* 68, 295–309. doi: 10.1016/j.brainresbull.2005.08.026.

Overton, P. G., and Clark, D. (1997). Burst firing in midbrain dopaminergic neurons. *Brain Research Reviews* 25, 312–334. doi: 10.1016/S0165-0173(97)00039-8.

Overton, P. G., Vautrelle, N., and Redgrave, P. (2014). Sensory regulation of dopaminergic cell activity: Phenomenology, circuitry and function. *Neuroscience* 282, 1–12. doi: 10.1016/j.neuroscience.2014.01.023.

Parker, S. M., and Sinnamon, H. M. (1983). Forward locomotion elicited by electrical stimulation in the diencephalon and mesencephalon of the awake rat. *Physiology & Behavior* 31, 581–587.

Paxinos, G., and Franklin, K. B. J. (2019). *Paxinos and Franklin's the Mouse Brain in Stereotaxic Coordinates*. Academic Press.

Petzold, A., van den Munkhof, H. E., Figge-Schlensok, R., and Korotkova, T. (2023). Complementary lateral hypothalamic populations resist hunger pressure to balance nutritional and social needs. *Cell Metabolism*. doi: 10.1016/j.cmet.2023.02.008.

Phillipson, O. T. (1979). The cytoarchitecture of the interfascicular nucleus and ventral tegmental area of tsai in the rat. *J. Comp. Neurol.* 187, 85–98. doi: 10.1002/cne.901870106.

Picciotto, M. R., Higley, M. J., and Mineur, Y. S. (2012). Acetylcholine as a Neuromodulator: Cholinergic Signaling Shapes Nervous System Function and Behavior. *Neuron* 76, 116–129. doi: 10.1016/j.neuron.2012.08.036.

Pignatelli, M., Beyeler, A., and Leinekugel, X. (2012). Neural circuits underlying the generation of theta oscillations. *Journal of Physiology-Paris* 106, 81–92. doi: 10.1016/j.jphysparis.2011.09.007.

Poirier, L. J., Giguére, M., and Marchand, R. (1983). Comparative morphology of the substantia nigra and ventral tegmental area in the monkey, cat and rat. *Brain Research Bulletin* 11, 371–397. doi: 10.1016/0361-9230(83)90173-9.

Qi, J., Zhang, S., Wang, H.-L., Wang, H., de Jesus Aceves Buendia, J., Hoffman, A. F., et al. (2014). A glutamatergic reward input from the dorsal raphe to ventral tegmental area dopamine neurons. *Nat Commun* 5, 5390. doi: 10.1038/ncomms6390.

Qualls-Creekmore, E., Yu, S., Francois, M., Hoang, J., Huesing, C., Bruce-Keller, A., et al. (2017). Galanin-Expressing GABA Neurons in the Lateral Hypothalamus Modulate Food Reward and Noncompulsive Locomotion. *J. Neurosci.* 37, 6053–6065. doi: 10.1523/JNEUROSCI.0155-17.2017.

Ranade, S., Hangya, B., and Kepecs, A. (2013). Multiple Modes of Phase Locking between Sniffing and Whisking during Active Exploration. *Journal of Neuroscience* 33, 8250–8256. doi: 10.1523/JNEUROSCI.3874-12.2013.

Robinson, J., Manseau, F., Ducharme, G., Amilhon, B., Vigneault, E., El Mestikawy, S., et al. (2016). Optogenetic Activation of Septal Glutamatergic Neurons Drive Hippocampal Theta Rhythms. *Journal of Neuroscience* 36, 3016–3023. doi: 10.1523/JNEUROSCI.2141-15.2016.

Root, D. H., Barker, D. J., Estrin, D. J., Miranda-Barrientos, J. A., Liu, B., Zhang, S., et al. (2020). Distinct Signaling by Ventral Tegmental Area Glutamate, GABA, and Combinatorial Glutamate-GABA Neurons in Motivated Behavior. *Cell Reports* 32, 108094. doi: 10.1016/j.celrep.2020.108094.

Root, D. H., Estrin, D. J., and Morales, M. (2018). Aversion or Salience Signaling by Ventral Tegmental Area Glutamate Neurons. *iScience* 2, 51–62. doi: 10.1016/j.isci.2018.03.008.

Root, D. H., Mejias-Aponte, C. A., Zhang, S., Wang, H.-L., Hoffman, A. F., Lupica, C. R., et al. (2014). Single rodent mesohabenular axons release glutamate and GABA. *Nat Neurosci* 17, 1543–1551. doi: 10.1038/nn.3823.

Rost, B. R., Wietek, J., Yizhar, O., and Schmitz, D. (2022). Optogenetics at the presynapse. *Nat Neurosci* 25, 984–998. doi: 10.1038/s41593-022-01113-6.

Sanchez-Catalan, M. J., Kaufling, J., Georges, F., Veinante, P., and Barrot, M. (2014). The antero-posterior heterogeneity of the ventral tegmental area. *Neuroscience* 282, 198–216. doi: 10.1016/j.neuroscience.2014.09.025.

Schultz, W. (1997). Dopamine neurons and their role in reward mechanisms. *Current Opinion in Neurobiology* 7, 191–197. doi: 10.1016/S0959-4388(97)80007-4.

Schultz, W. (1999). The Reward Signal of Midbrain Dopamine Neurons. *Physiology* 14, 249–255. doi: 10.1152/physiologyonline.1999.14.6.249.

Schultz, W. (2016). Dopamine reward prediction-error signalling: a two-component response. *Nat Rev Neurosci* 17, 183–195. doi: 10.1038/nrn.2015.26.

Scott, N., Prigge, M., Yizhar, O., and Kimchi, T. (2015). A sexually dimorphic hypothalamic circuit controls maternal care and oxytocin secretion. *Nature* 525, 519–522. doi: 10.1038/nature15378.

Sheffield, M. E. J., Edgerton, G. B., Heuermann, R. J., Deemyad, T., Mensh, B. D., and Spruston, N. (2013). Mechanisms of retroaxonal barrage firing in hippocampal interneurons. *The Journal of Physiology* 591, 4793–4805. doi: 10.1113/jphysiol.2013.258418.

Simon, P., Dupuis, R., and Costentin, J. (1994). Thigmotaxis as an index of anxiety in mice. Influence of dopaminergic transmissions. *Behavioural Brain Research* 61, 59–64. doi: 10.1016/0166-4328(94)90008-6.

Sinnamon, H., Lee, S., Adams, D., and Stopford, C. (1984). Locomotor stepping elicited by electrical stimulation of the lateral hypothalamus requires an ipsilateral descending pathway☆. *Physiology & Behavior* 33, 209–215. doi: 10.1016/0031-9384(84)90101-X.

Sinnamon, H. M. (1993). Preoptic and hypothalamic neurons and the initiation of locomotion in the anesthetized rat. *Progress in Neurobiology* 41, 323–344. doi: 10.1016/0301-0082(93)90003-B.

Sinnamon, H. M. (2006). Decline in hippocampal theta activity during cessation of locomotor approach sequences: Amplitude leads frequency and relates to instrumental behavior. *Neuroscience* 140, 779–790. doi: 10.1016/j.neuroscience.2006.02.058.

Smythe, J. W., Colom, L. V., and Bland, B. H. (1992). The extrinsic modulation of hippocampal theta depends on the coactivation of cholinergic and GABA-ergic medial septal inputs. *Neuroscience & Biobehavioral Reviews* 16, 289–308. doi: 10.1016/S0149-7634(05)80203-9.

Sotty, F., Danik, M., Manseau, F., Laplante, F., Quirion, R., and Williams, S. (2003). Distinct electrophysiological properties of glutamatergic, cholinergic and GABAergic rat

septohippocampal neurons: novel implications for hippocampal rhythmicity. *The Journal of Physiology* 551, 927–943. doi: 10.1113/jphysiol.2003.046847.

Steffensen, S. C., Svingos, A. L., Pickel, V. M., and Henriksen, S. J. (1998). Electrophysiological Characterization of GABAergic Neurons in the Ventral Tegmental Area. *J. Neurosci.* 18, 8003–8015. doi: 10.1523/JNEUROSCI.18-19-08003.1998.

Stuber, G. D., Sparta, D. R., Stamatakis, A. M., van Leeuwen, W. A., Hardjoprajitno, J. E., Cho, S., et al. (2011). Excitatory transmission from the amygdala to nucleus accumbens facilitates reward seeking. *Nature* 475, 377–380. doi: 10.1038/nature10194.

Sturman, O., Germain, P.-L., and Bohacek, J. (2018). Exploratory rearing: a context- and stress-sensitive behavior recorded in the open-field test. *Stress* 21, 443–452. doi: 10.1080/10253890.2018.1438405.

Swanson, L. W. (1982). The projections of the ventral tegmental area and adjacent regions: A combined fluorescent retrograde tracer and immunofluorescence study in the rat. *Brain Research Bulletin* 9, 321–353. doi: 10.1016/0361-9230(82)90145-9.

Tan, K. R., Yvon, C., Turiault, M., Mirzabekov, J. J., Doehner, J., Labouèbe, G., et al. (2012). GABA Neurons of the VTA Drive Conditioned Place Aversion. *Neuron* 73, 1173–1183. doi: 10.1016/j.neuron.2012.02.015.

Tolman, E. C. (1948). Cognitive maps in rats and men. *Psychological Review* 55, 189–208. doi: 10.1037/h0061626.

Tracy, M. E., Tesic, V., Stamenic, T. T., Joksimovic, S. M., Busquet, N., Jevtovic-Todorovic, V., et al. (2018). CaV3.1 isoform of T-type calcium channels supports excitability of rat and mouse ventral tegmental area neurons. *Neuropharmacology* 135, 343–354. doi: 10.1016/j.neuropharm.2018.03.028.

Tsai, C. (1925). The optic tracts and centers of the opossum. Didelphis virginiana. *Journal of Comparative Neurology* 39, 173–216. doi: 10.1002/cne.900390202.

Turrero García, M., Stegmann, S. K., Lacey, T. E., Reid, C. M., Hrvatin, S., Weinreb, C., et al. (2021). Transcriptional profiling of sequentially generated septal neuron fates. *eLife* 10, e71545. doi: 10.7554/eLife.71545.

Vanderwolf, C. H. (1969). Hippocampal electrical activity and voluntary movement in the rat. *Electroencephalography and Clinical Neurophysiology* 26, 407–418. doi: 10.1016/0013-4694(69)90092-3.

van Zessen, R., Phillips, J. L., Budygin, E. A., and Stuber, G. D. (2012). Activation of VTA GABA Neurons Disrupts Reward Consumption. *Neuron* 73, 1184–1194. doi: 10.1016/j.neuron.2012.02.016.

Varga, V., Hangya, B., Kránitz, K., Ludányi, A., Zemankovics, R., Katona, I., et al. (2008). The presence of pacemaker HCN channels identifies theta rhythmic GABAergic neurons in the medial septum: Characterization of medial septal HCN neurons. *The Journal of Physiology* 586, 3893–3915. doi: 10.1113/jphysiol.2008.155242.

Vertes, R. P., and Kocsis, B. (1997). Brainstem-diencephalo-septohippocampal systems controlling the theta rhythm of the hippocampus. *Neuroscience* 81, 893–926. doi: 10.1016/s0306-4522(97)00239-x.

Vickstrom, C. R., Liu, X., Liu, S., Hu, M.-M., Mu, L., Hu, Y., et al. (2021). Role of endocannabinoid signaling in a septohabenular pathway in the regulation of anxiety- and depressive-like behavior. *Mol Psychiatry* 26, 3178–3191. doi: 10.1038/s41380-020-00905-1.

Vinogradova, O. S. (2001). Hippocampus as comparator: Role of the two input and two output systems of the hippocampus in selection and registration of information. *Hippocampus* 11, 578–598. doi: 10.1002/hipo.1073.

Vinogradova, O. S., Kitchigina, V. F., and Zenchenko, C. I. (1998). Pacemaker neurons of the forebrain medical septal area and theta rhythm of the hippocampus. *Membr Cell Biol* 11, 715–725.

Walsh, J. J., and Han, M. H. (2014). The heterogeneity of ventral tegmental area neurons: Projection functions in a mood-related context. *Neuroscience* 282, 101–108. doi: 10.1016/j.neuroscience.2014.06.006.

Walsh, T. J., Gandhi, C., and Stackman, R. W. (1998). Reversible inactivation of the medial septum or nucleus basalis impairs working memory in rats: A dissociation of memory and performance. *Behavioral Neuroscience* 112, 1114–1124. doi: 10.1037/0735-7044.112.5.1114.

Wang, H.-L., and Morales, M. (2008). Corticotropin-releasing factor binding protein within the ventral tegmental area is expressed in a subset of dopaminergic neurons. *Journal of Comparative Neurology* 509, 302–318. doi: 10.1002/cne.21751.

Wang, H.-L., Qi, J., Zhang, S., Wang, H., and Morales, M. (2015). Rewarding Effects of Optical Stimulation of Ventral Tegmental Area Glutamatergic Neurons. *Journal of Neuroscience* 35, 15948–15954. doi: 10.1523/JNEUROSCI.3428-15.2015.

Watanabe, K., Irie, K., Hanashima, C., Takebayashi, H., and Sato, N. (2018). Diencephalic progenitors contribute to the posterior septum through rostral migration along the hippocampal axonal pathway. *Sci Rep* 8, 11728. doi: 10.1038/s41598-018-30020-9.

Wei, B., Huang, Z., He, S., Sun, C., You, Y., Liu, F., et al. (2012). The onion skin-like organization of the septum arises from multiple embryonic origins to form multiple adult neuronal fates. *Neuroscience* 222, 110–123. doi: 10.1016/j.neuroscience.2012.07.016.

Wickersham, I. R., Finke, S., Conzelmann, K.-K., and Callaway, E. M. (2007). Retrograde neuronal tracing with a deletion-mutant rabies virus. *Nat Methods* 4, 47–49. doi: 10.1038/nmeth999.

Wiltschko, A. B., Johnson, M. J., Iurilli, G., Peterson, R. E., Katon, J. M., Pashkovski, S. L., et al. (2015). Mapping Sub-Second Structure in Mouse Behavior. *Neuron* 88, 1121–1135. doi: 10.1016/j.neuron.2015.11.031.

Winson, J. (1978). Loss of Hippocampal Theta Rhythm Results in Spatial Memory Deficit in the Rat. *Science* 201, 160–163. doi: 10.1126/science.663646.

Wu, Z., Autry, A. E., Bergan, J. F., Watabe-Uchida, M., and Dulac, C. G. (2014). Galanin neurons in the medial preoptic area govern parental behaviour. *Nature* 509, 325–330. doi: 10.1038/nature13307.

Wyble, B. P., Hyman, J. M., Rossi, C. A., and Hasselmo, M. E. (2004). Analysis of theta power in hippocampal EEG during bar pressing and running behavior in rats during distinct behavioral contexts. *Hippocampus* 14, 662–674. doi: 10.1002/hipo.20012.

Yamaguchi, T., Qi, J., Wang, H.-L., Zhang, S., and Morales, M. (2015). Glutamatergic and dopaminergic neurons in the mouse ventral tegmental area. *Eur J Neurosci* 41, 760–772. doi: 10.1111/ejn.12818.

Yang, H., de Jong, J. W., Tak, Y., Peck, J., Bateup, H. S., and Lammel, S. (2018). Nucleus Accumbens Subnuclei Regulate Motivated Behavior via Direct Inhibition and Disinhibition of VTA Dopamine Subpopulations. *Neuron* 97, 434-449.e4. doi: 10.1016/j.neuron.2017.12.022.

Yoo, J. H., Zell, V., Gutierrez-Reed, N., Wu, J., Ressler, R., Shenasa, M. A., et al. (2016). Ventral tegmental area glutamate neurons co-release GABA and promote positive reinforcement. *Nat Commun* 7, 13697. doi: 10.1038/ncomms13697.

Yu, X., Li, W., Ma, Y., Tossell, K., Harris, J. J., Harding, E. C., et al. (2019). GABA and glutamate neurons in the VTA regulate sleep and wakefulness. *Nat Neurosci* 22, 106–119. doi: 10.1038/s41593-018-0288-9.

Zell, V., Steinkellner, T., Hollon, N. G., Warlow, S. M., Souter, E., Faget, L., et al. (2020). VTA Glutamate Neuron Activity Drives Positive Reinforcement Absent Dopamine Co-release. *Neuron* 107, 864-873.e4. doi: 10.1016/j.neuron.2020.06.011.

Zhang, G.-W., Shen, L., Zhong, W., Xiong, Y., Zhang, L. I., and Tao, H. W. (2018a). Transforming Sensory Cues into Aversive Emotion via Septal-Habenular Pathway. *Neuron* 99, 1016-1028.e5. doi: 10.1016/j.neuron.2018.07.023.

Zhang, G.-W., Sun, W.-J., Zingg, B., Shen, L., He, J., Xiong, Y., et al. (2018b). A Non-canonical Reticular-Limbic Central Auditory Pathway via Medial Septum Contributes to Fear Conditioning. *Neuron* 97, 406-417.e4. doi: 10.1016/j.neuron.2017.12.010.

Zhang, T. A., Placzek, A. N., and Dani, J. A. (2010). In vitro identification and electrophysiological characterization of dopamine neurons in the ventral tegmental area. *Neuropharmacology* 59, 431–436. doi: 10.1016/j.neuropharm.2010.06.004.

9. Acknowledgements

It takes a village to raise a child, and no doubt it takes a village also to raise a doctoral researcher. Several exceptional people have dotted my path during the past five years, and each one of them contributed deeply to my personal and professional development.

First on the list, my PhD supervisor Prof. Dr. Stefan Remy. He welcomed me into his lab as a Master student, and trusted my scientific vision and my ideas from start to finish. It has been a long road, and I am extremely grateful for the many opportunities he has given me to learn, experiment, and interact with the neuroscientific community all over the world.

I am also thankful to have Prof. Dr. Dirk Isbrandt as my second reviewer, whose passion for science truly inspired me every time we met; along with the other two members of my committee: Prof. Dr. Susanne Schoch-McGovern and Prof. Dr. Sandra Blaess.

This work wouldn’t have been possible without the support of the Remy group. In particular, I want to thank Dr. Christina Müller who defined with me the early steps of this project and Dr. Hiroshi Kaneko for his kindness, valuable help, and patience in teaching me everything I needed to know about electrophysiology and set-up manufacturing. This journey would have not been the same without my fellow PhD companions Dennis Dalügge, with whom I shared countless coffee breaks and uncountable scientific discussions, and Kevin Luxem, who spent infinite coding sessions with me and put up with all my rants against Python. Special thanks go to Dr. Oliver Barnstedt whose enthusiasm for science, wise words and advices encouraged me even in the most difficult moments. Not to mention the help he gave in shaping this work and finalizing this thesis. Another huge thank you goes to Dr. Sanja Mikulovic, for always being by my side, for the endless chats, for the scientific and personal support she has given me over the years, and for always finding the time to discuss, correct, or simply read everything I came up with.

Moving from Bonn to Magdeburg was not easy: it was hard to say goodbye to “my” lab in DZNE; to Nancy, whose door was always open and with a smile could solve all problems; and to the whole Fuhrmann group, not only lab neighbours but also friends with whom I shared so many hiking and conference trips. But without the move to Magdeburg, I would not have met Silvia, with her experience and determination. Without her, everything would

have been more difficult and less enjoyable. I also want to thank the entire CNeu department, for the support and help they have given me in the past years, and in particular Alessandro, for always providing me with freshly brewed coffee when needed.

It takes a village, and this village is also made up of all the friends I have at my side. Anna, Antonio, Caterina, Francesca, Gabriele, Margherita, and Matteo, who despite the years and distance have been a common thread throughout this time. Zoe, Lorenzo, and Cecilia, with whom I shared the path at the University of Trieste and who never left me alone since, despite the countless moves around Europe for all of us. Laura, who always has her door open for me and who will prepare the Pastiera in August just to lift me up. My D&D party: Lorenzo, Alessandro, Mattia and Pietro, and the countless weekends ordering food from Mogul and arguing about the best strategy to adopt. Matilde, Maria, Giulio, and Stefano, they became my second family when I arrived in Bonn 8 years ago, and they still are. André, Irina, Hyundai, Qëndresa, and Geni: my haven in Bonn whenever I return. Their presence and support have been and still are invaluable to me. Tamara, with her incredible strength and creativity, always manages to show me reality from a different angle and I want to thank her for that. Silvia: neuroscience brough us together, and gave me an extraordinary friend. Last but not least, Nora: I don’t know how I would have survived this journey without her constant support.

Finally, my gratitude goes to my family. Alberto, mum, and dad, for supporting me now and always; for trusting me and never doubt any of my decisions, for always being there when I need them the most. To my grandfather, whose eyes sparkle every time I tell him of my trips and my successes, and to my grandmother, the hearth of our family, who has never failed to show me her unconditional love. Not to forget my aunt Anna and my uncle Roberto, for being always there, listening to me, and giving me the best advices. This work, all that I have learned, and all that I have achieved, would not have been possible without you.

It took a village, and I cannot express how grateful I am to have shared this path with each and every of these incredible people. It has not always been easy, but it has been an extraordinary journey.